National Aeronautics and Space Administration

HOUSTON, TEXAS

Manned Spacecraft Center

MSC INTERNAL NOTE NO. 66-EG-4

PROJECT APOLLO

VISIBILITY OF LUNAR CRATERS DURING THE LEM FINAL APPROACH PHASE

Prepared by: Indulis Saulietis
Indulis Saulietis

Approved: Paul E. Ebersole
Paul E. Ebersole
Chief, Guidance Development Branch

Approved: R. G. Chilton
Robert G. Chilton
Deputy Chief
Guidance and Control Division

NATIONAL AERONAUTICS AND SPACE ADMINISTRATION

MANNED SPACECRAFT CENTER

HOUSTON, TEXAS

January 10, 1966

INTRODUCTION

The present strategy for the lunar landing approach of the LEM provides for a spacecraft attitude such that the landing area can be seen through the window. The LEM crew will visually survey the intended landing area to determine if the terrain is suitable for a landing. The trajectory must be shaped through the guidance logic in order to provide spacecraft attitudes suitable for the viewing process and this shaping results in a greater expenditure of descent engine fuel than would a trajectory designed solely to a constraint of minimum fuel expenditure. There is then a tradeoff between the descent engine fuel cost and the requirement to visually survey the lunar terrain. The cost of providing visibility during the final approach phase has been analyzed in Reference No. 4. The advantage gained by the visual survey of the lunar terrain during the approach is partially dependent upon how soon in the final approach the pilot can begin to detect lunar surface features and, subsequently, make judgment about the suitability of the terrain for landing.

because the lunar photometric function is not duplicated naturally at any location on earth, the determination of capability to detect lunar surface features in a formidable task. Some success has been obtained by covering scale models of the lunar surface with cupric oxide and observing the model from various angles in the presence of a light source simulating the sun. The difficulty of properly lighting large models and the subsequent scaling problems limits this approach. An approach, which appeared to have promise, involved programing the photometric function together with visual detection criteria in order to have a flexible analytical tool that could be applied to any combination of viewing angle, sun angle, and crater size. This approach was developed and the description of the analytical method and results are discussed in this internal note.

ABSTRACT

Visibility curves for idealized 10:1 depth to diameter ratio craters were found for sun elevations of 10°, 15°, 20°, 30°, 45°, and 60° at observer's altitudes of 1,000 to 10,000 feet. A field of view of 140° total observer azimuth and 8° to 60° observer altitude were evaluated.

SCOPE

This study on the visibility of lunar craters was initiated in support of the working group presently redefining the LEM descent and touchdown logic. It was desired that the results of this study indicate what size craters the LEM pilot will be able to detect on the lunar surface at any point in his field of view at various combinations of vehicle altitude and sun elevation angle, and then make recommendations with regard to optimum sun angles and glide path angles. It was also desired to find the maximum altitude at which the pilot can begin landing site selection by visual means, assuming optimum visibility around the site.

It was decided to present this data in the form of range plots in which the area that the pilot can see is analyzed at each point to determine the detectable size of the crater. These sizes were then to be plotted on the orthogonal range plot at their respective locations. After this was done, contour lines separating arbitrarily selected crater size ranges were drawn. The resulting plot represents the visibility conditions from a single point on the trajectory with some sun elevation specified.

Several basic assumptions were made in this study. In summary, these are:

a. Craters are spherical depressions (10:1 diameter to depth ratio).

b. Craters have sharp edges.

c. Tiffany data assumed applicable.

d. No search time specified.

e. No human factors or hardware limitations.

f. Detection criterion of visibility is used and not recognition.

With these assumptions in mind, it should be recognized that the data generated represents a "best case" situation as far as analysis methods are concerned. There are several other variables that can be applied to the study to make the results more realistic, but at the present time these are not well defined. Among these are search times, hardware constraints, and human factors. It is hoped that further studies will include these factors and that more realistic data will result.

METHOD

Brightness Distribution on the Crater Floor - A study of available information on lunar craters indicated that craters of less than 500' diameter have, in general, the same 10:1 diameter to depth ratio (Figure 1) and are approximately spherical in surface form. With this assumption, it is possible to calculate the necessary parameters in normalized form so the data for any one size is applicable to any other by use of a scale factor. A crater size of 10' diameter and 1' depth was assumed for this purpose.

Figure 2 defines the prime coordinate system in which the relative positions of the sun and observer are shown. In this coordinate system, the sphere describing the crater surface has the equation

$$X^2 + Y^2 + (Z - (R - d))^2 = R^2 \qquad (1)$$

where

R = radius of sphere
r = radius of crater = 5'
d = depth of crater = 1'

$$R = \frac{r^2 + d^2}{2d} = 13 \tag{1a}$$

$$R - d = 12$$

The crater rim presents an ellipse to the observer having the equation

$$\frac{Y_1^2}{r^2} = \frac{Z_1^2}{(r \sin\lambda)^2} = 1 \tag{2}$$

in the coordinate system of the observer as shown in Figure 3 where X_1, Y_1, and Z_1 have gone through the successive rotations (ψ) and (λ) about the prime coordinate system X, Y, and Z.

The transforms

$$\begin{aligned} X &= (X_1 \cos\lambda + Z_1 \sin\lambda) \cos\psi + Y_1 \sin\psi \\ Y &= Y_1 \cos\psi - (X_1 \cos\lambda + Z_1 \sin\lambda) \sin\psi \\ Z &= Z_1 \cos\lambda - X_1 \sin\lambda \end{aligned} \tag{3}$$

and

$$\begin{aligned} X_1 &= (X \cos\psi - Y \sin\psi) \cos\lambda - Z \sin\lambda \\ Y_1 &= Y \cos\psi + X \sin\psi \\ Z_1 &= Z \cos\lambda + (X \cos\psi - Y \sin\psi) \sin\lambda \end{aligned} \tag{3a}$$

are used between X_1, Y_1, and Z_1 and X, Y, and Z.

Similarly, the crater rim presents the ellipse

$$\frac{Y_2^2}{r^2} + \frac{Z_2^2}{(r \sin \phi)^2} = 1 \qquad (4)$$

to the Sun Line of Sight (SLOS) in the sun coordinate system X_2, Y_2, and Z_2 as shown in Figure 4.

The sun coordinate system X_2, Y_2, and Z_2 is rotated (ϕ) about Y in the X, Y, and Z system

The transforms

$$\begin{aligned} X_2 &= X \cos \phi - Z \sin \phi \\ Y_2 &= Y \\ Z_2 &= Z \cos \phi + X \sin \phi \end{aligned} \qquad (5)$$

and

$$\begin{aligned} X &= X_2 \cos \phi + Z_2 \sin \phi \\ Y &= Y_2 \\ Z &= Z_2 \cos \phi - X_1 \sin \phi \end{aligned} \qquad (5a)$$

are used between X, Y, and Z and X_2, Y_2, and Z_2.

The procedure used was to choose a point $X_{10} = C$, Y_{10}, Z_{10} within the ellipse (2) in the observer coordinate system and transform it into the prime coordinate system using equation (3) obtaining X_0, Y_0, and Z_0 in X, Y, and Z. It was then necessary to find the intersection point (X_a, Y_a, and Z_a) on the sphere surface (see Figure 5).

This was done by solving the equation of the line normal to the (Y_1 and Z_1) plane at (X_{10}, Y_{10}, and Z_{10}) with the sphere equation (1) and discarding that solution having Z_a positive. (All points on the crater floor have negative Z_a values between 0 and -1.) A reverse procedure was used to project this point into the Y_2 Z_2 plane (see Figure 6).

Having obtained the intersect point (Y_{20} and Z_{20}) in the sun plane (Y_2 and Z_2), it remains only to determine whether (Y_{20} and Z_{20}) lies inside or outside the sun ellipse (4). If it lies inside, we can conclude that the point (X_a, Y_a, and Z_a) on the crater floor is sunlit. If it lies outside the ellipse (4), that point lies within the geometric shadow cast by the crater rim.

If it has been found that the point (X_a, Y_a, and Z_a) is sunlit, a local viewing geometry is found relative to the local normal to the sphere at that point by determining the direction cosines of the three lines OLOS, SLOS, and local normal. The brightness along OLOS can then be found from the lunar photometric function. This brightness is then assigned to the original point Y_{10} and Z_{10} selected on the observer's ellipse. By an iterative process, the brightness distribution as seen by the observer on the floor of the crater can be found (Figures 7 and 8).

In the present configuration, the computer program selects (Y_{10} and Z_{10}) in intervals of .25, so each point represents a projected area of .0625. It sums all the geometric shadow points and multiplies the sum by .0625 to find a total projected area. This area is then normalized by dividing by 25π (the projected normal area of the crater). An average brightness of zero is assigned to this area. A separate normalized area is obtained by summing those points which have a brightness less than that of the background. An average brightness is found for these points. Similarly, those points having a brightness greater than the background are summed and a third area and average brightness are obtained.

Crater Visibility - A preliminary method of evaluating the visibility of lunar craters gave results that were too conservative when compared to experimental visibility tests conducted at a later time. A discussion of this preliminary method is included since some of the techniques are applicable to the final experimentally verified method.

Using the method outlined under "Brightness Distribution on the Crater Floor", three sets of data were obtained for the assumed crater configuration. These consisted of three normalized areas and three average brightnesses. A separate visibility calculation was done for each.

a. Geometric Shadow Visibility - An average brightness of zero was assumed for this area of the craters which immediately fixes the contract at -1, using the contrast equation

$$C_T = \frac{B_T - B_0}{B_0} \tag{6}$$

where

B_T = brightness of target
B_0 = brightness of background
C_T = target contrast

To this, contract C_T was applied a field factor to give 99% probability of detection. Using the Tiffany data (Reference no. 3), a threshold angle (θ) was found for each background brightness at a set of angles (ϕ), (ψ), and (λ). From this angle, we can find the diameter (d) of a circular spot necessary for detection at any range R. By converting the normalized area found earlier into an equal area circular spot with this diameter (d), we can find the range at which this equivalent spot can be seen.

$$R = \frac{d}{\tan(\theta)} \tag{7}$$

Or conversely, the diameter from a given range can be obtained

$$d = R \tan(\theta) \tag{7a}$$

Figure 10 shows the equivalent view geometry from the LEM from which we find the slant range R to be

$$R = \frac{h}{\sin(\lambda)} \tag{8}$$

The diameter d' of the crater producing (at (ϕ), (ψ), and (λ)) this equivalent area is given by

$$d' = \frac{d}{\sqrt{A}}$$

where A is the normalized decimal fraction area of the spot. By iterating through the values of h, (ϕ), (ψ), and (λ), a crater size visible due to geometric shadows at any point on the surface can be found.

b. Photometric Shadow Visibility - The photometric shadow was defined as that area of the crater floor having a brightness less than that of the background but greater than zero. The calculation of visible size, due to these shadows, is similar to that used in the geometric shadow case with the exception that the contrast is also a variable. This posed no problems in estimating the visible crater size since a (θ) can be found for each contrast and background brightness in the Tiffany data.

c. Bright Side Visibility - The bright side of the crater floor was defined as that area having a brightness greater than that of the background. Contrasts and crater sizes were found as in (b.) above.

Data obtained from nos. 1, 2, and 3 above was plotted separately in range form and can be seen in Figures 36-41. The same data was again plotted by combining the three sets of data at each altitude and sun angle and then selecting at each point the smallest crater visible due to either no. 1, 2, or 3. These can be seen in Figures 42-44.

A series of observational tests on a lunar surface model were made to test the validity of the method described above. The results indicated that the method of treating each type of contrast, exhibited by the crater separately and then choosing the one giving the best visibility, is too pessimistic particularly at high sun angles and low observer elevation angles. It was felt that an elongated target (such as a crater foreshortened by the viewing geometry) is more detectable than a circular spot having the same area and contrast.

A second test was made to confirm this hypothesis and the results confirmed that this was the case. It now remained to find a better technique of treating the craters as single contrast targets. The assumption was made that any given crater, at its detection range, presents to the observer only a small blurred disk having a diameter equal to that of the crater and a contract equivalent to that obtained by distributing the crater contrasts evenly over this disk. Figure 9 illustrates this method and the formula used to calculate the equivalent contrast.

Using this formula, a series of computer runs were made and the results plotted as described earlier. A much better fit to the observed data was obtained.

The method used to obtain the observational data is described in Appendix B of this internal note.

In the process of generating equivalent targets, much labor was saved by having the computer print out the results automatically in orthogonal range coordinates. This enabled quick evaluation of the merits of any given scheme without having to hand plot the results. Data was also generated for sun angles of 10°, 20°, and 60° in addition to 15°, 30°, and 45° sun angles already analyzed.

CONCLUSIONS

Figures 10-35 represent the visibility conditions existing on the lunar surface for various combinations of sun elevation angle and spacecraft altitude. The retro-reflective nature of the surface produces a "washout" condition (indicated by regions on the range visibility plots in which craters must be 500' or greater in diameter to be detected) which gets worse with increasing sun elevations. For sun angles less than 23°, there is one such region on each plot. In this case, geometric (black) shadows are present at all times and aid in visibility. For sun elevations above 23°, the shadows disappear and the visibility gets poorer as indicated by the presence of two "washout"

regions. One of these is located at the point on the surface where the vehicle shadow is case and the other is further down range. The first is caused by the retro-reflective property of the surface and the second by the low vision angle relative to the surface (i.e., only the sunlit rear walls of the crater are seen.)

The data in Figures 10-34 is considered to be fairly reliable since some experimental verification has been obtained (Appendix B). It should be remembered that the data assumes detection criteria only with no indication of whether the pilot can identify the detected feature as a crater.

ANALYSIS OF RESULTS

The effect of LEM altitude and sun angle on visibility is summarized in Table I. An evaluation of Figures 12-35 resulted in a set of acceptable glide path angles for each combination of altitude and sun angle. These represent glide paths on which the pilot can detect 10, 15, 20, and 30-foot diameter craters in the vicinity of the nominal landing site that corresponds to the glide path in question. Setting an upper limit on the glide path of 20° eliminates most of the altitude-sun angle combinations leaving those underlined in Table I. For example at an altitude of 5,000', the sun angles at which site selection can be made from a glide path of less than 20° lie between 10° and 15° with a lower limit on glide path of 13°.

Effect of 3-Day Launch Window on Visibility Conditions - Assuming the first day to be the optimum launch time, one can select a sun angle (local to the nominal landing site) which will given optimum visibility, say 10°. If the launch slips 24 hours and no change in the nominal landing site is made, the sun elevation will have changed by 13° to 23°. Referring to Table I, it will be found that visibility is marginal. For descent glide path angles of less than 20° if the launch slips another 24 hours, the sun elevation at the site will be 36° at which a site could be visually selected from a 500' altitude and 20° glide path.

It was found that there is no combination of three consecutive sun angles differing by 13° each that will give even marginal visibility on all launch days. This is, of course, for the same landing site on all three days.

It is therefore recommended that the landing site be reselected as the launch slips from day-to-day to preserve optimum visibility during the descent phase. Ideally, these would lie 13° apart on the moon's surface in the orbit plane so 24-hour slips would simply mean reselection to the next adjacent site to preserve an optimum sun elevation. Practically, this is not possible so there will be some variation in the sun elevation at different launch window days. Hopefully, these will be no more than ±5°.

Dog Leg Trajectory Advantages - Table I also includes the results of analyzing Figures 12-35 to determine if a dog leg (out of plane) descent gives any advantage in so far as visibility is concerned. Again, this includes the

constraints of 20° maximum glide path angle and 10', 15', 20', and 30' diameter observable craters. For example at 1,000' altitude with a sun angle of 30°, an in-plane descent would not be possible with the 20° maximum glide path angle constraint. But if a 15° dog leg is made in azimuth, the pilot can select a site with a 17° flight path angle (see Figure 21). This example is for 10' diameter craters visible in the landing site vicinity.

In summary, visibility is acceptable for those sun angles and altitudes for which a "yes" answer exists under dog leg feasibility or for which the in-plane glide path can be less than 20° (underlined items).

The question of window interference can be raised at this point. It is understood at the present time that for glide path angles of 10° to 20°, the nominal landing site is always visible to the pilot from 10,000' on down to hover altitude.

ACCEPTABLE GLIDE PATH ANGLES AND DOG LEG FEASIBILITY SUMMARY, FOR DETECTABLE CRATER SIZES OF 10', 15', 20', & 30'

ALTITUDE, FT.	FIG. #	SUN ELEV.	DOG LEG FEASIBILITY				ACCEPTABLE GLIDE PATH ANGLES			
			10'	15'	20'	30'	10'	15'	20'	30'
10,000	30	10°	NO	NO	NO	NO	gt16°	gt16°	gt15°	gt13.5°
	31	15°	NO	NO	NO	NO	gt25°	gt20°	gt19°	gt18.5°
	32	20°	NO	NO	NO	NO	gt30°	gt27°	gt25°	gt23°
	33	30°	NO	NO	NO	NO	gt40°	gt40°	gt38°	gt38°
	34	45°	NO	NO	NO	NO	gt55°	gt55°	gt55°	gt55°
	35	60°	NO	NO	NO	NO	gt65°	gt65°	45-55°, gt65°	35-55°, gt65°
5,000	24	10°	NO	NO	NO	NO	gt13°	gt13°	gt12.5°	gt12°
	25	15°	NO	NO	NO	YES	gt20°	gt18°	gt18°	gt17°
	26	20°	NO	NO	YES	YES	gt25°	gt23°	gt23°	[illegible]°
	27	30°	NO	NO	NO	YES	gt35°	gt34°	gt33°	gt33°
	28	45°	NO	NO	NO	NO	gt55°	gt55°	30-40°, gt55°	gt55°, 2[illegible]-40°
	29	60°	NO	NO	NO	NO	40-50°, gt65°	3[illegible]-50°, gt65°	33-50°, gt65°	2[illegible]-50°, gt65°
	18	10°	NO	NO	NO	NO	gt11°	gt10°	gt10°	gt10°
	19	15°	YES	YES	YES	YES	gt15°	gt17°	gt17°	gt15.5°
	20	20°	YES	YES	YES	YES	gt23°	gt23°	gt22°	gt22°
	21	30°	YES	YES	YES	YES	gt32°	19-23°, gt32°	18-23°, gt32°	17-23°, gt32°
	22	45°	NO	NO	NO	NO	20-40°, gt55°	19-40°, gt55°	19-40°, gt55°	18-40°, gt55°
	23	60°	NO	NO	NO	NO	20-50°, gt65°	18-50°, gt65°	17-50°, gt65°	16-50°, gt65°
500	12	10°	NO	NO	NO	NO	gt10°	gt10°	gt10°	gt10°
	13	15°	YES	YES	YES	YES	gt17°	gt17°	gt17°	gt17°
	14	20°	YES	YES	YES	YES	gt23°	gt23°	gt22°	gt22°
	15	30°	YES	YES	YES	YES	19-23°, gt35°	19-23°, gt35°	19-23°, gt32°	19-23°, gt32°
	16	45°	NO	NO	NO	NO	19-40°, gt65°	18-40°, gt55°	18-40°, gt55°	17-40°, gt55°
	17	60°	NO	NO	NO	NO	16-50°, gt65°	15-50°, gt65°	14-50°, gt65°	13.5-50°, gt65°

TABLE I

Underlined items meet the requirement of Glide Path Angle between 10 and 20°

gtXX° means greater than XX°

RECOMMENDATIONS FOR FURTHER STUDY INTO THE VISIBILITY PROBLEM

a. Target recognition data is currently being generated. A study similar to the one here discussed will be done on lunar terrain recognitions and its effects on visual site selection.

b. Better simulations are needed to verify the conclusions reached in these studies which are based on analytic data only.

c. Data is needed on desired landing site characteristics and hardware constraints.

REFERENCES

1. Eastman Kodak Company, Apparatus and Optical Division, Final Report, Report No. Z-3841, "Lunar Photo Study", Contract NAS 9-3826, December 1, 1964 - October 1, 1965.

2. Jet Propulsion Laboratory, Technical Report No. 32-664, "The Lunar Reflectivity Model for Range Block III Analysis", D. Willingham, November 2, 1964.

3. Massachusetts Institute of Technology/Instrumentation Laboratory, Report No. E-1385, "Visibility Data and the Use of Optical Aids", Arthur C. Hardy, July 1963.

4. NASA TN D-2426, "Study of Powered-Descent Trajectories for Manned Lunar Landings", Floyd V. Bennett and Thomas G. Price, August 1964.

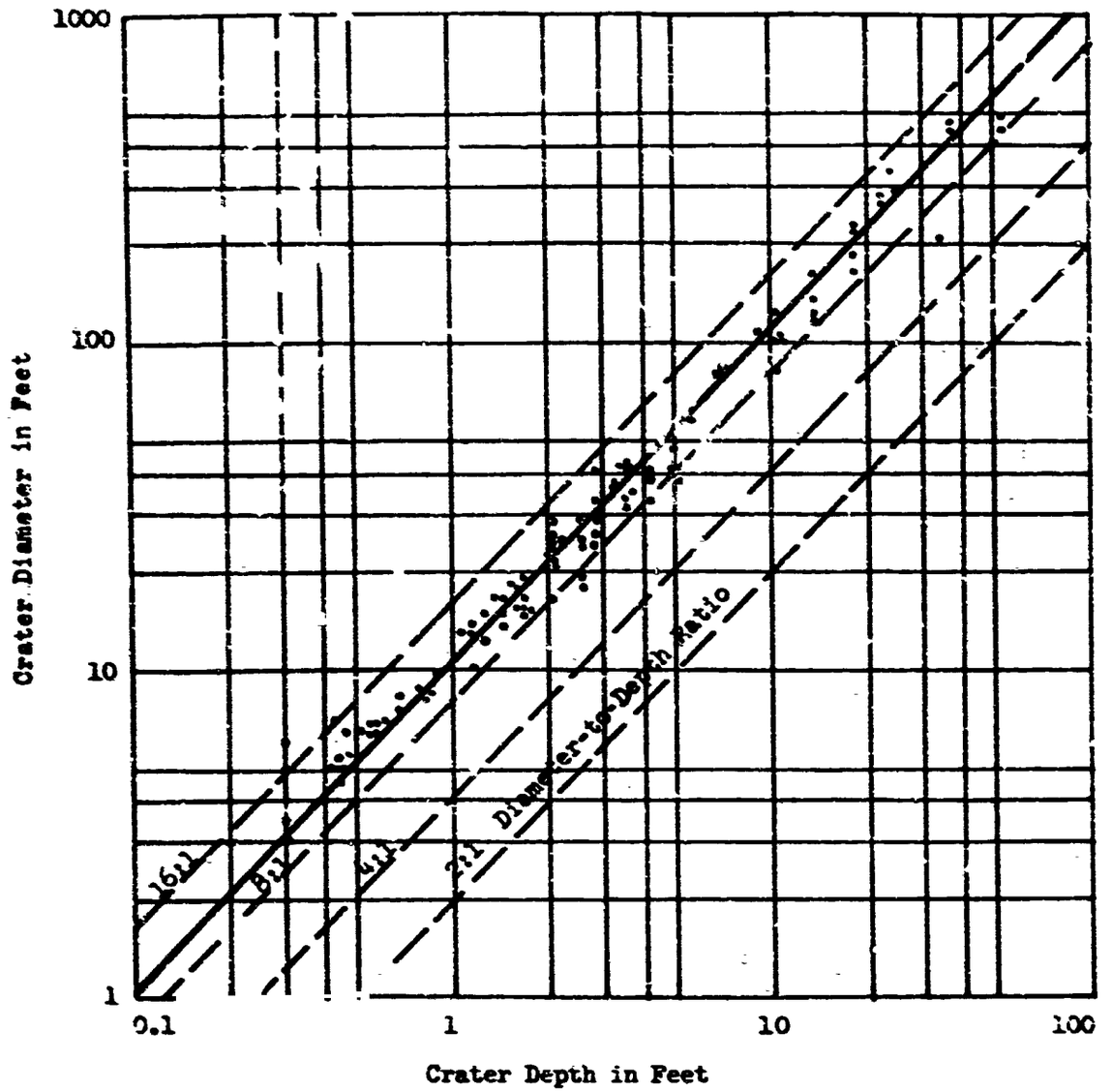

Figure 1 Diameter and Depth of Craters on the Moon. Obtained from Photographs Taken by Ranger VII and IX.

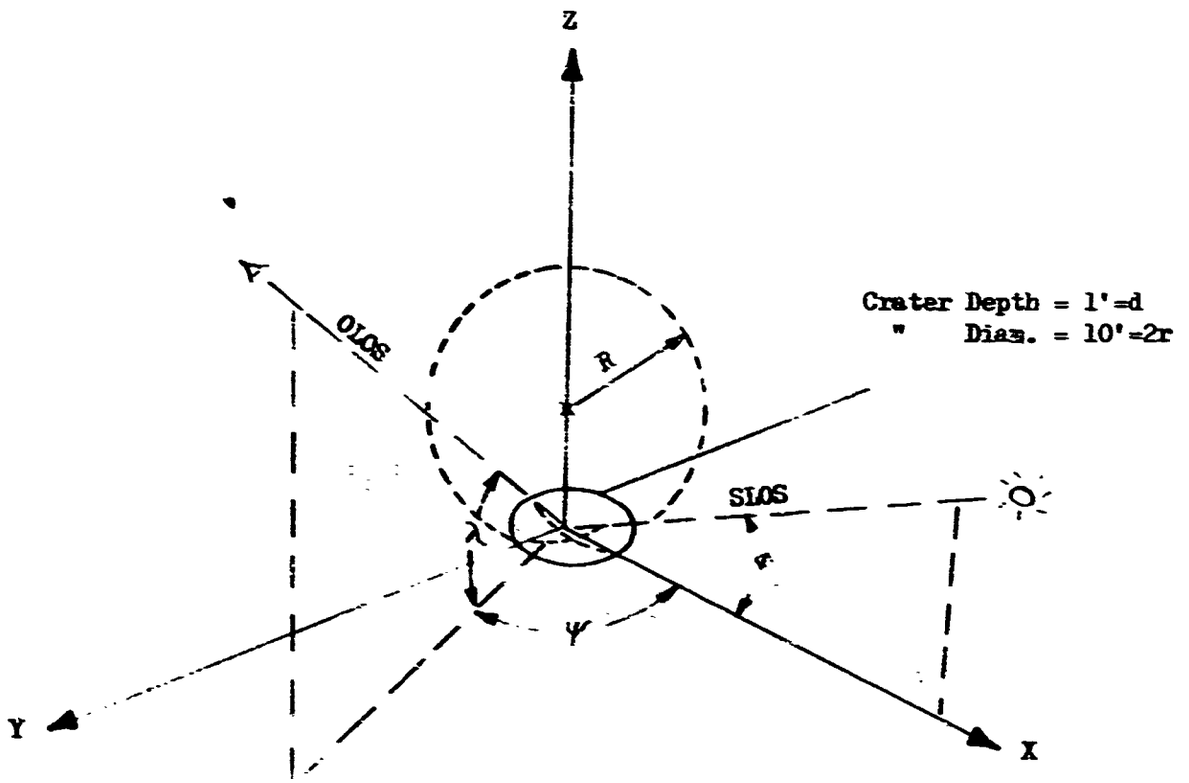

FIGURE 2

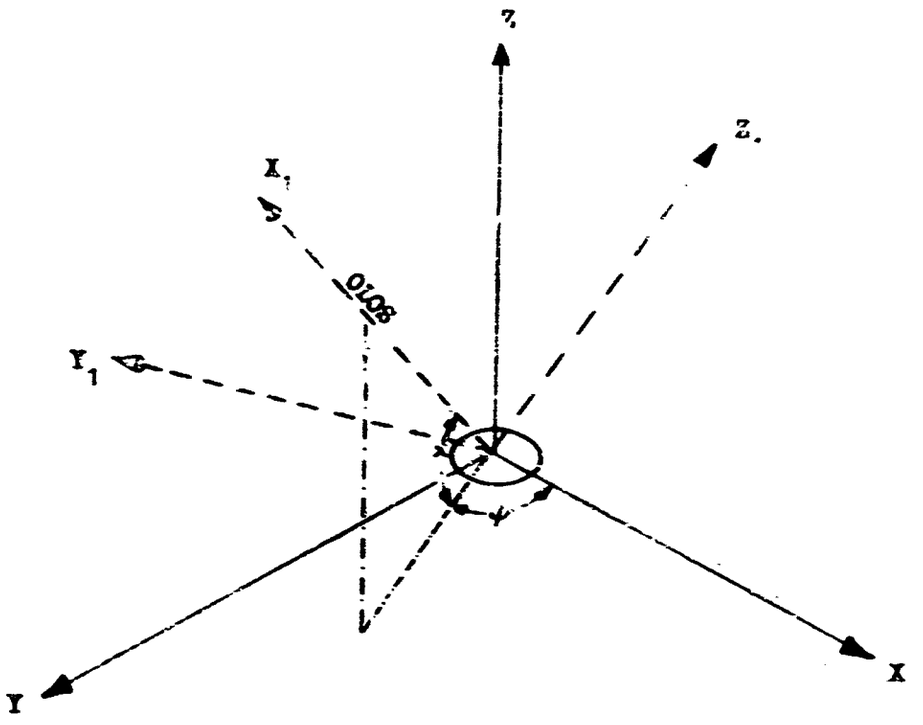

FIGURE 3

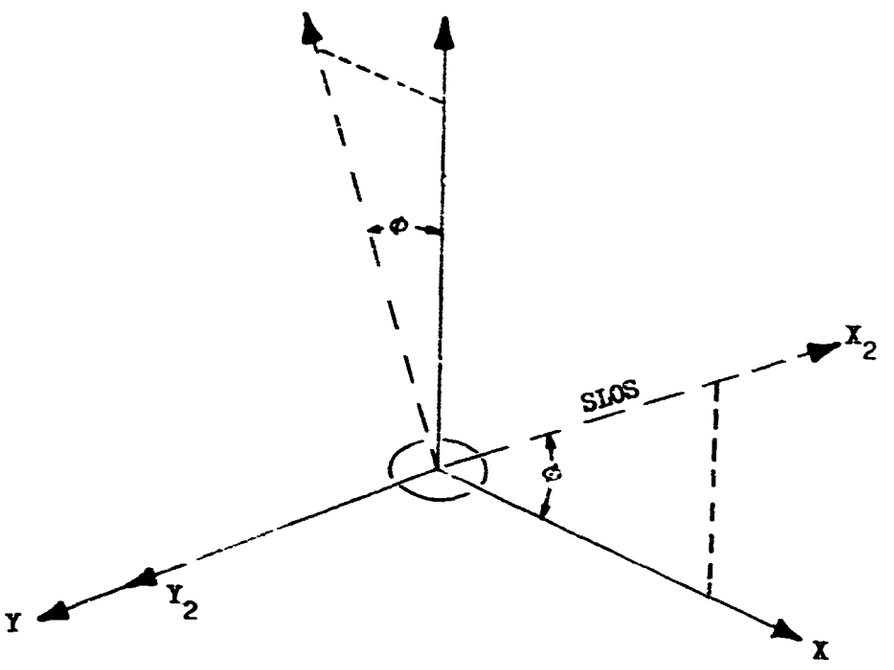

FIGURE 4

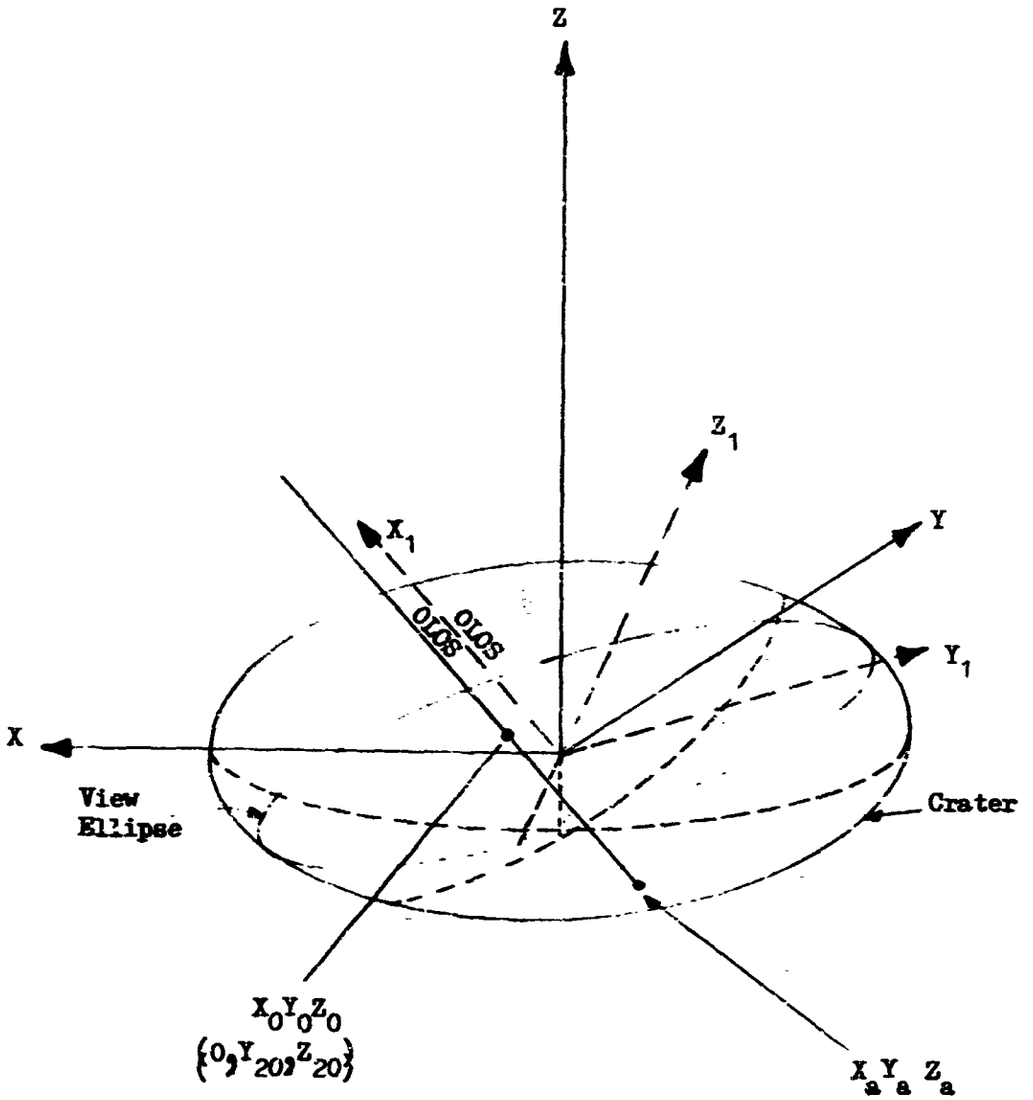
Z
Z_1
X_1
Y
Y_1
X
SOTO
OTOS
View
Ellipse
Crater
$X_0Y_0Z_0$
$(0, Y_{20}, Z_{20})$
$X_a Y_a Z_a$

FIGURE 5

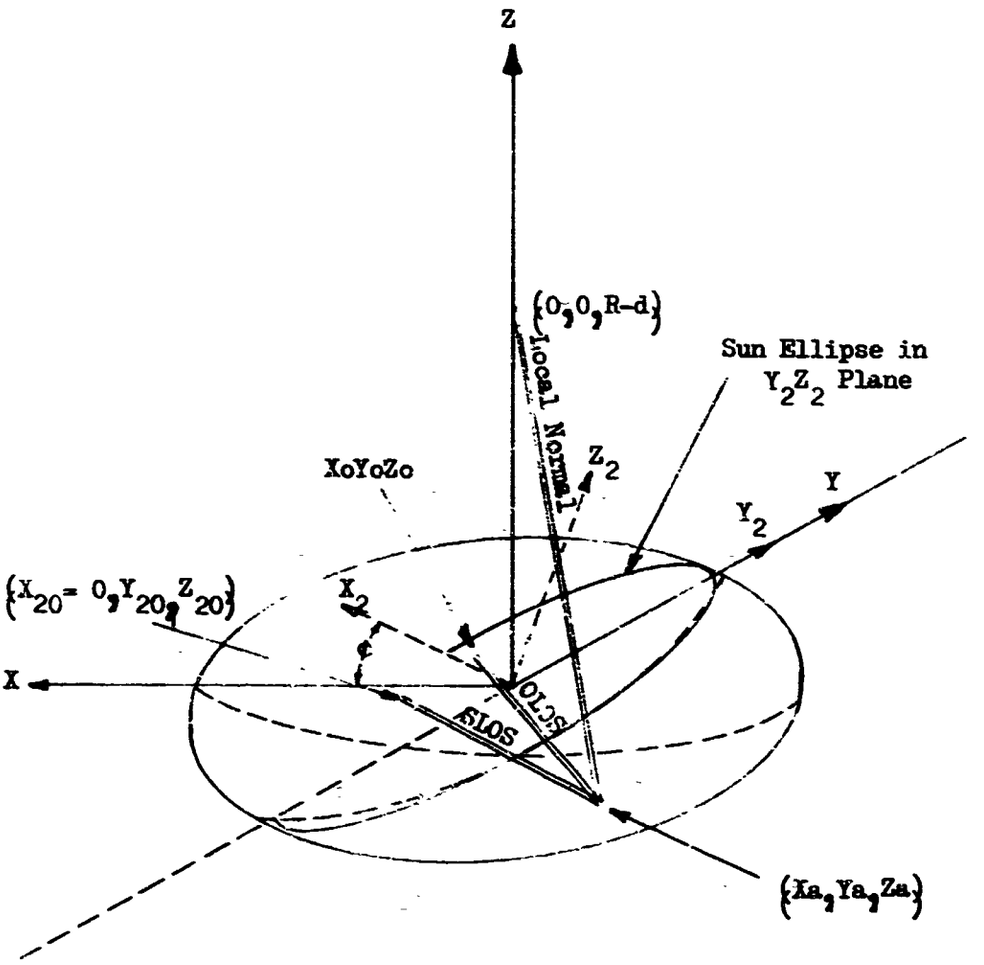
Z
(0,0,R-d)
Local Normal
Sun Ellipse in
Y_2Z_2 Plane
XoYoZo
Z_2
Y
Y_2
$(X_{20}=0, Y_{20}, Z_{20})$
X_2
X
SOTS
SOTO
(Xa, Ya, Za)

FIGURE 6

S = 15° Bo = 137 ft. 1. $\psi = \lambda = 45°$

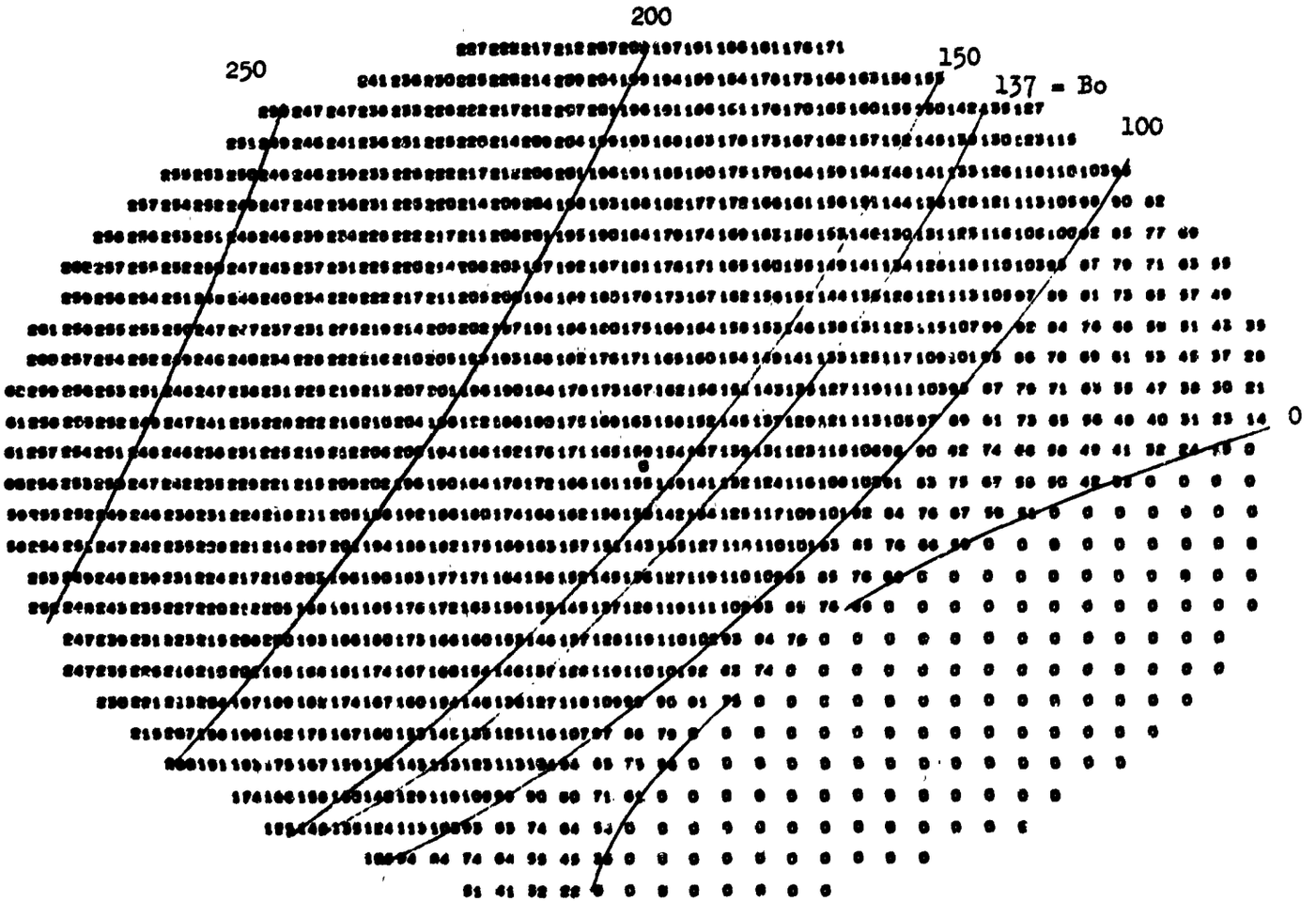

BRIGHTNESS DISTRIBUTION ON FLOOR OF TYPICAL CRATER

FIGURE 7

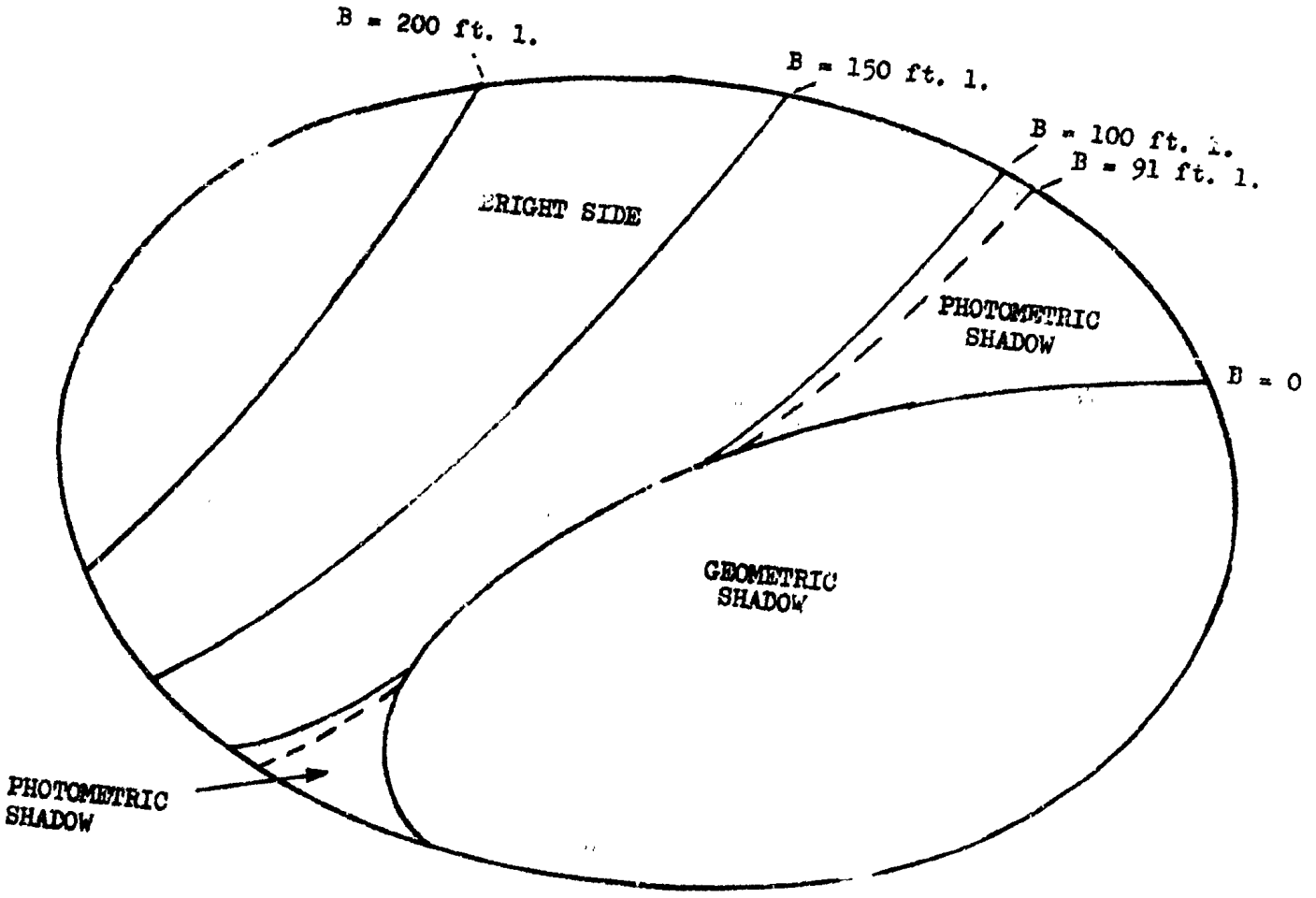

BRIGHTNESS DISTRIBUTION ON CRATER FLOOR

OBSERVER ELEVATION = 45° OBSERVER AZIMUTH = 45° SUN ELEV. = 10°

BACKGROUND BRIGHTNESS = 91 FOOT LAMBERTS

FIGURE 8

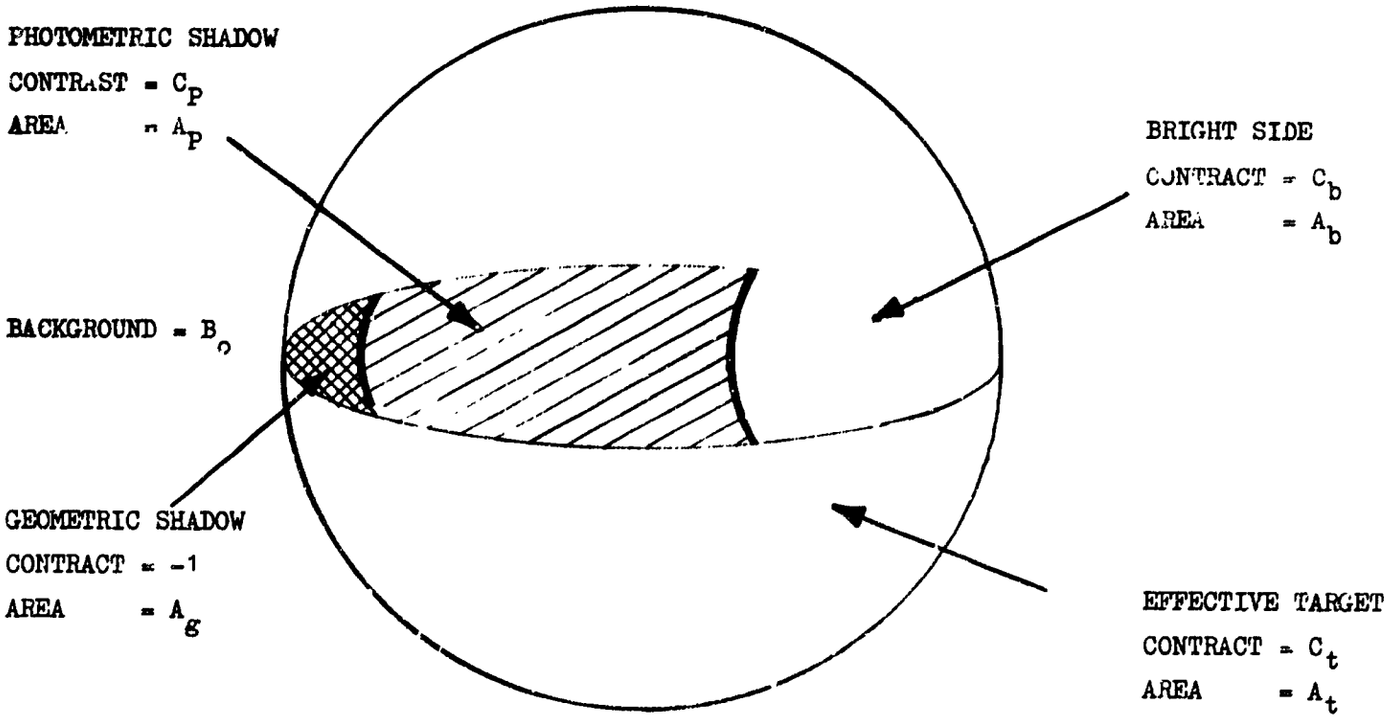

$$C_t = \frac{1}{2.29}\left[\frac{A_g}{A_t} + \frac{|C_p|A_p}{A_t} + \frac{|C_b|A_b}{A_t}\right]$$

FIGURE 9

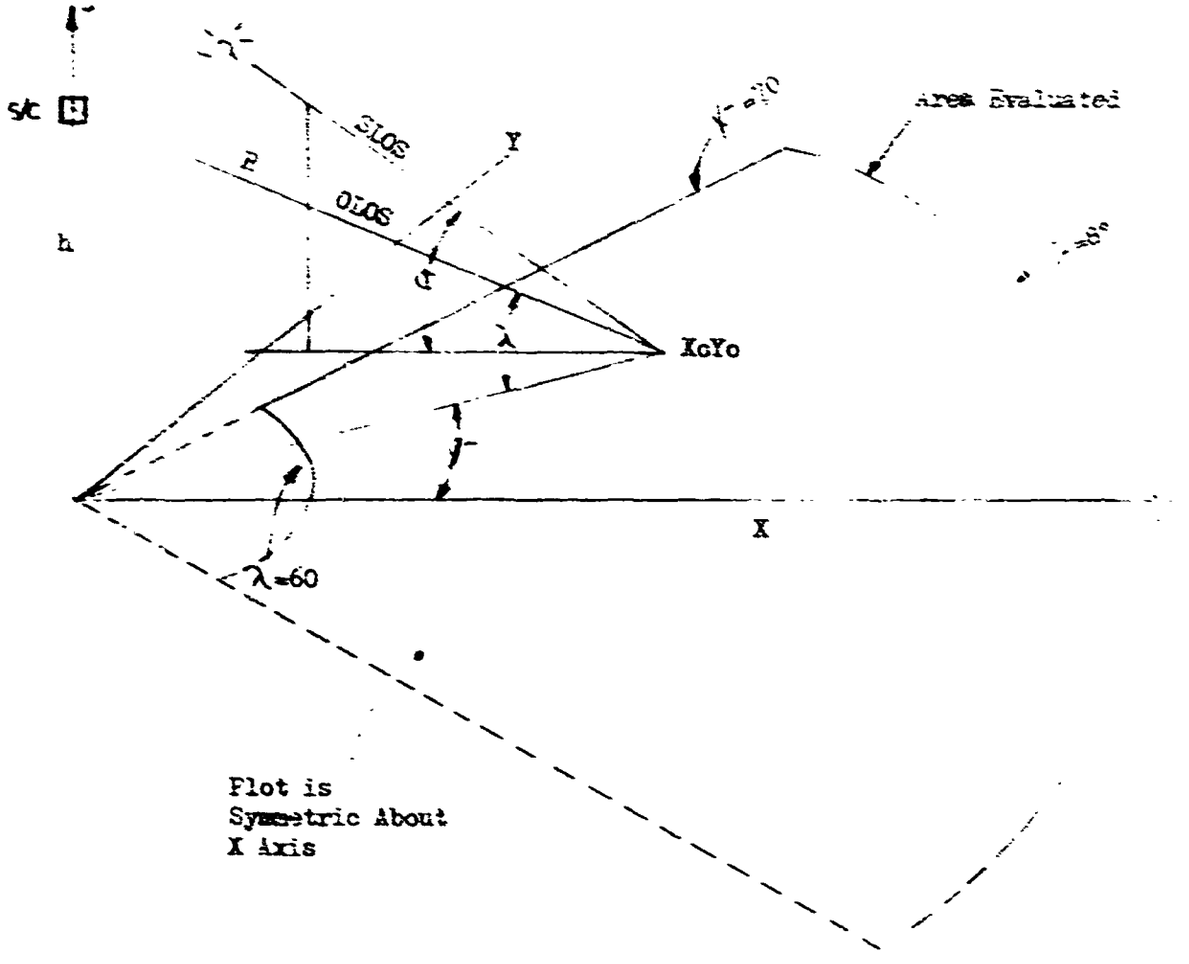
S/C
SOLS
SOLO
Y
h
XcYo
X
λ=60
Area Evaluated
Plot is
Symmetric About
X Axis

FIGURE 10

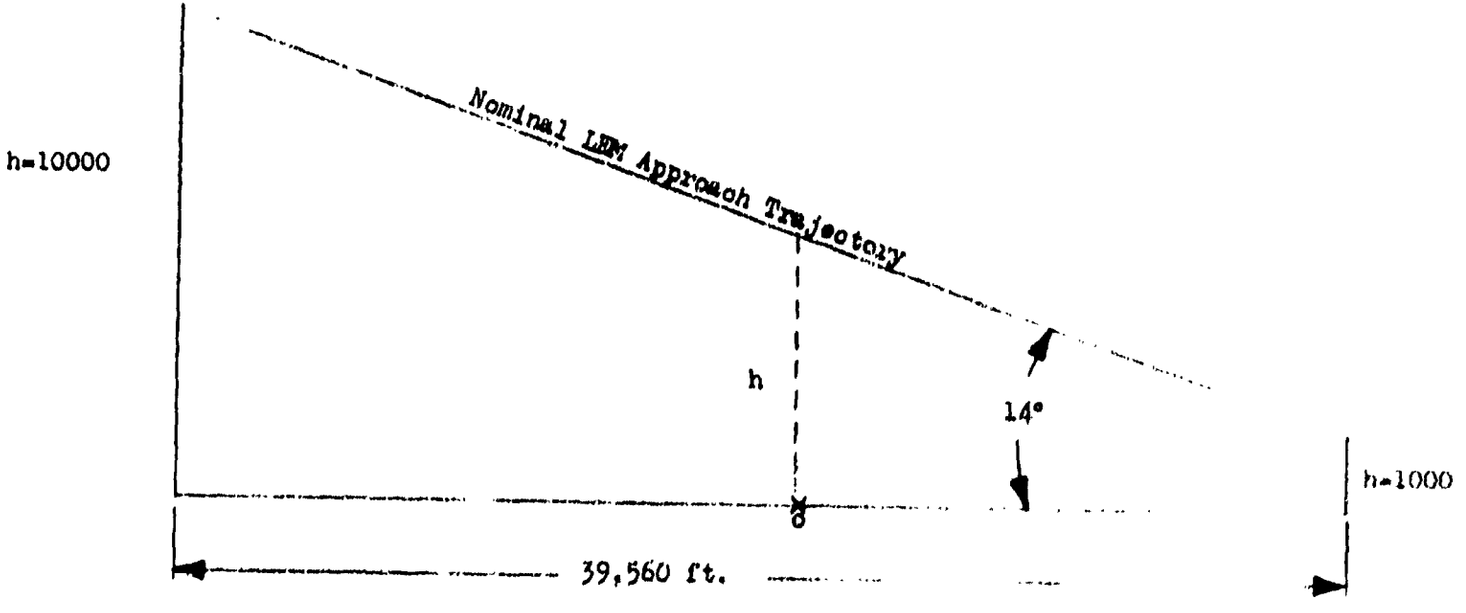

FIGURE 11

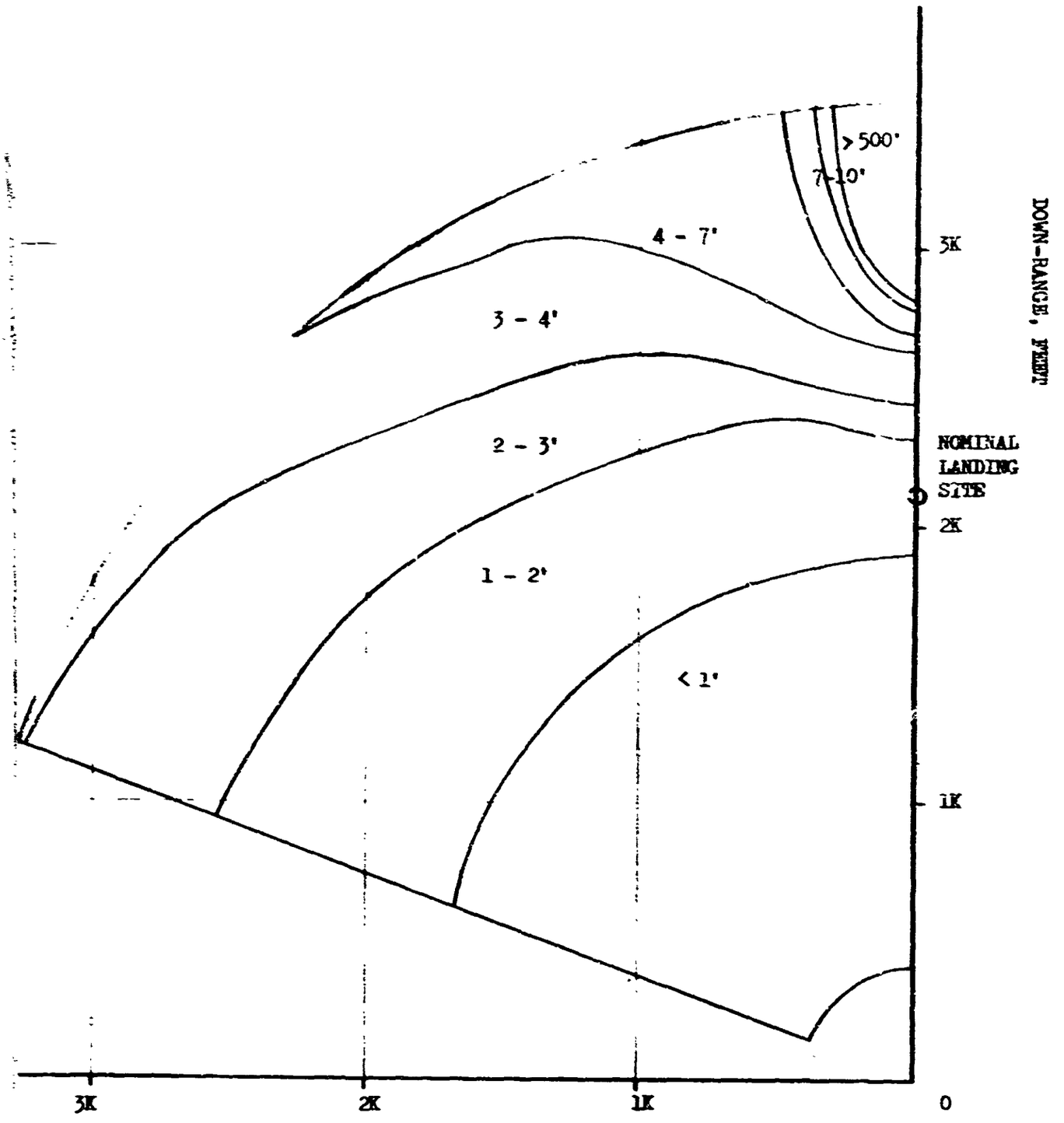

LEM ALTITUDE = 500 FEET

SUN ELEVATION 10°

CRATER VISIBILITY CONTOUR LINES

FIGURE 12

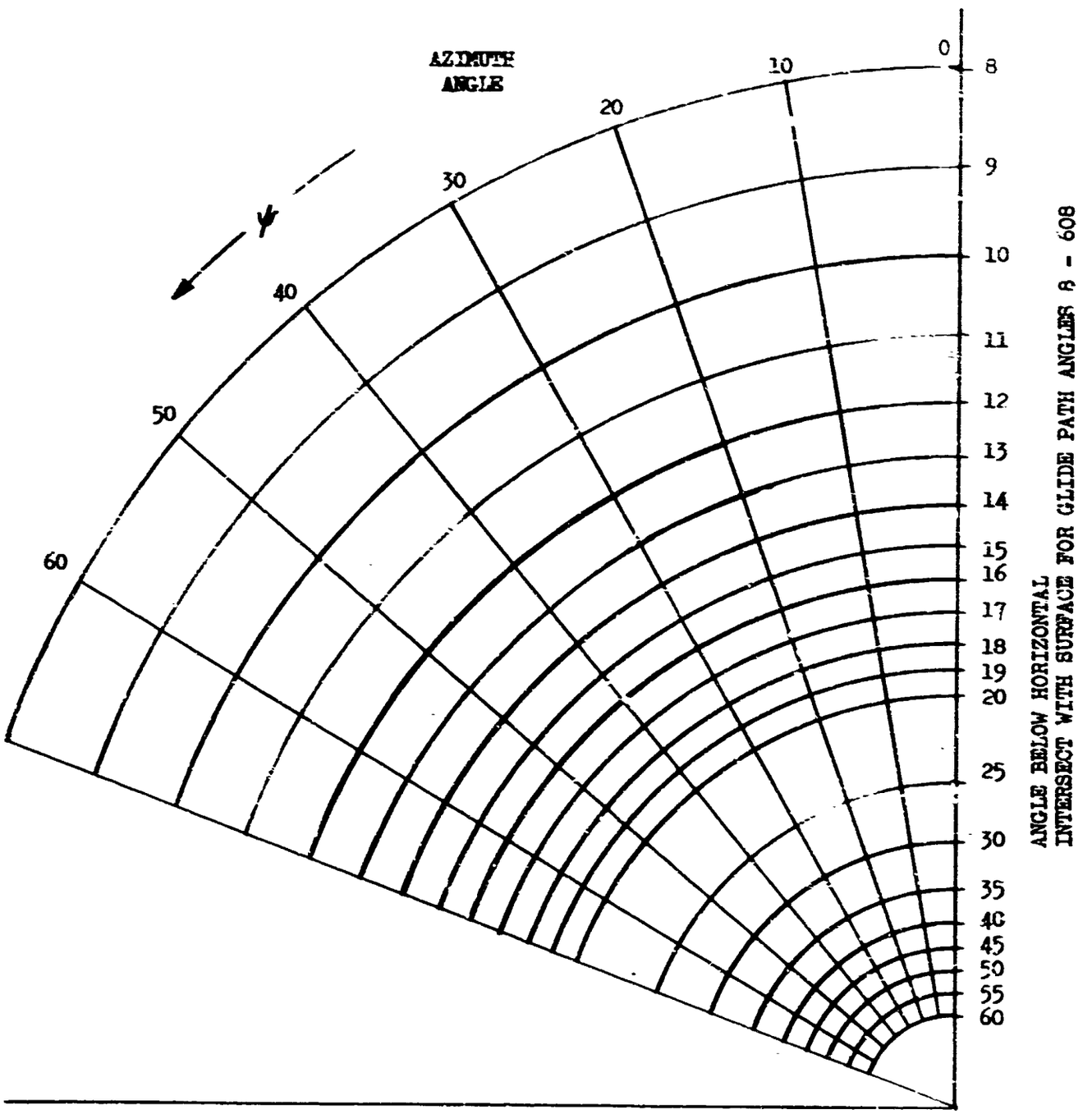

NORMALIZED VIEWING GEOMETRY

(to scale for Figures 12-35)

FIGURE 12A

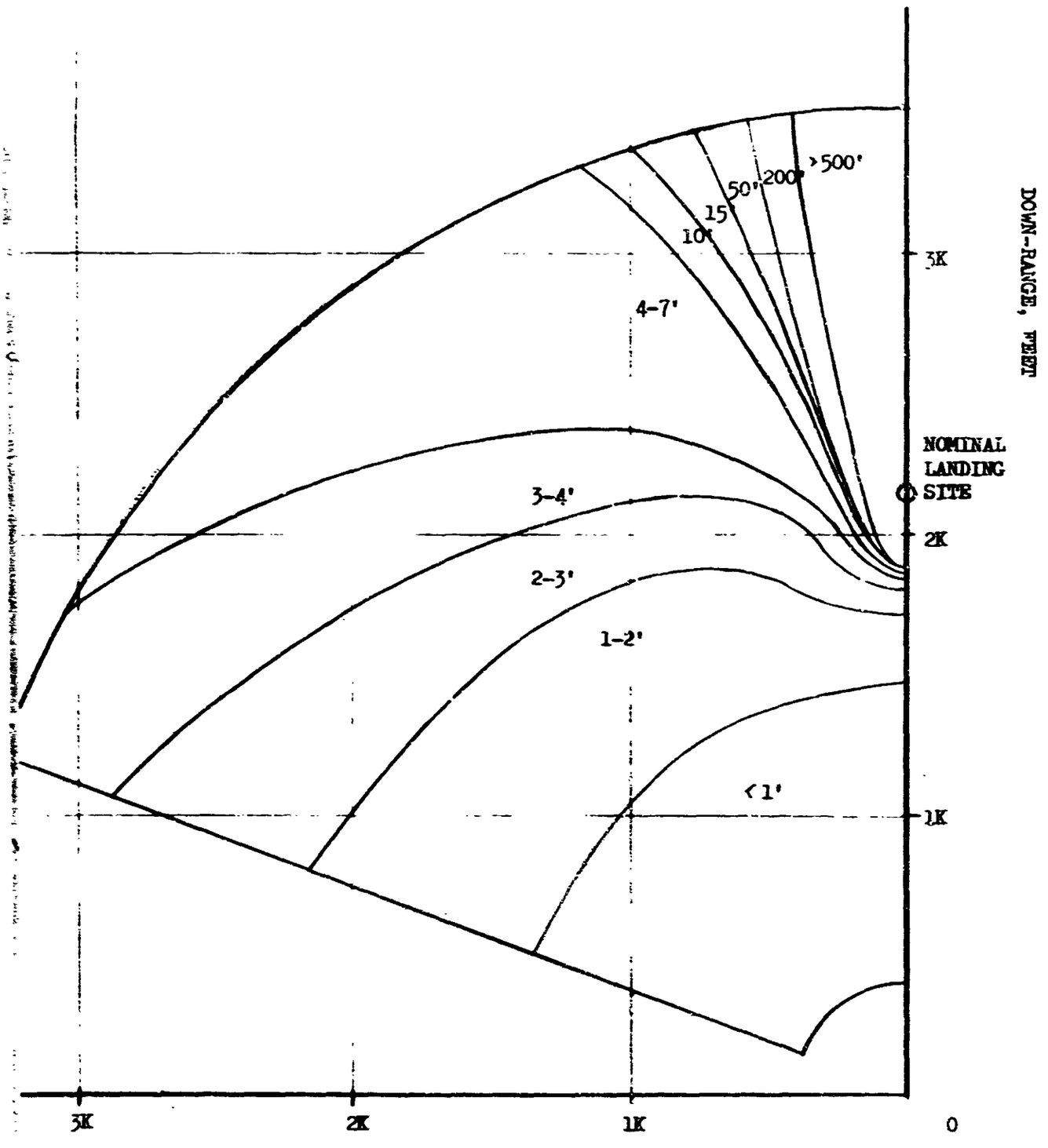

LEM ALTITUDE = 500 FEET

SUN ELEVATION 15°

CRATER VISIBILITY CONTOUR LINES

FIGURE 13

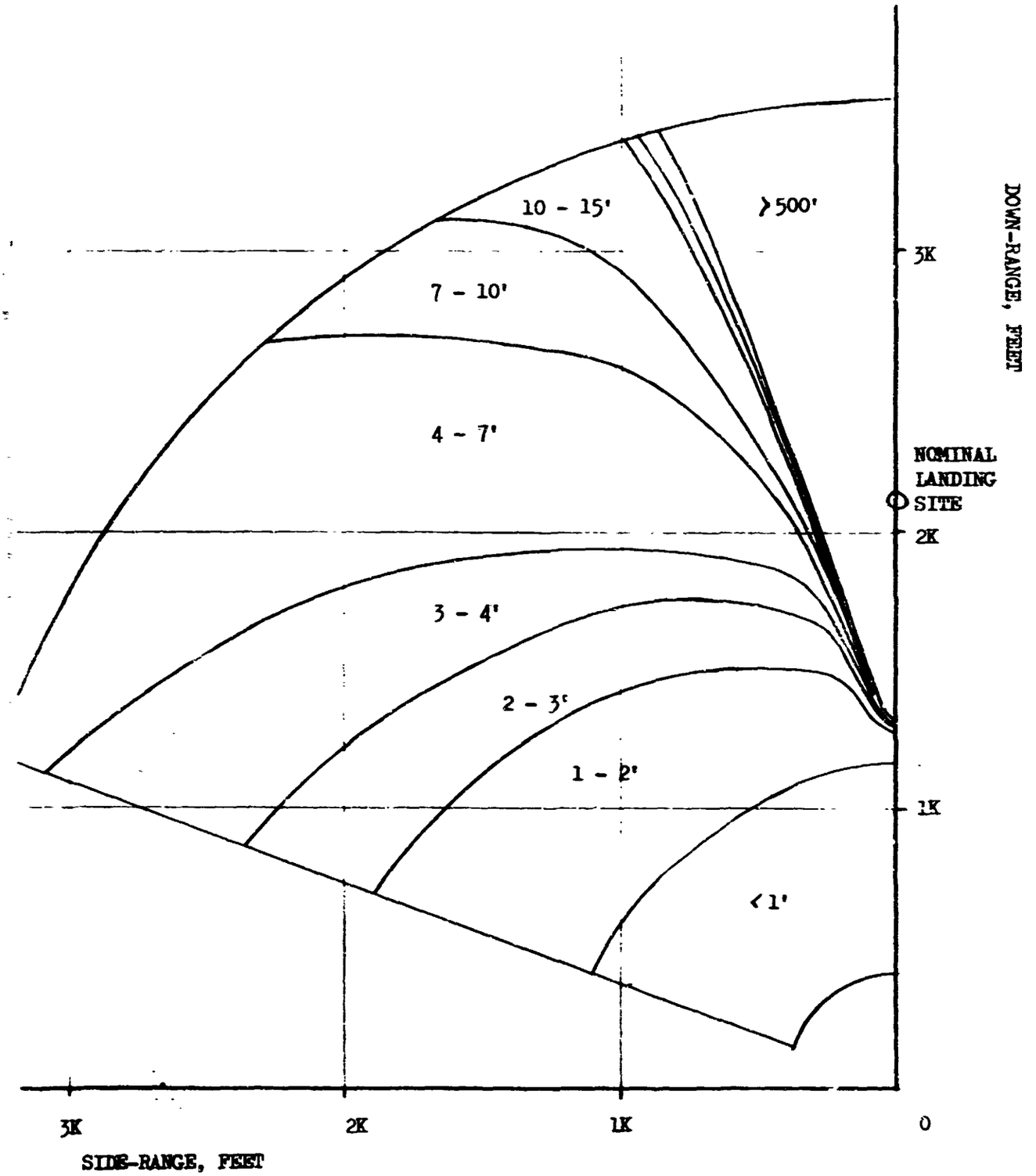

LEM ALTITUDE = 500 FEET

SUN ELEVATION 20°

CRATER VISIBILITY CONTOUR LINES

FIGURE 14

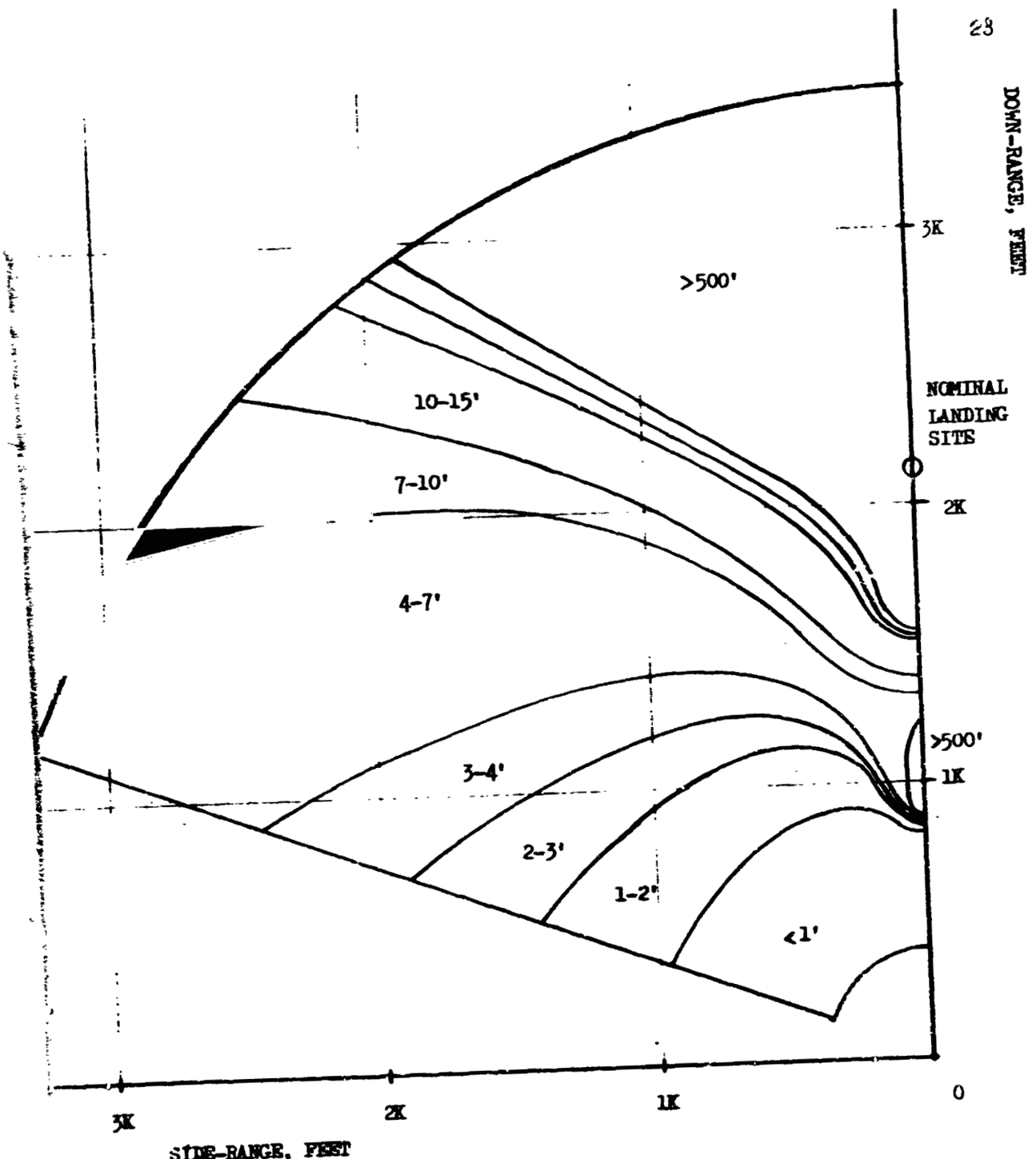

LEM ALTITUDE = 500 FEET

SUN ELEVATION 30°

CRATER VISIBILITY CONTOUR LINES

FIGURE 15

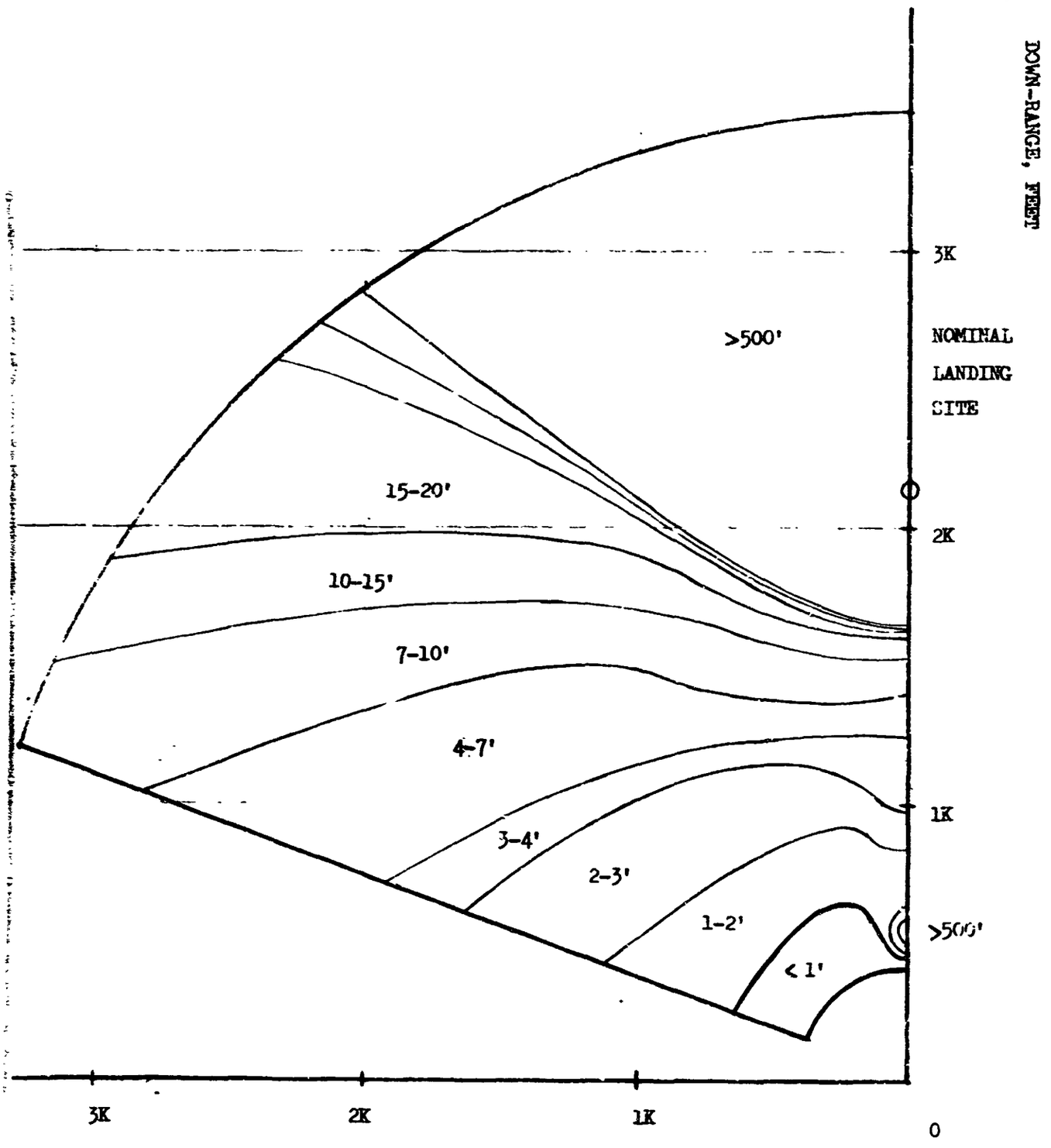

LEM ALTITUDE = 500 FEET

SUN ELEVATION 45°

CRATER VISIBILITY CONTOUR LINES

FIGURE 16

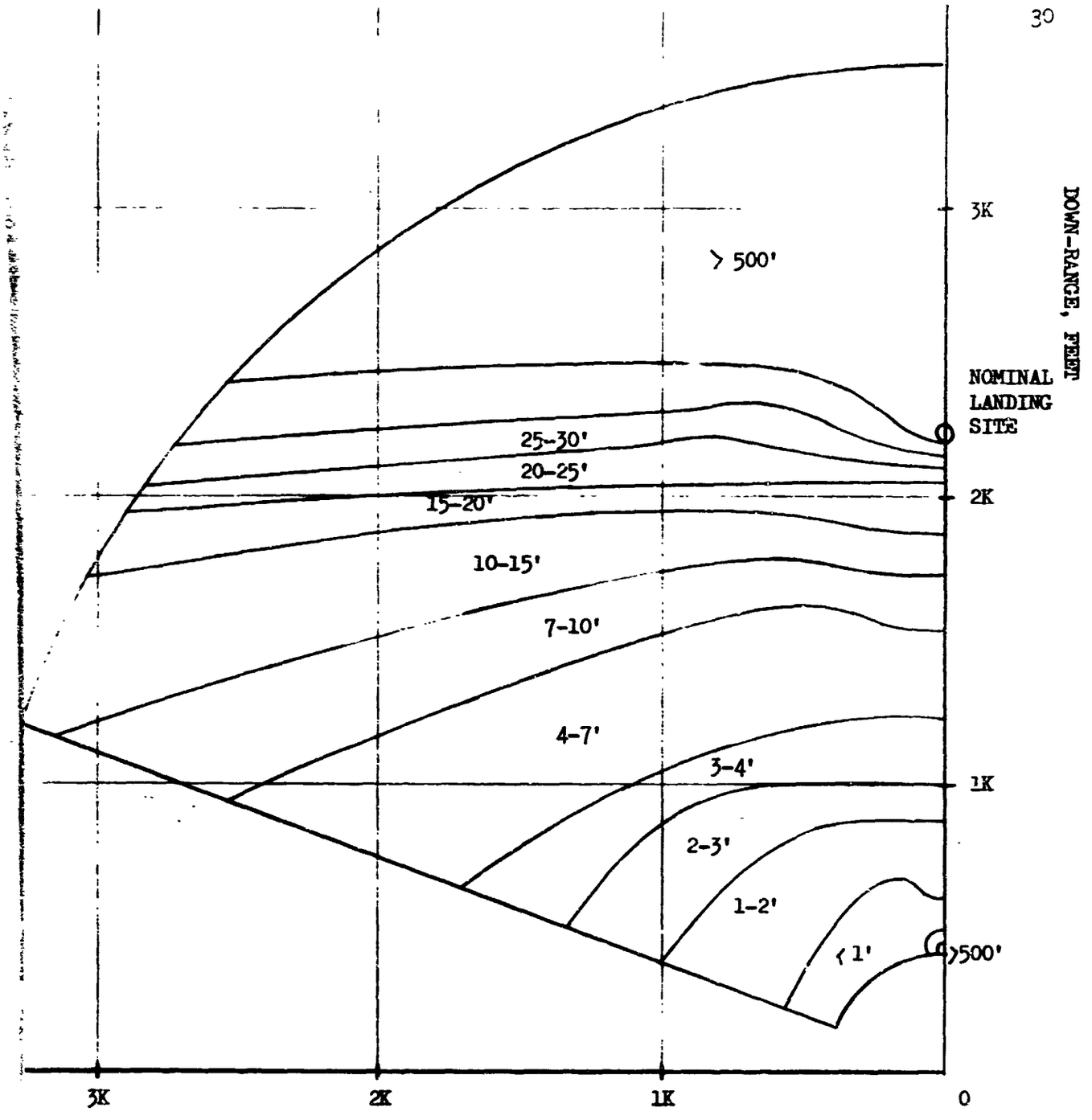

LEM ALTITUDE = 500FEET

SUN ELEVATION 60°

CRATER VISIBILITY CONTOUR LINES

FIGURE 17

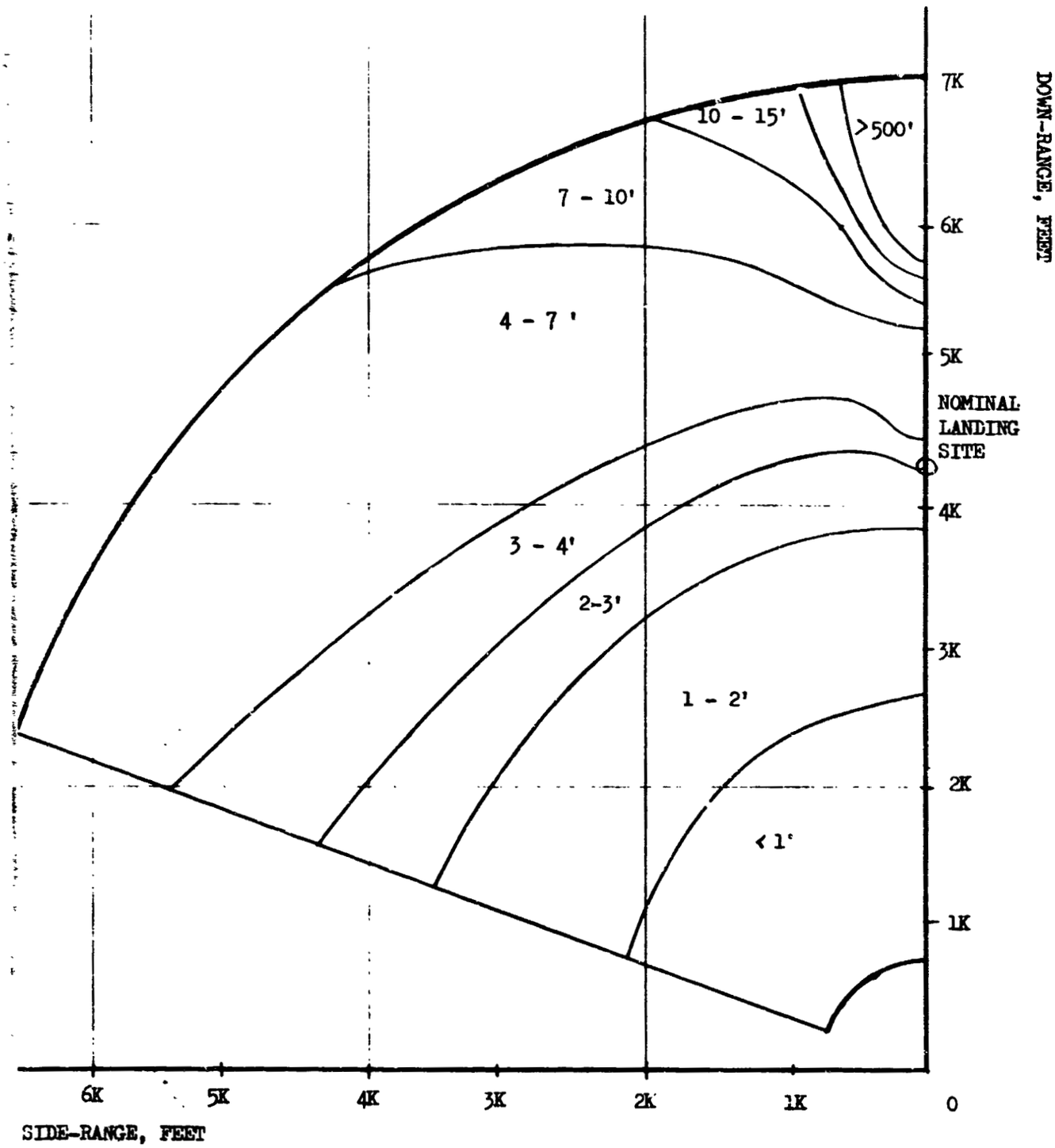

LEM ALTITUDE = 1000 FEET
SUN ELEVATION 10°

CRATER VISIBILITY CONTOUR LINES

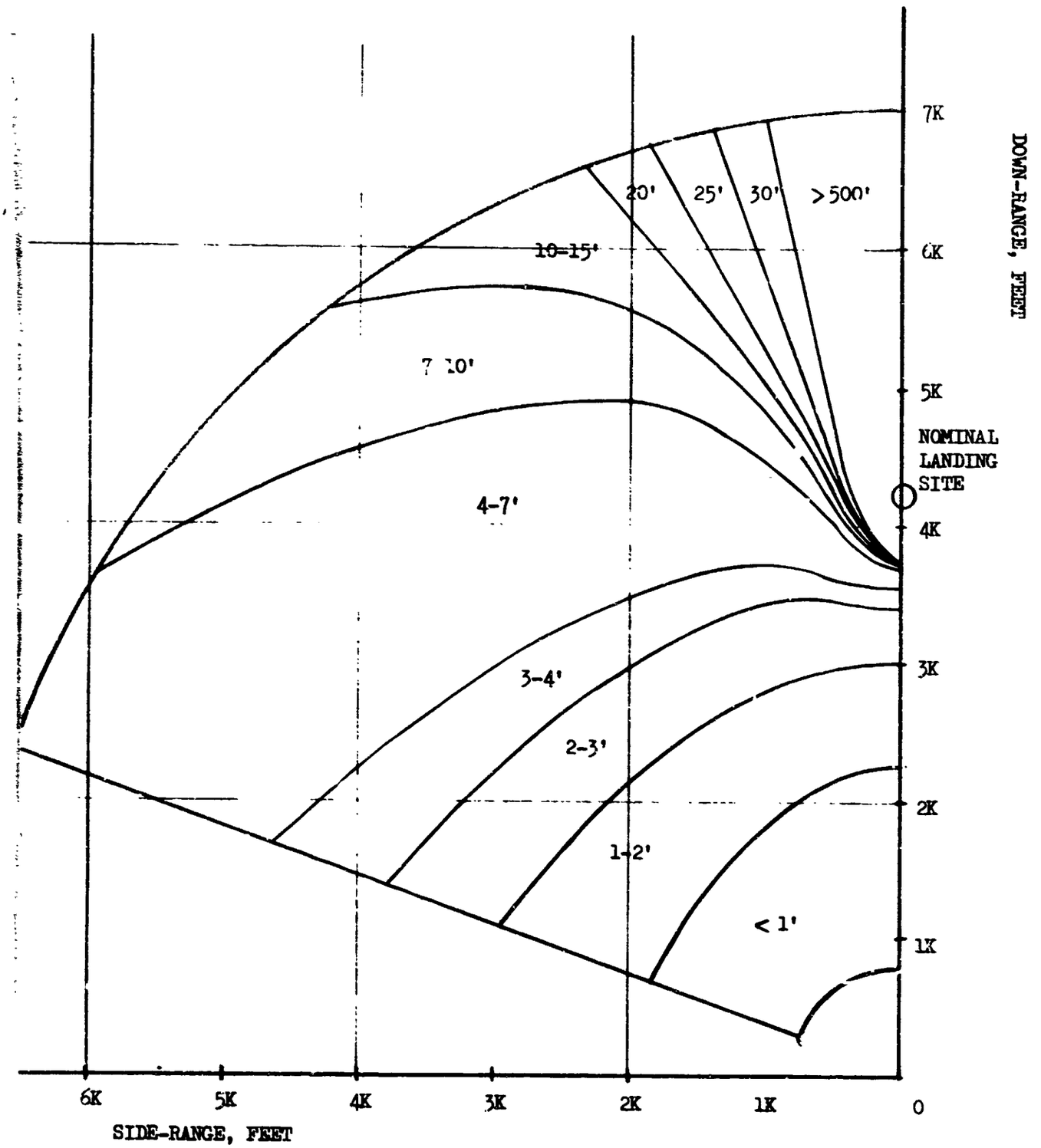

LEM ALTITUDE = 1000 FEET

SUN ELEVATION 15°

CRATER VISIBILITY CONTOUR LINES

FIGURE 19

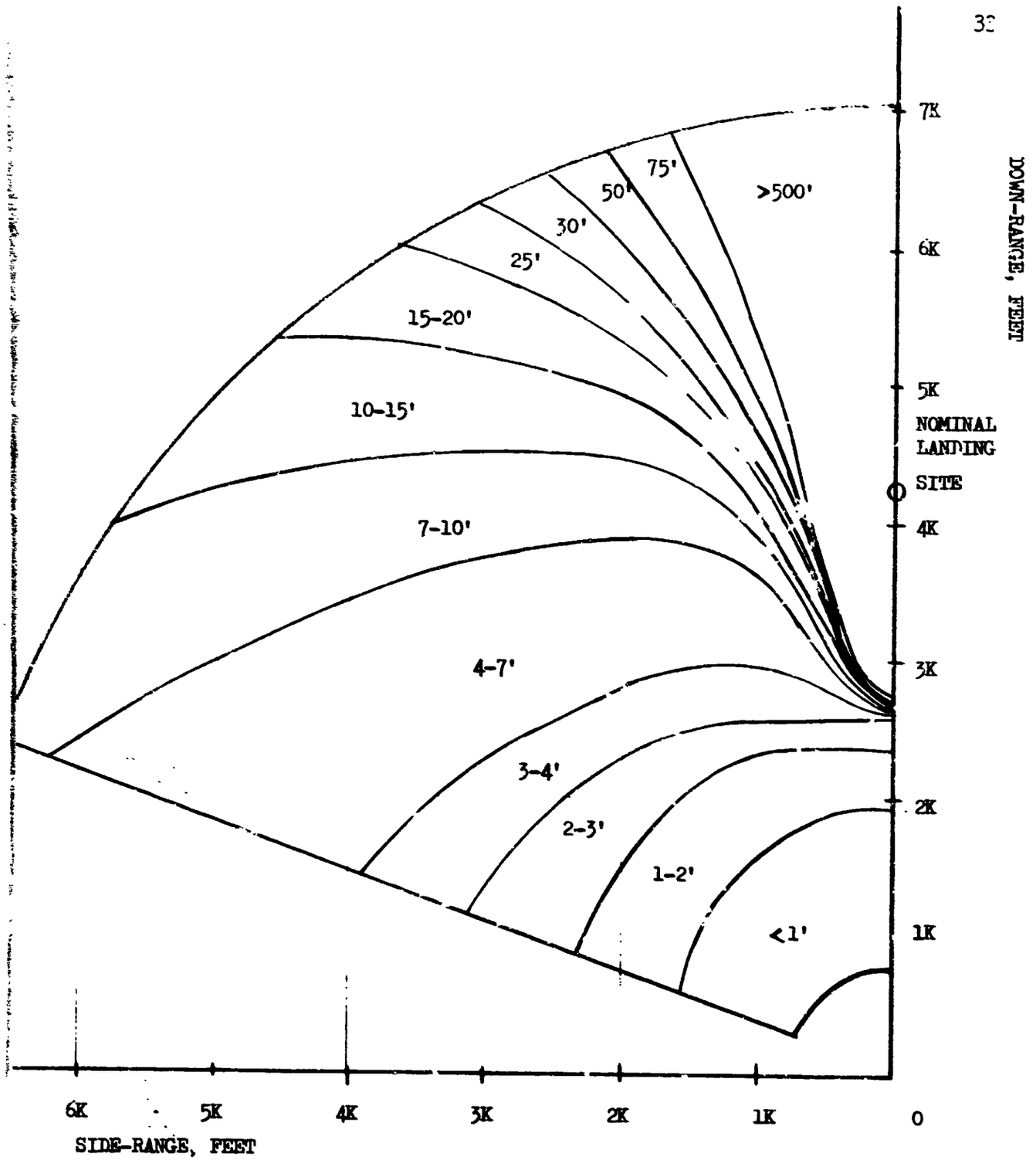

LEM ALTITUDE = 1000 FEET

SUN ELEVATION 20°

CRATER VISIBILITY CONTOUR LINES

FIGURE 20

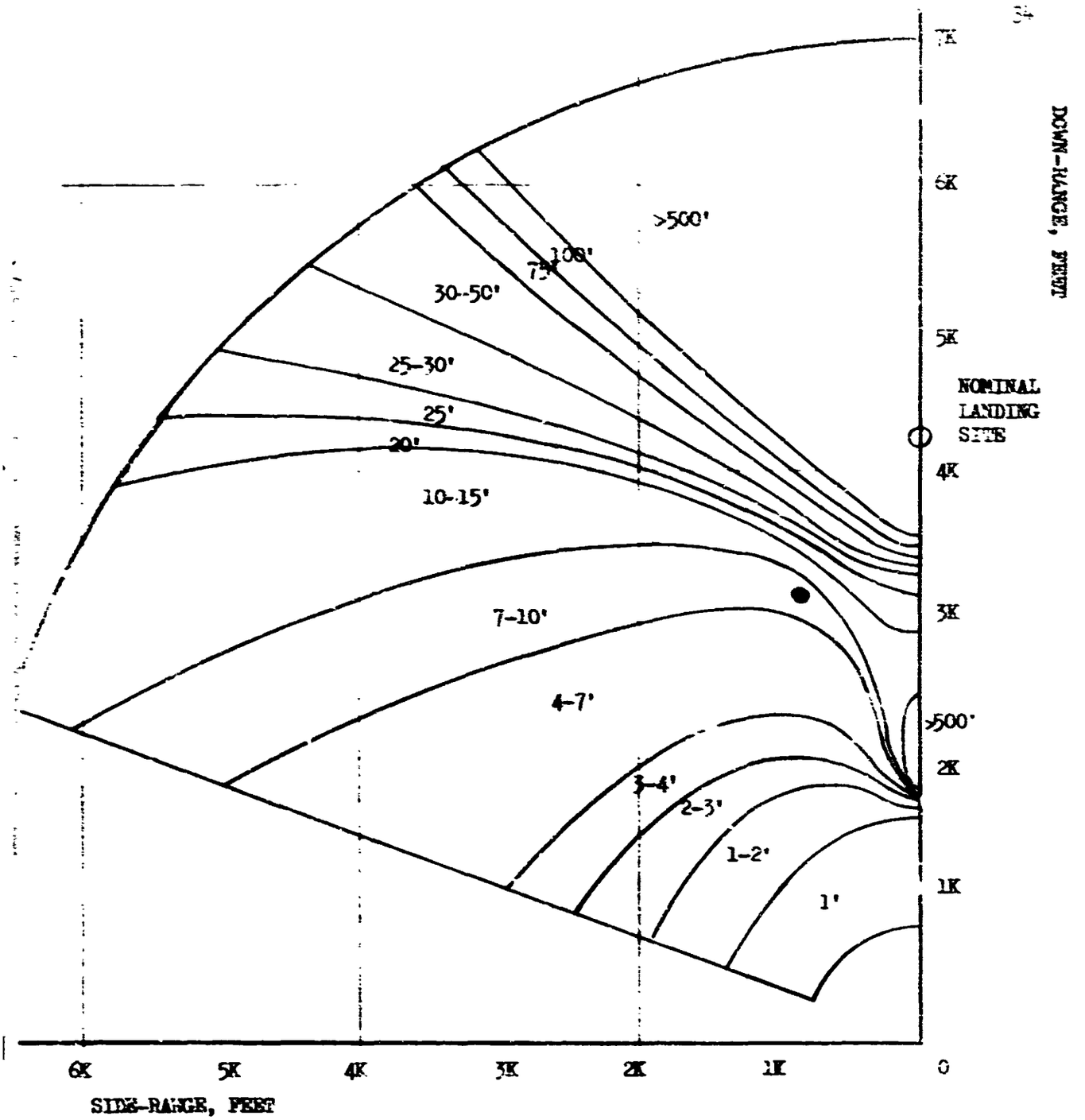

LEM ALTITUDE = 1000 FEET

SUN ELEVATION 30°

CRATER VISIBILITY CONTOUR LINES

FIGURE 21

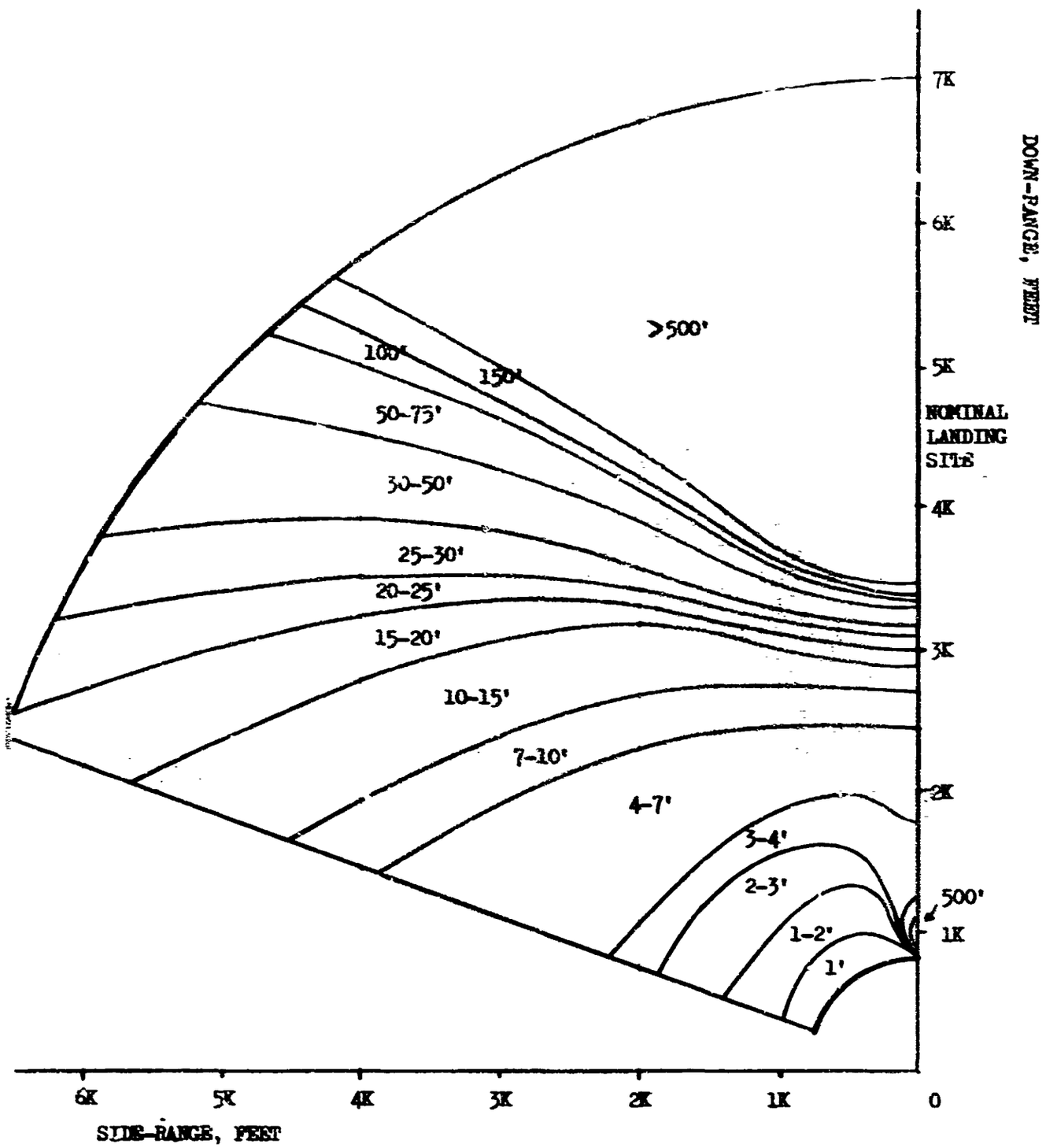

LEM ALTITUDE = 1000 FEET

SUN ELEVATION 45°

CARTER VISIBILITY CONTOUR LINES

FIGURE 22

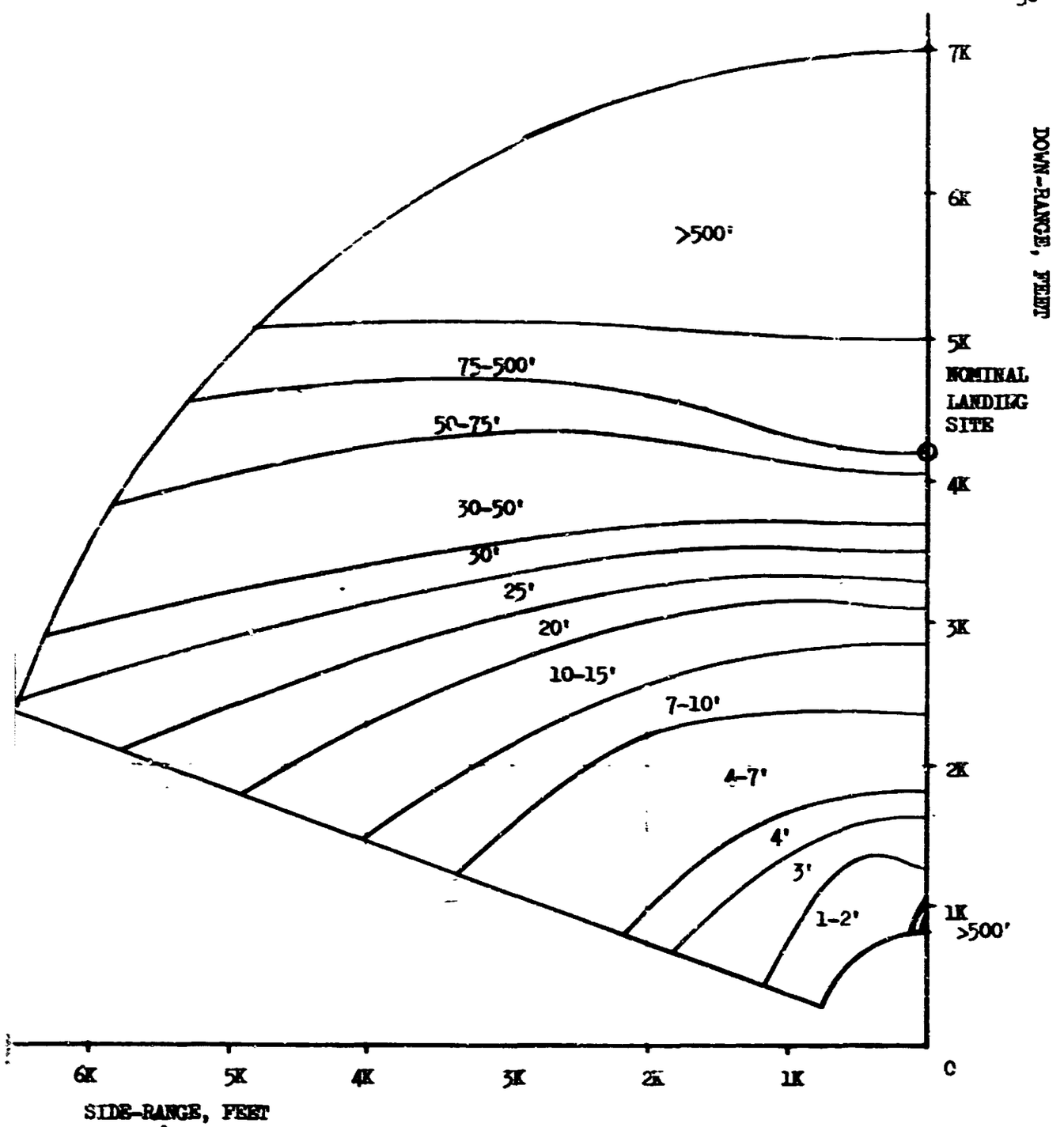

LEM ALTITUDE = 1000 FEET

SUN ELEVATION 60°

CARTER VISIBILITY CONTOUR LINES

FIGURE 23

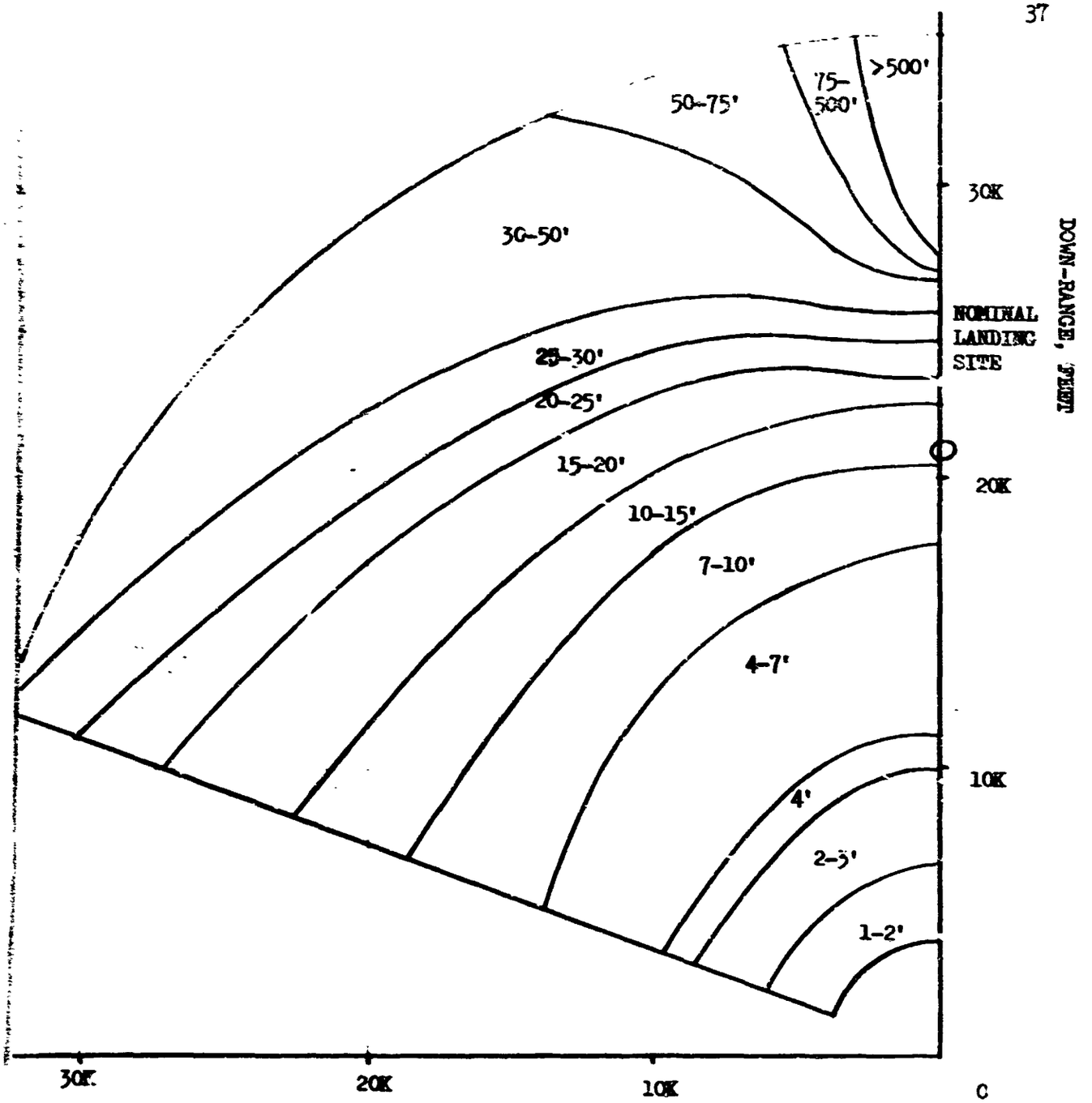

LEM ALTITUDE - 5000 FEET

SUN ELEVATION 10°

CRATER VISIBILITY CONTOUR LINES

FIGURE 24

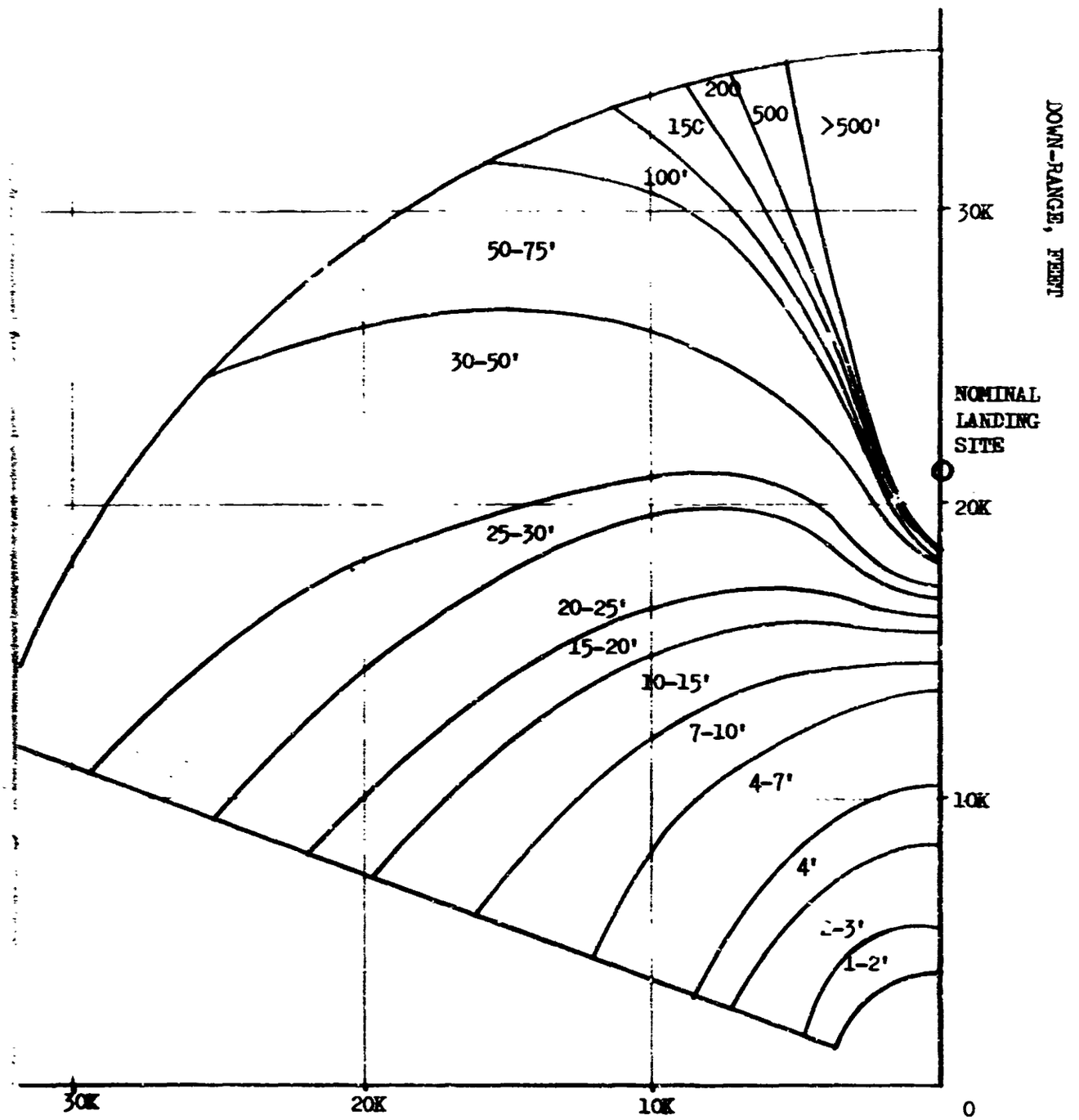

LEM ALTITUDE = 5000 FEET

SUN ELEVATION 15°

CRATER VISIBILITY CONTOUR LINES

FIGURE 25

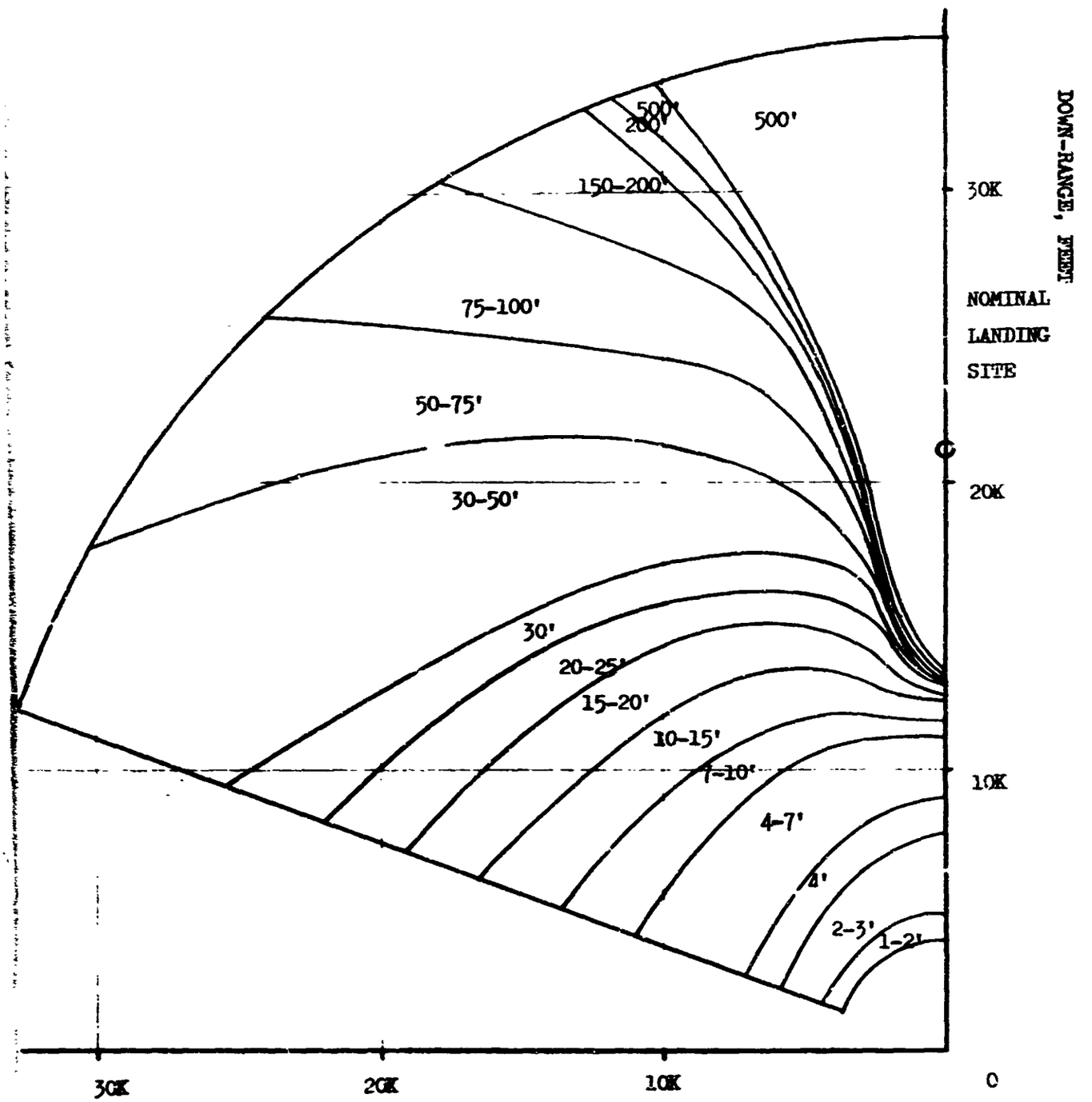

LEM ALTITUDE = 5000 FEET

SUN ELEVATION 20°

CRATER VISIBILITY CONTOUR LINES

FIGURE 26

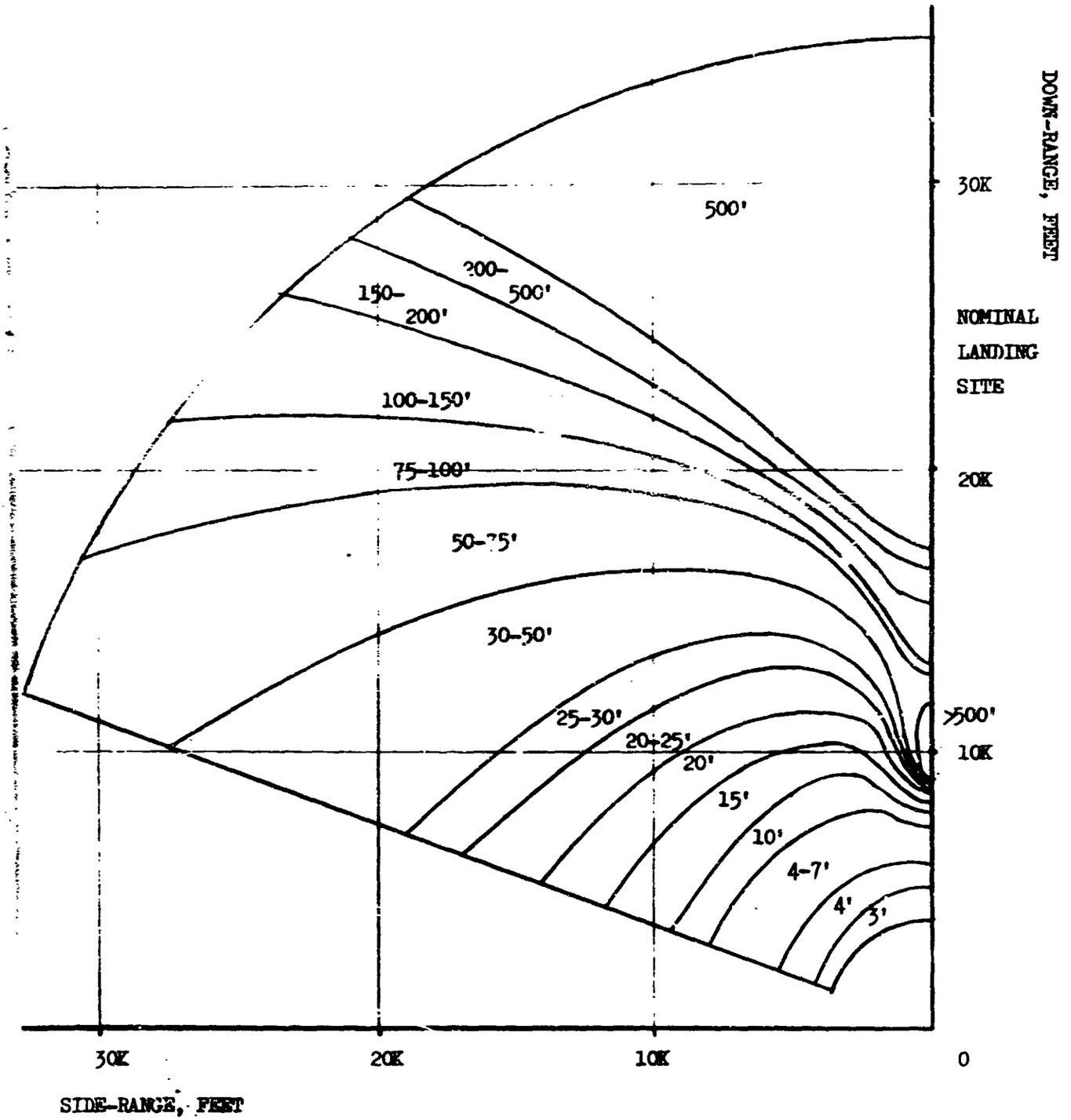

LEM ALTITUDE = 5000 FEET

SUN ELEVATION 30°

CRATER VISIBILITY CONTOUR LINES

FIGURE 47

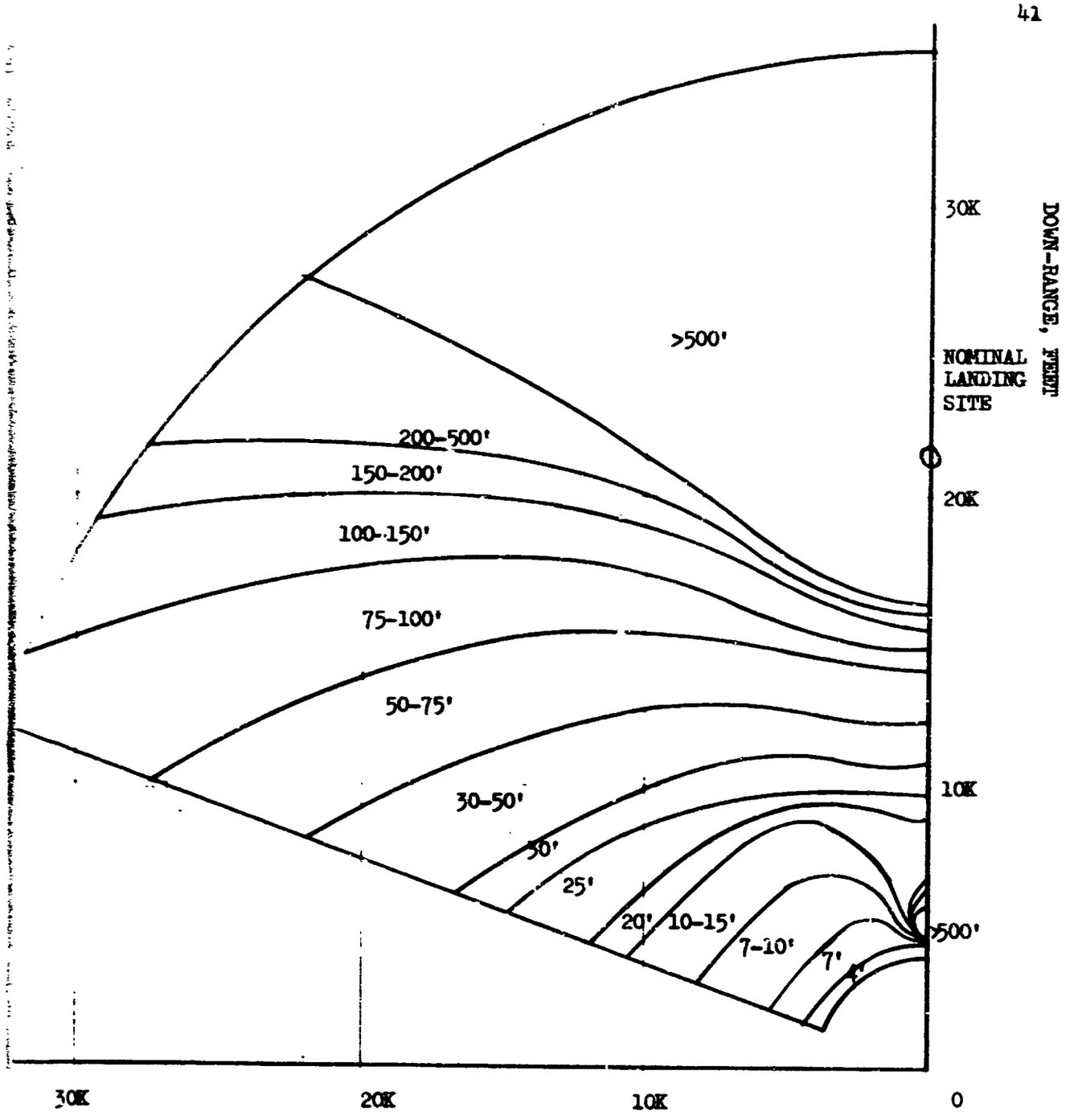

LEM ALTITUDE = 5000 FEET

SUN ELEVATION 45°

CRATER VISIBILITY CONTOUR LINES

FIGURE 28

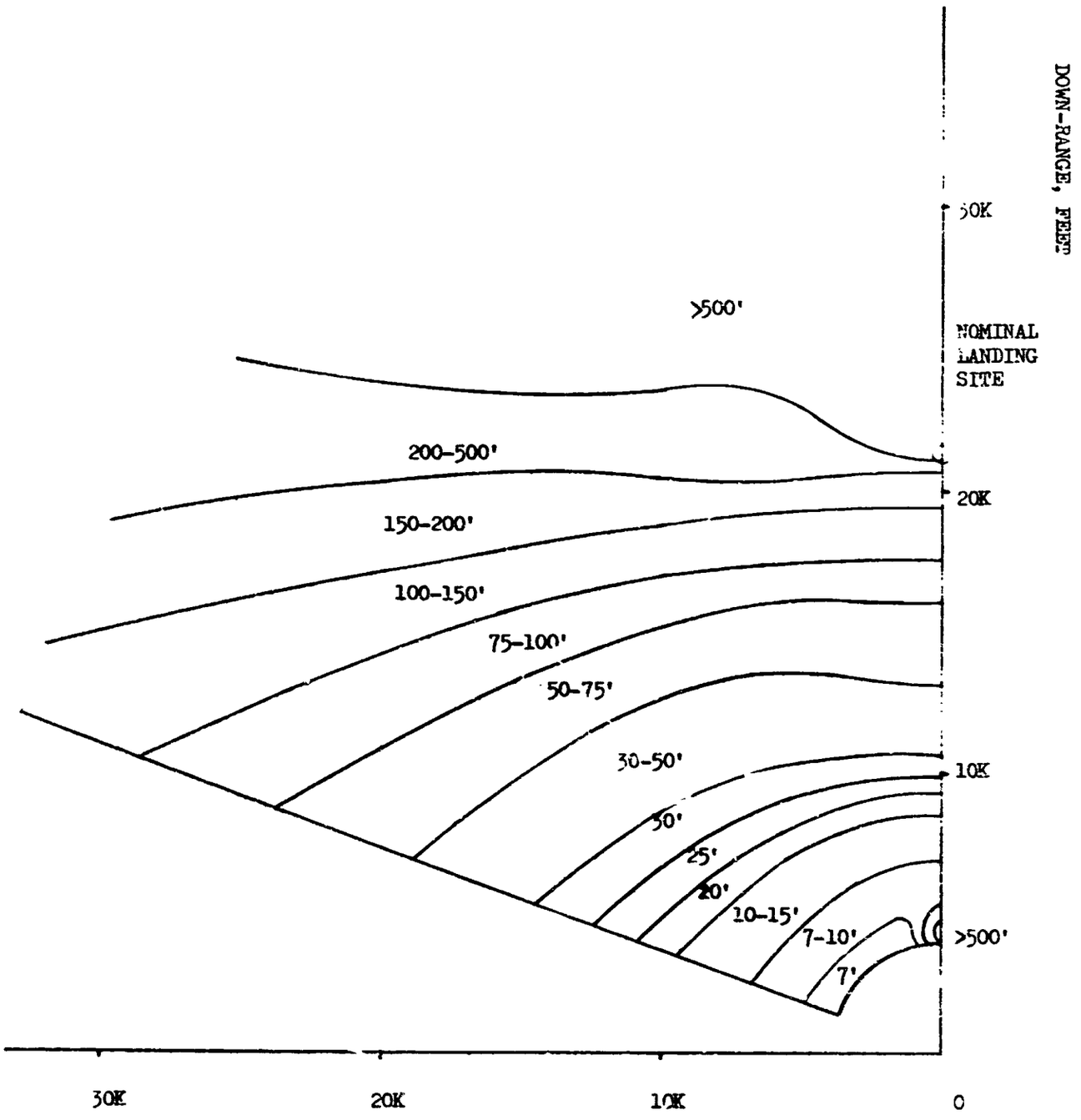

LEM ALTITUDE- 5000 FEET

SUN ELEVATION 60°

CRATER VISIBILITY CONTOUR LINES

FIGURE 29

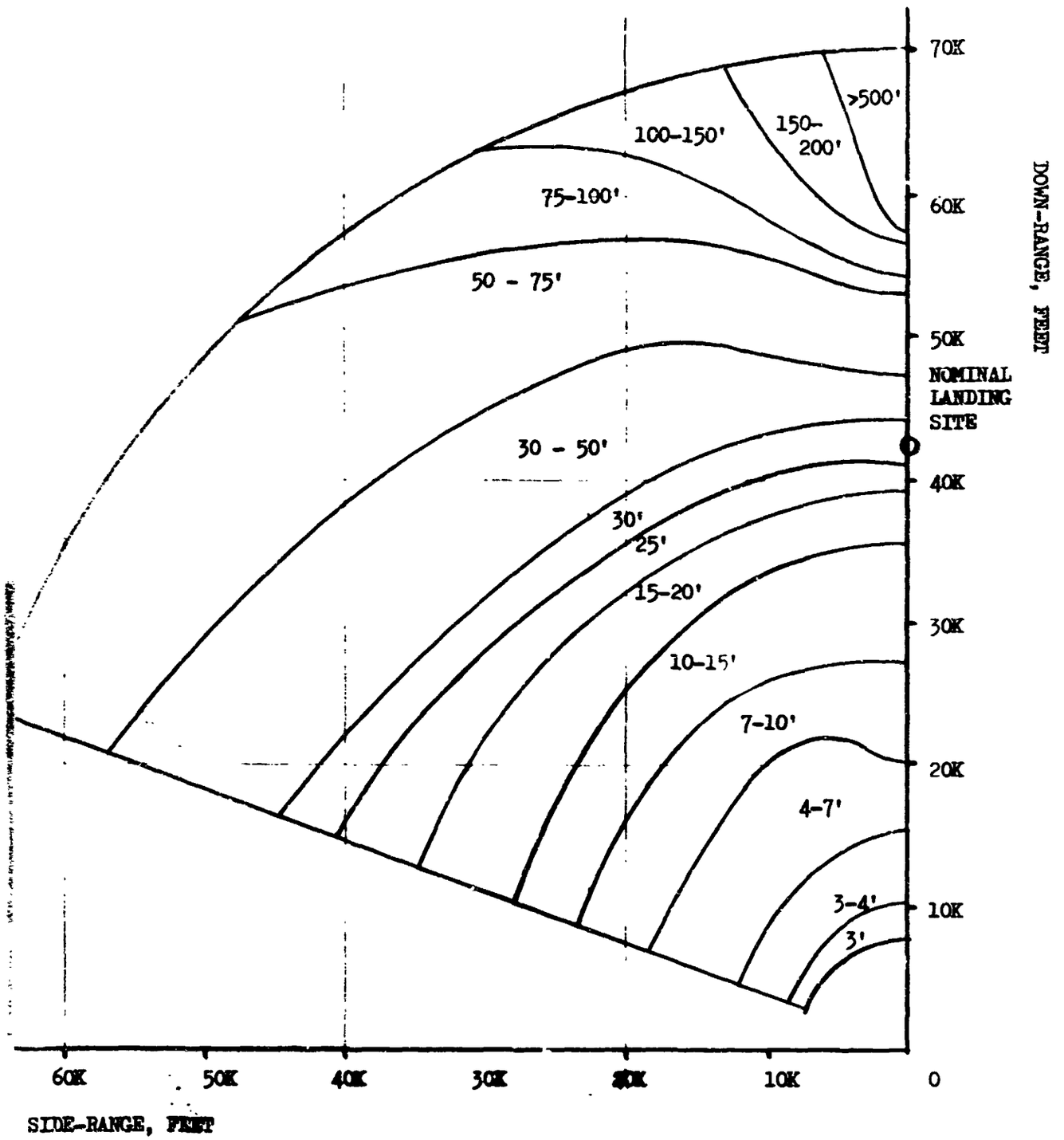

LEM ALTITUDE = 10000 FEET

SUN ELEVATION 10°

CRATER VISIBILITY CONTOUR LINES

FIGURE 30

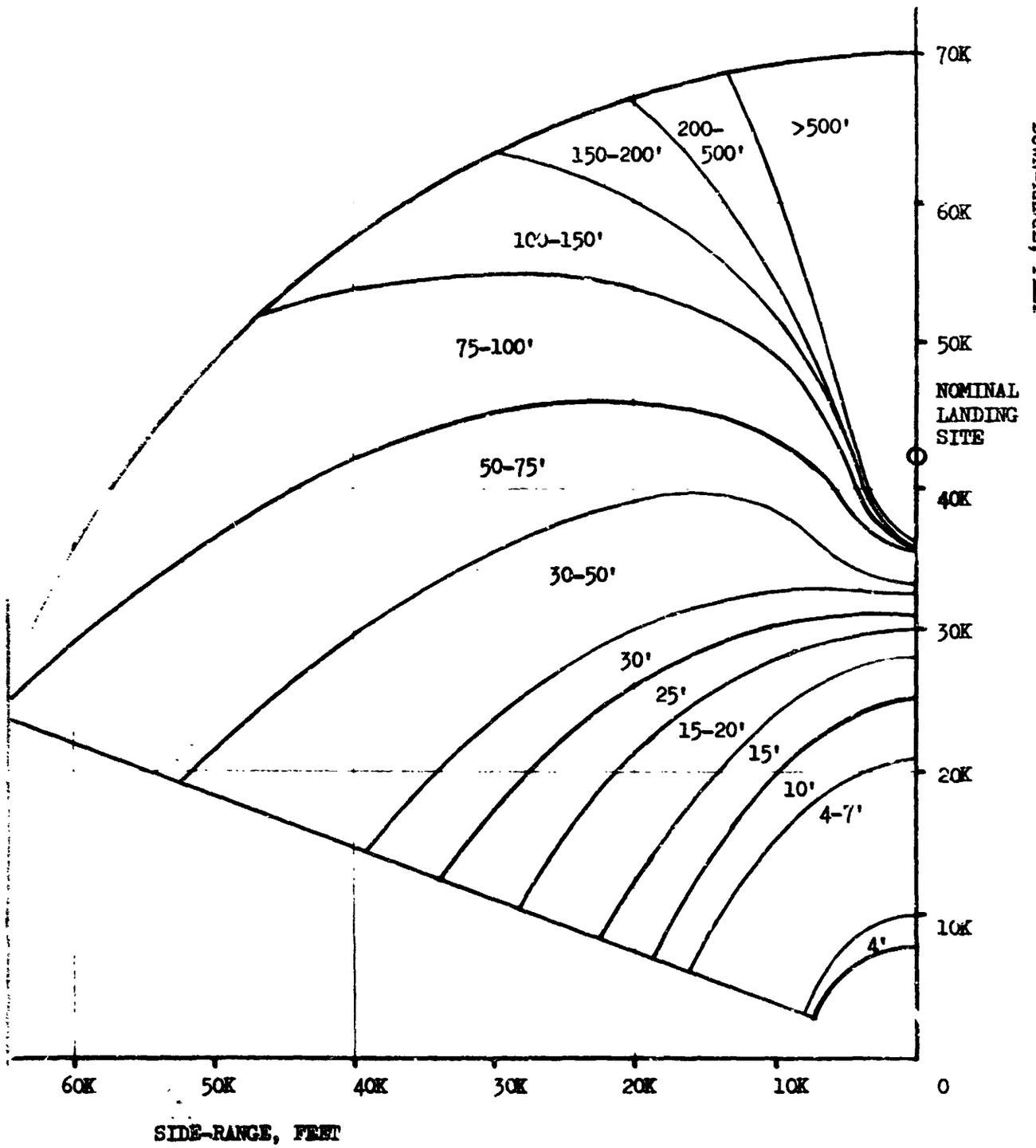

LEM ALTITUDE = 10000 FEET

SUN ELEVATION 15°

CRATER VISIBILITY CONTOUR LINES

FIGURE 31

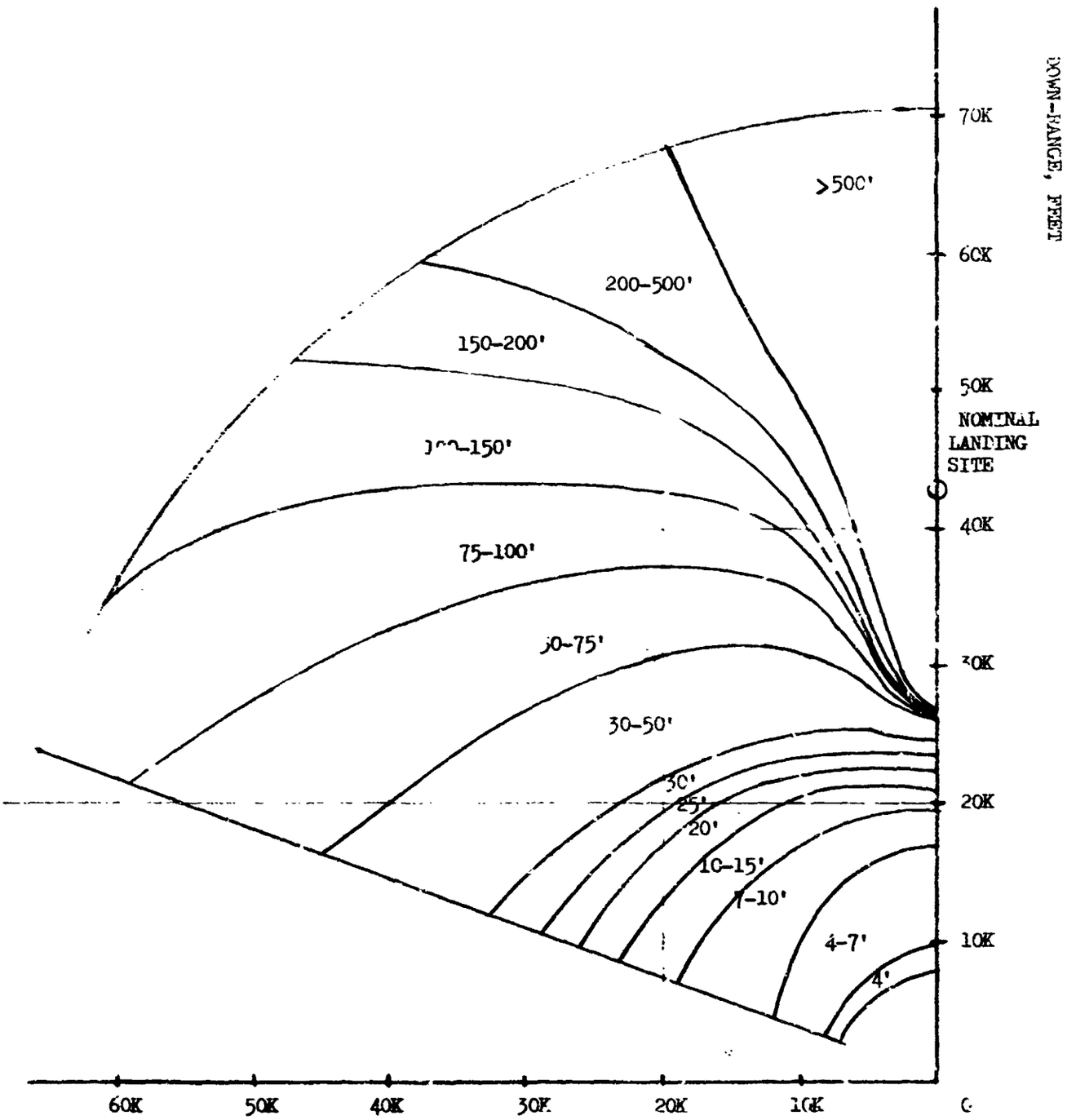

LEM ALTITUDE = 10000 FEET

SUN ELEVATION 20°

CRATER VISIBILITY CONTOUR LINES

FIGURE 32

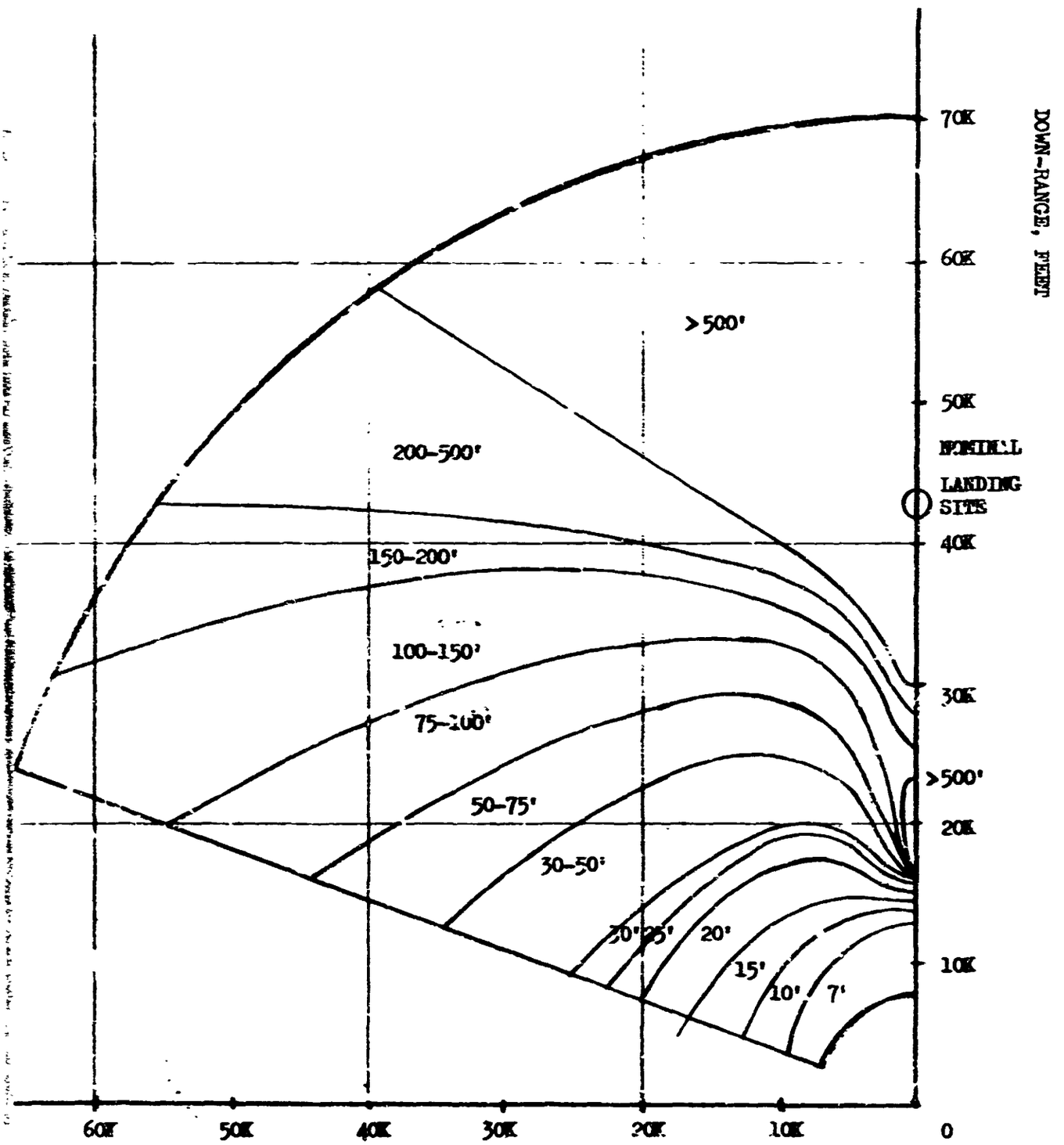

ALTITUDE = 10000 FEET

ELEVATION 30°

VISIBILITY CONTOUR LINES

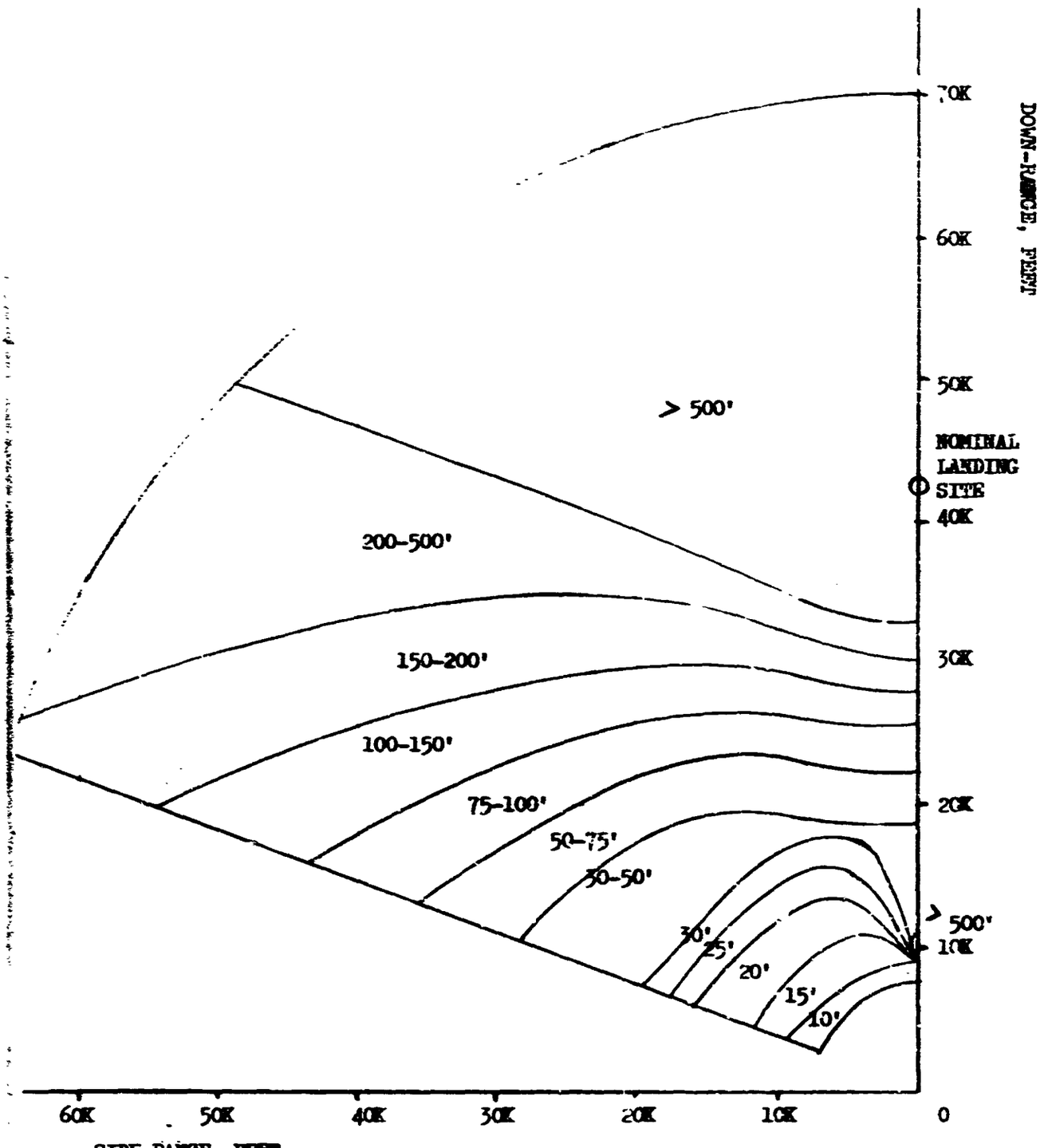

LEM ALTITUDE = 10000 FEET

SUN ELEVATION 45°

CRATER VISIBILITY CONTOUR LINES

FIGURE 34

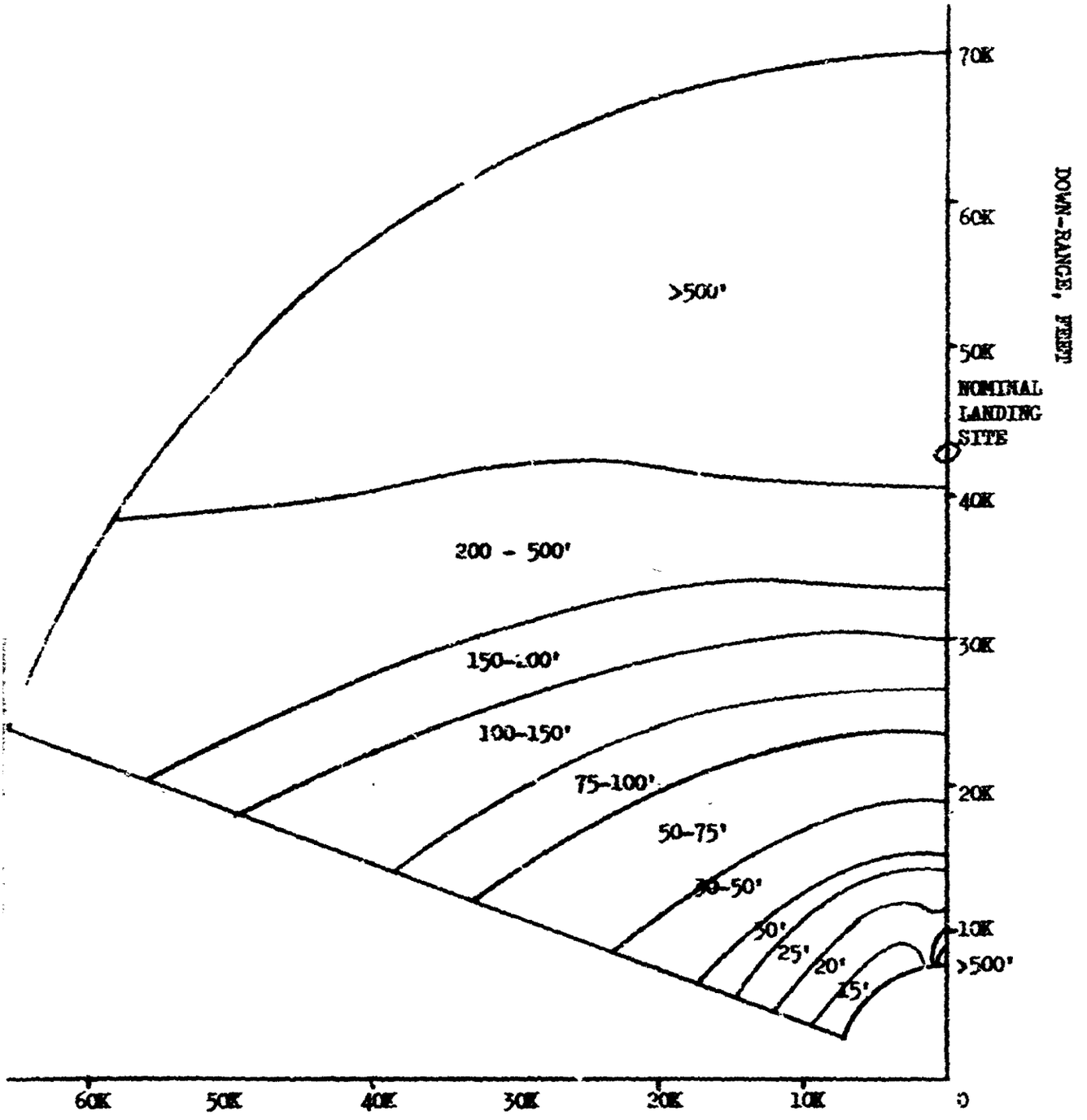

LEM ALTITUDE = 10000 FEET

SUN ELEVATION 60°

CRATER VISIBILITY CONTOUR LINES

FIGURE 35

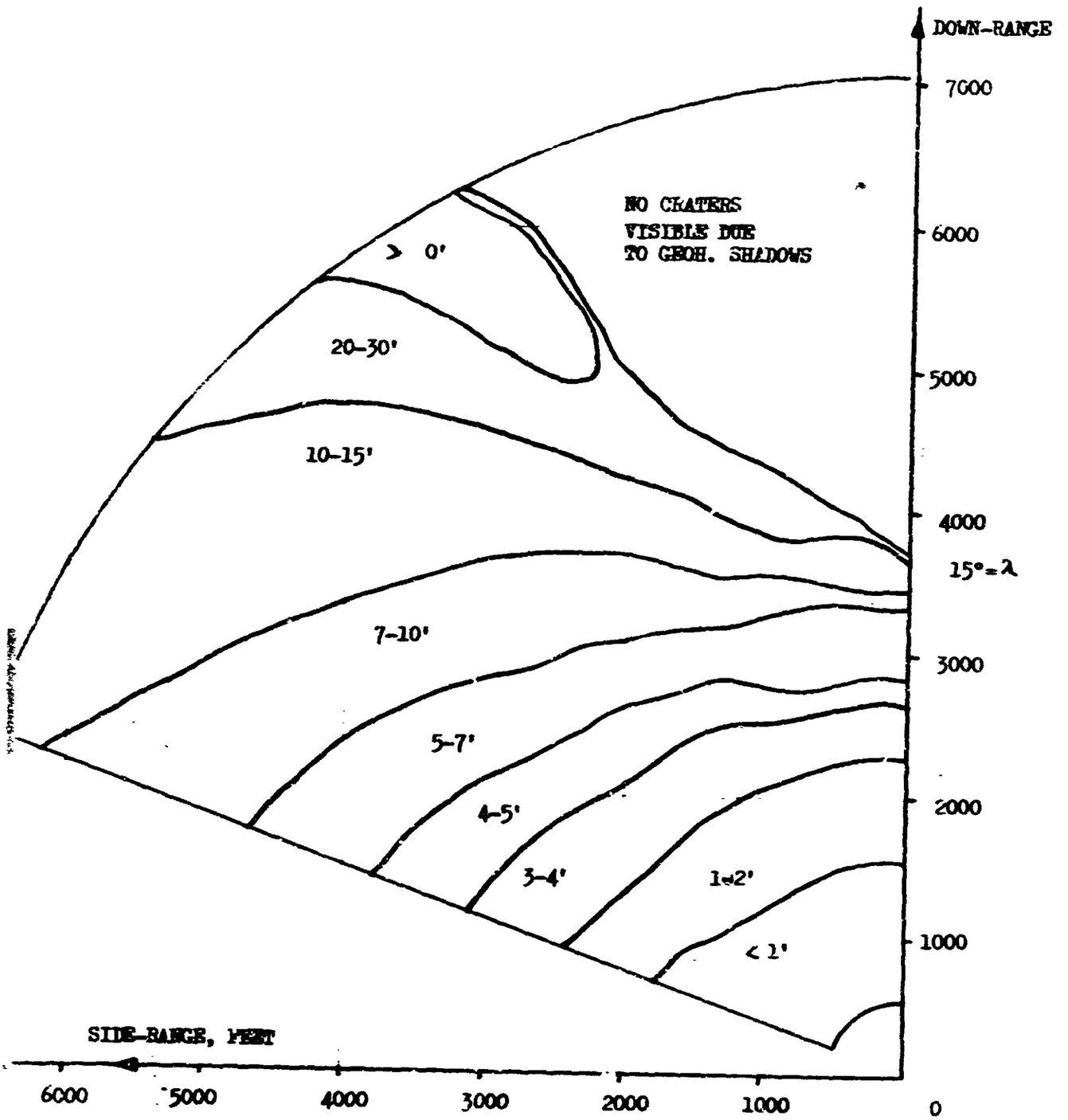

h=1000 ft.

Sun = 15°

GEOMETRIC SHADOW VISIBILITY

FIGURE 36

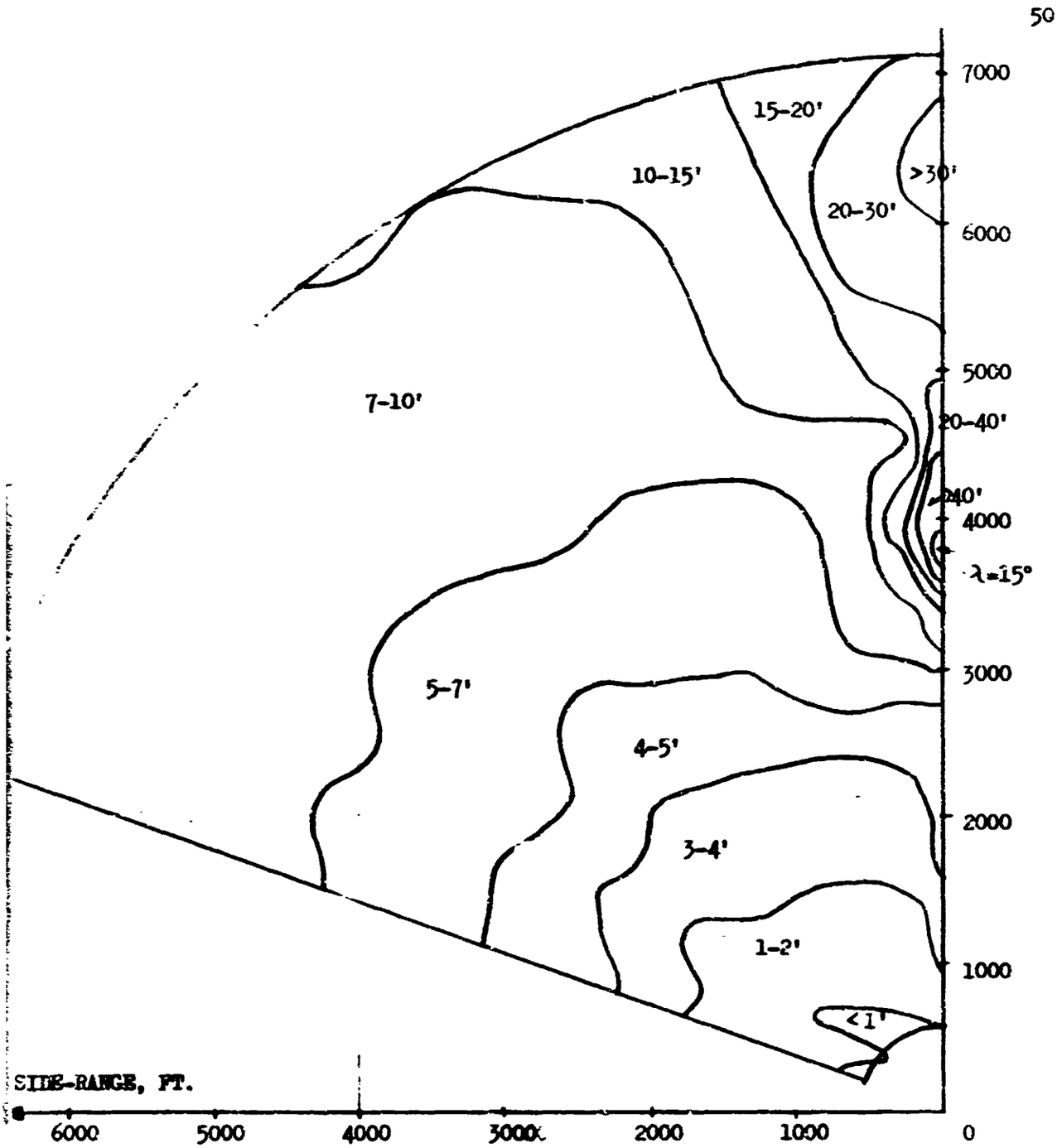

h = 1000 ft.

SUN ∢ = 15°

PHOTOMETRIC SHADOW VISIBILITY

FIGURE 37

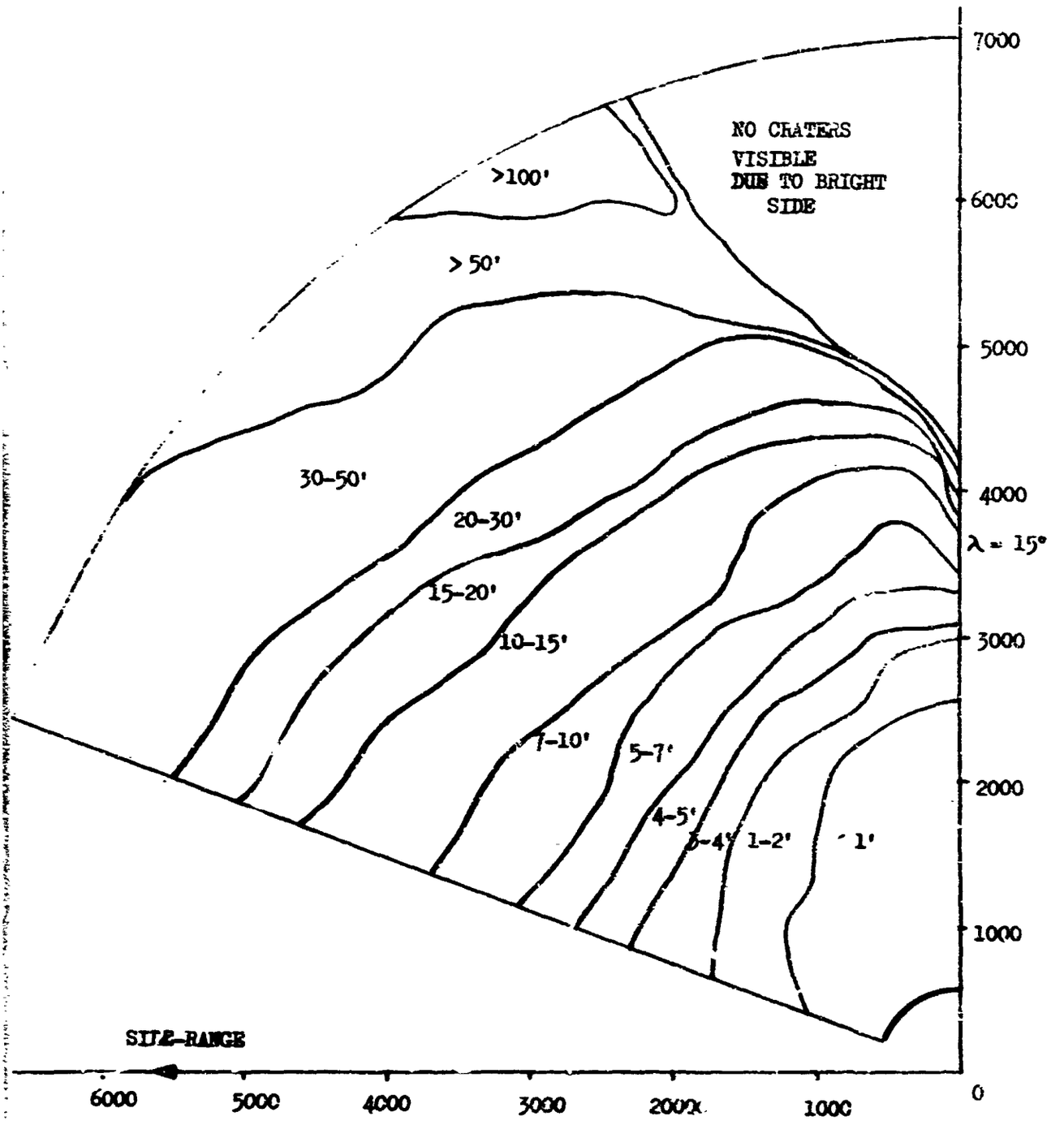

h = 1000 ft.

SUN = 15°

BRIGHT SIDE VISIBILITY

FIGURE 38

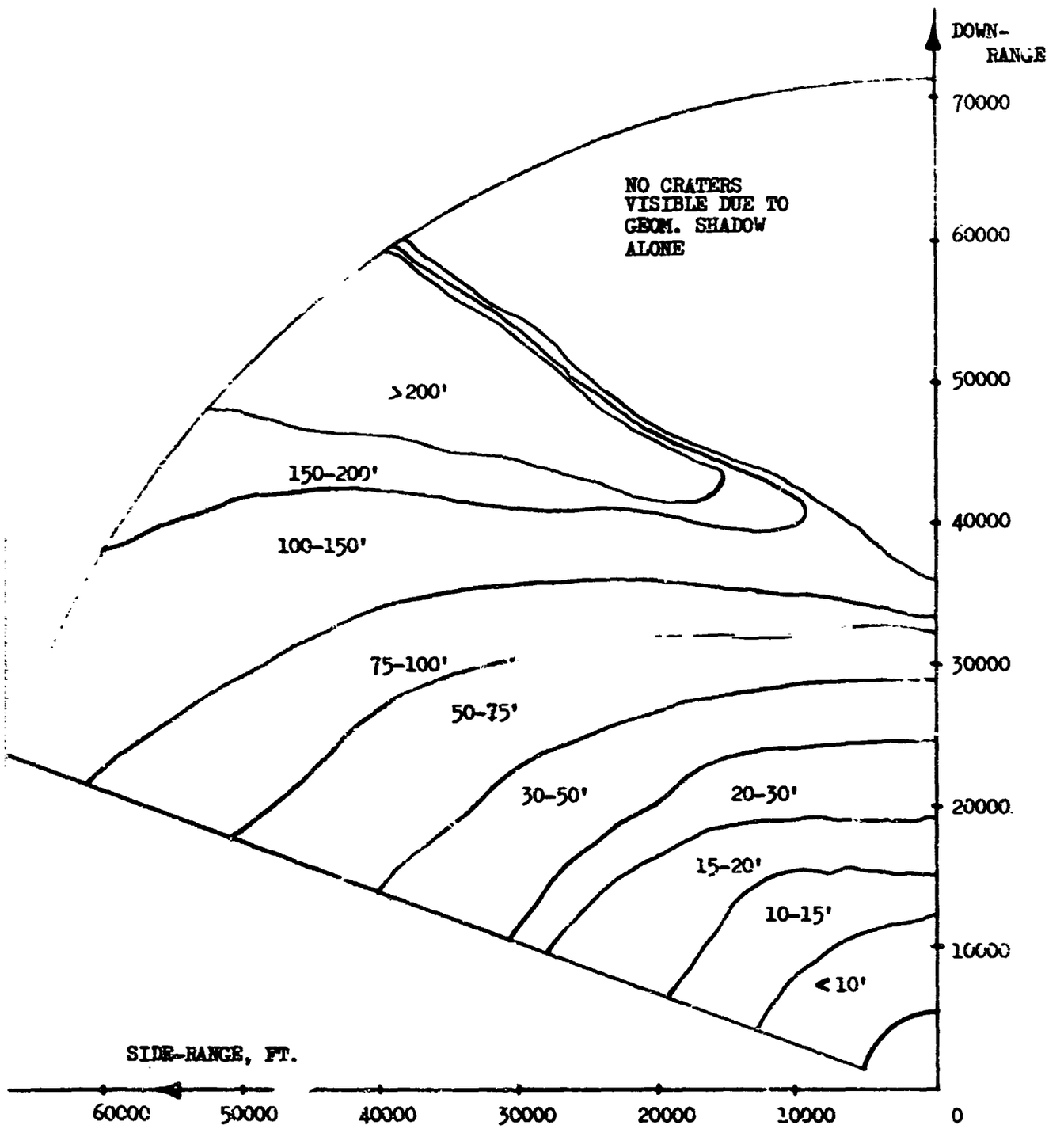

h = 10000 FEET

SD. = 15°

GEOMETRIC SHADOW VISIBILITY

FIGURE 39

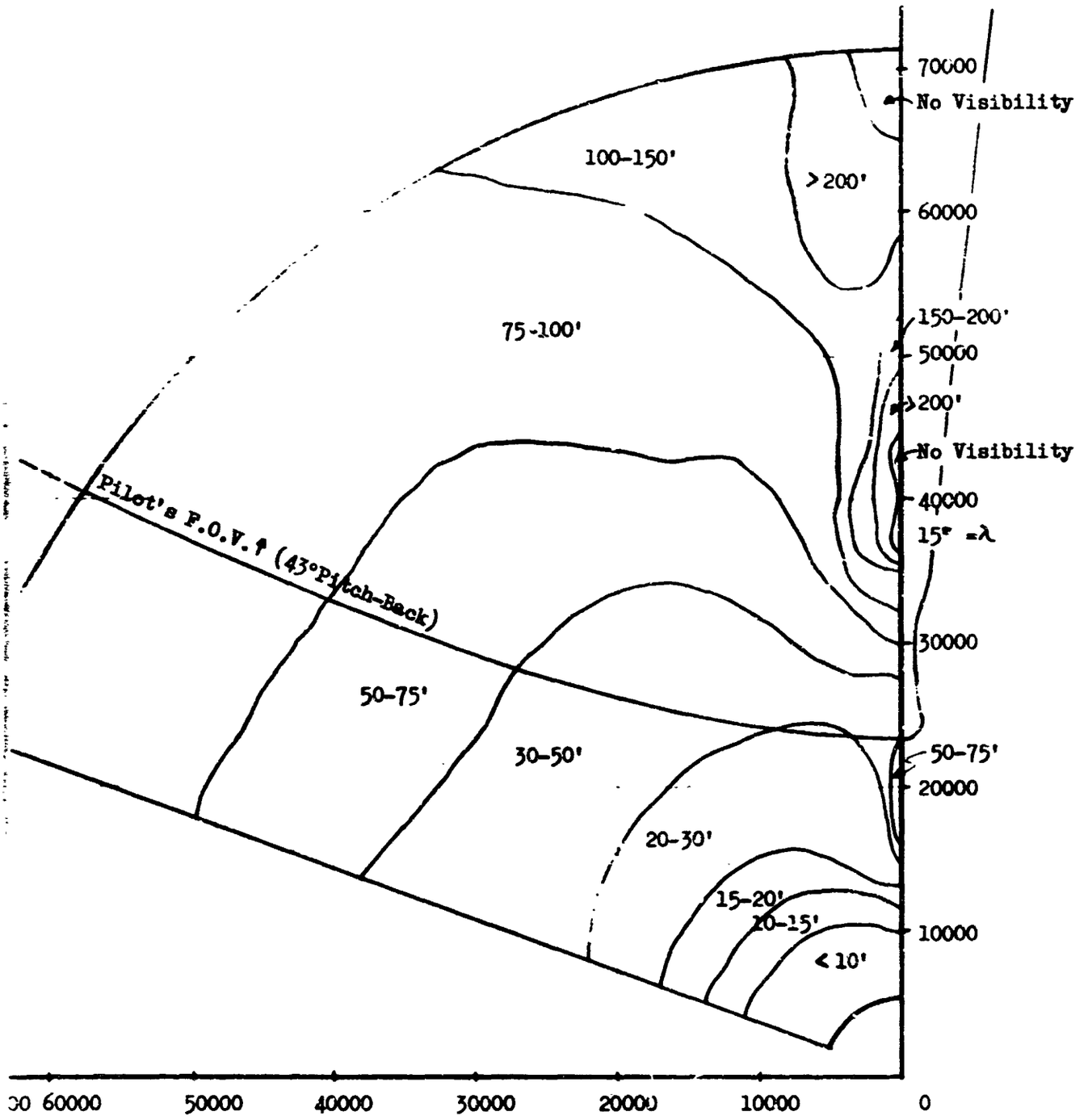

h = 10000 FT.

SUN $\measuredangle$ = 15°

PHOTOMETRIC SHADOW VISIBILITY

FIGURE 40

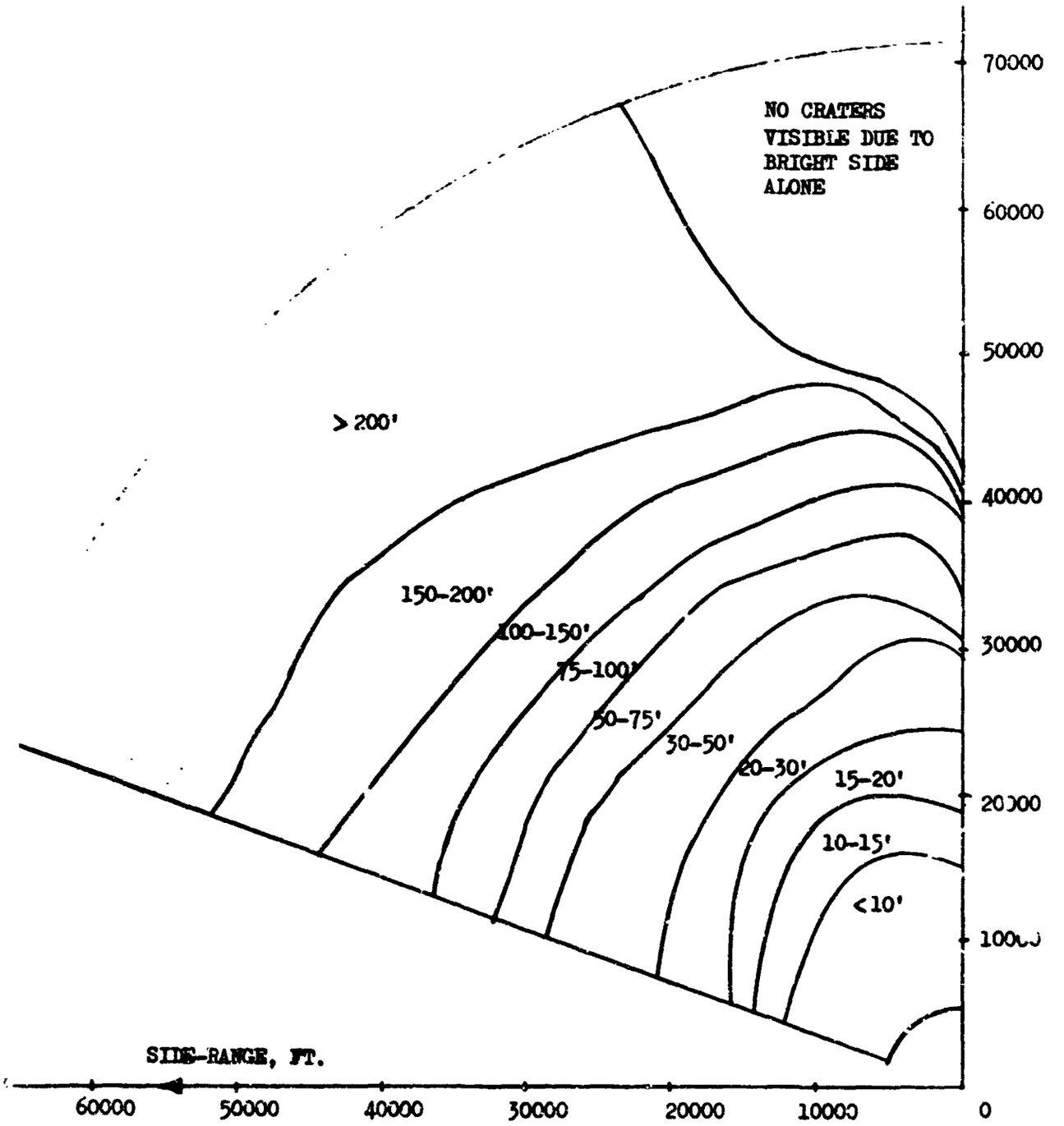

h= 10,000 FEET

SUN Φ = 15°

BRIGHT SIDE VISIBILITY

FIGURE 41

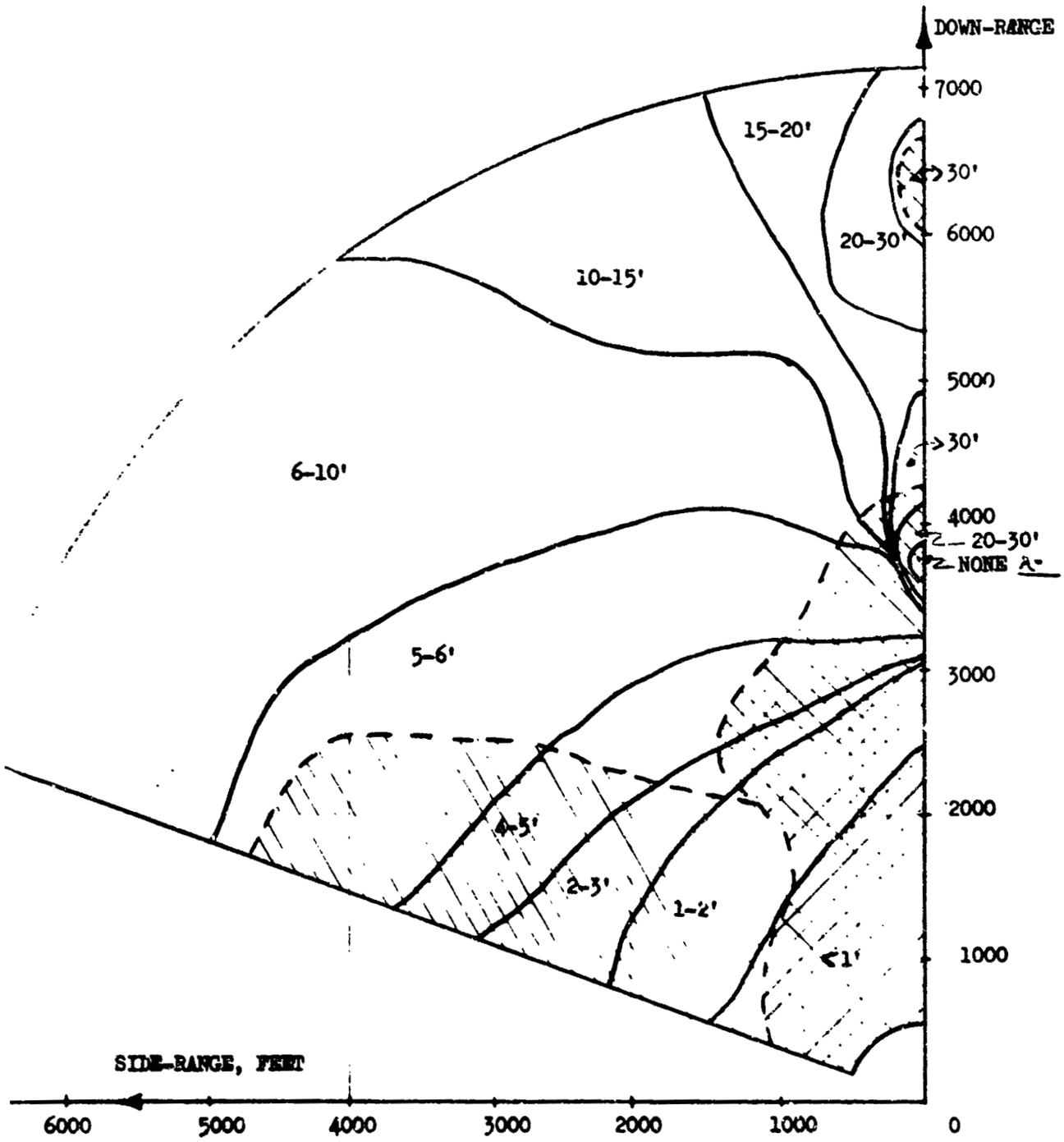

COMBINED VISIBILITY

h = 1000'

SUN = 15°

GEOMETRIC

BRIGHT SIDE

PHOTOMETRIC

FIGURE 42

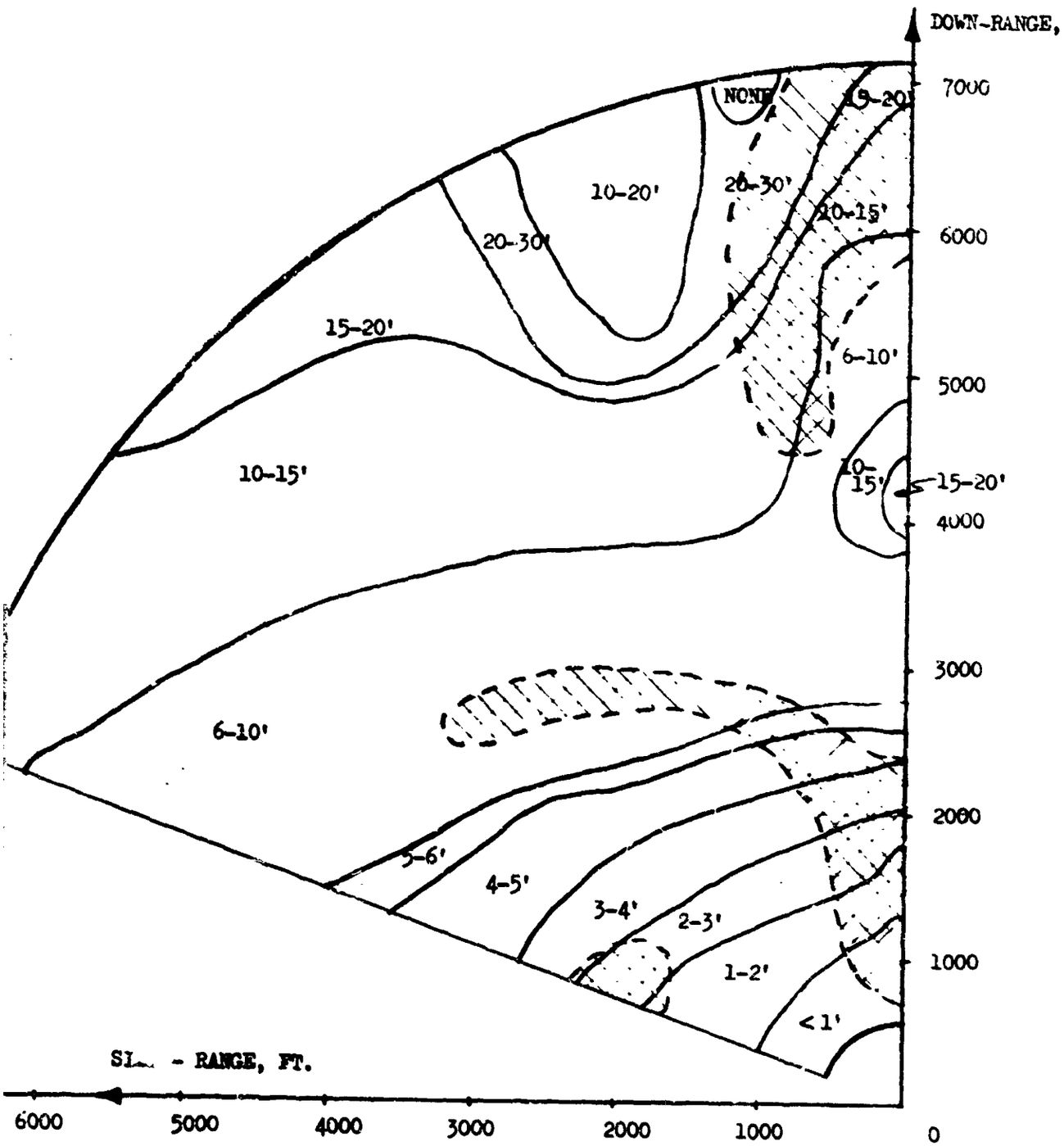

COMBINED VISIBILITY

h = 1000

SUN∠ = 30°

(NO GEOMETRIC SHADOWS)

FIGURE 43

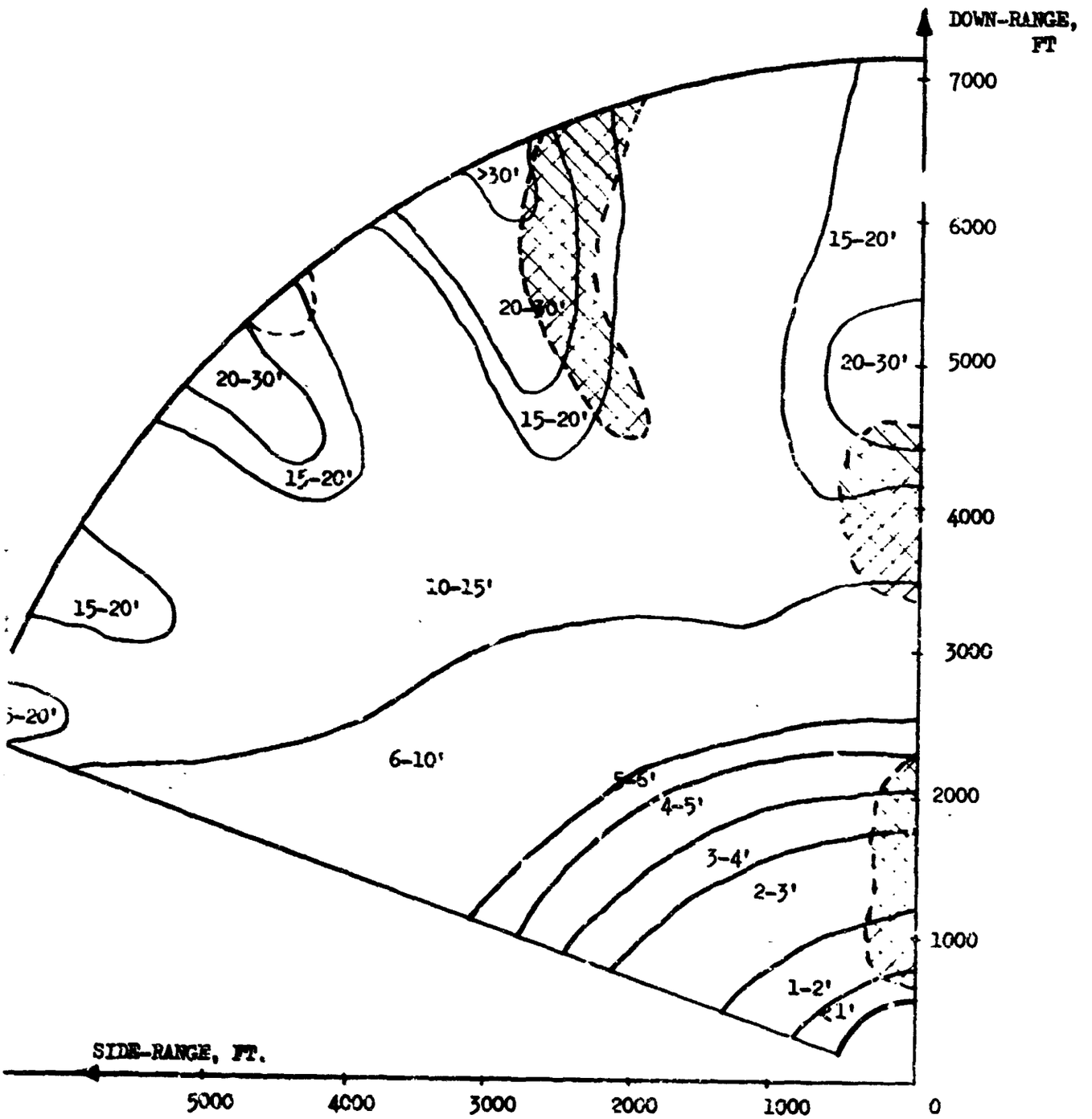

COMBINED VISIBILITY

h = 1000

SUN ∠ = 45°

(NO GEOMETRIC SHADOWS)

FIGURE 44

APPENDIX A

A parallel study was done on craters in sand in order to compare the lunar visibility curves with those we might expect on similar earth terrain. Since a photometric function was not available for sand, a set of laboratory experiments was done to determine one. It was found that sand closely approximates a Lambertian diffuse reflector with the brightness along any OLOS being

$$B' = B_0 (\rho) (a) \cos (90 - \phi) \tag{10}$$

where

B_0 = normal sun brightness, ft-Lamberts
(ρ) = normal albedo of sand, = 0.3
a = atmospheric absorption, = 0.7
ϕ = sun elevation above local horizontal plane

A set of curves, similar in form to those of the lunar case, were plotted and can be seen in Figures A1 - A6.

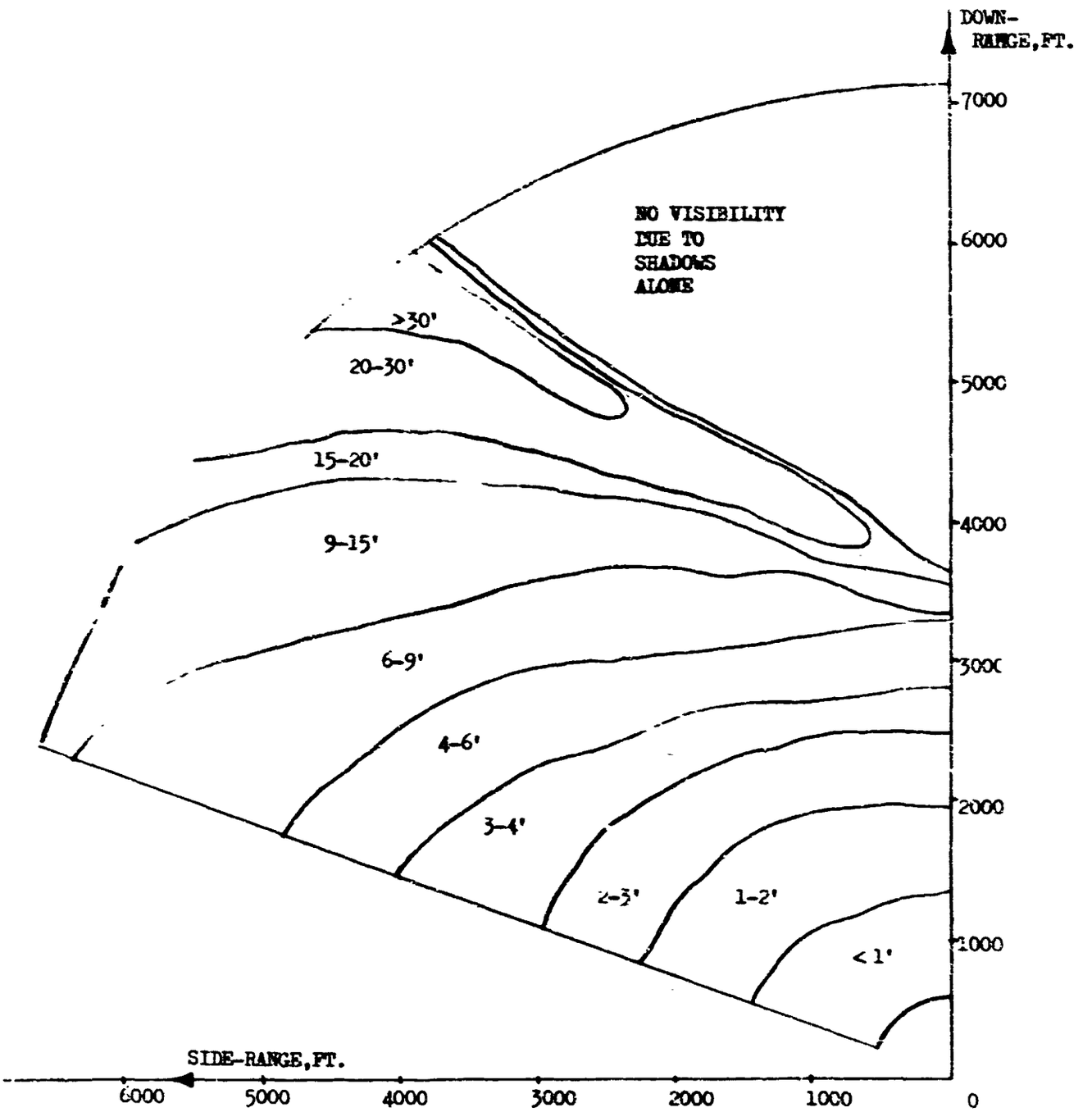

VISIBILITY OF CRATERS IN SAND

EARTH ATMOSPHERE ABSORPTION INCL.

GEOMETRIC SHADOW CRITERION ONLY

h = 1000 ft. (NO SKY-LIGHTING)

SUN $\measuredangle$ = 15°

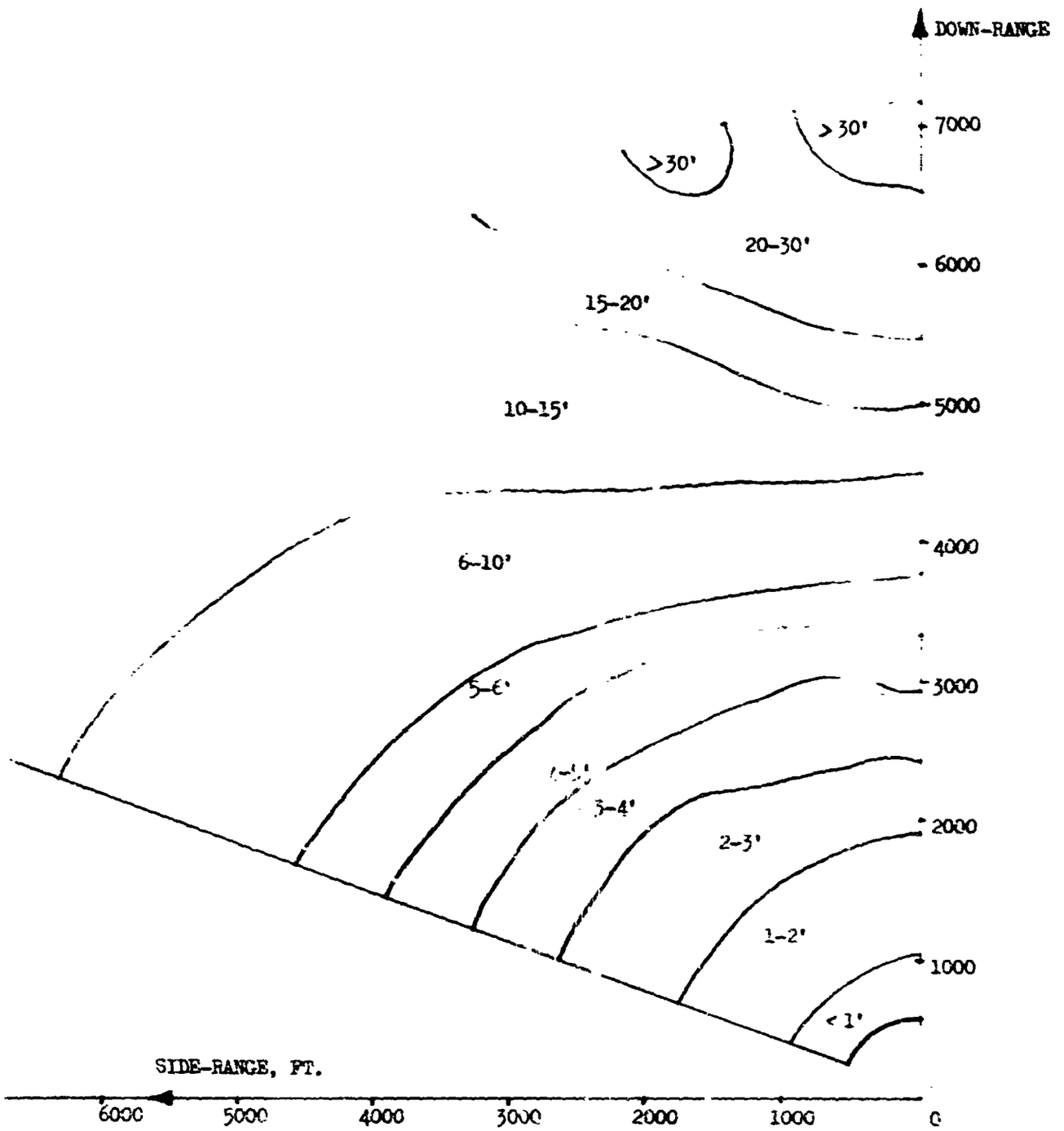

PHOTOMETRIC SHADOW VIS.

SUN ϕ = 15°, n = 1000

SAND CRATERS

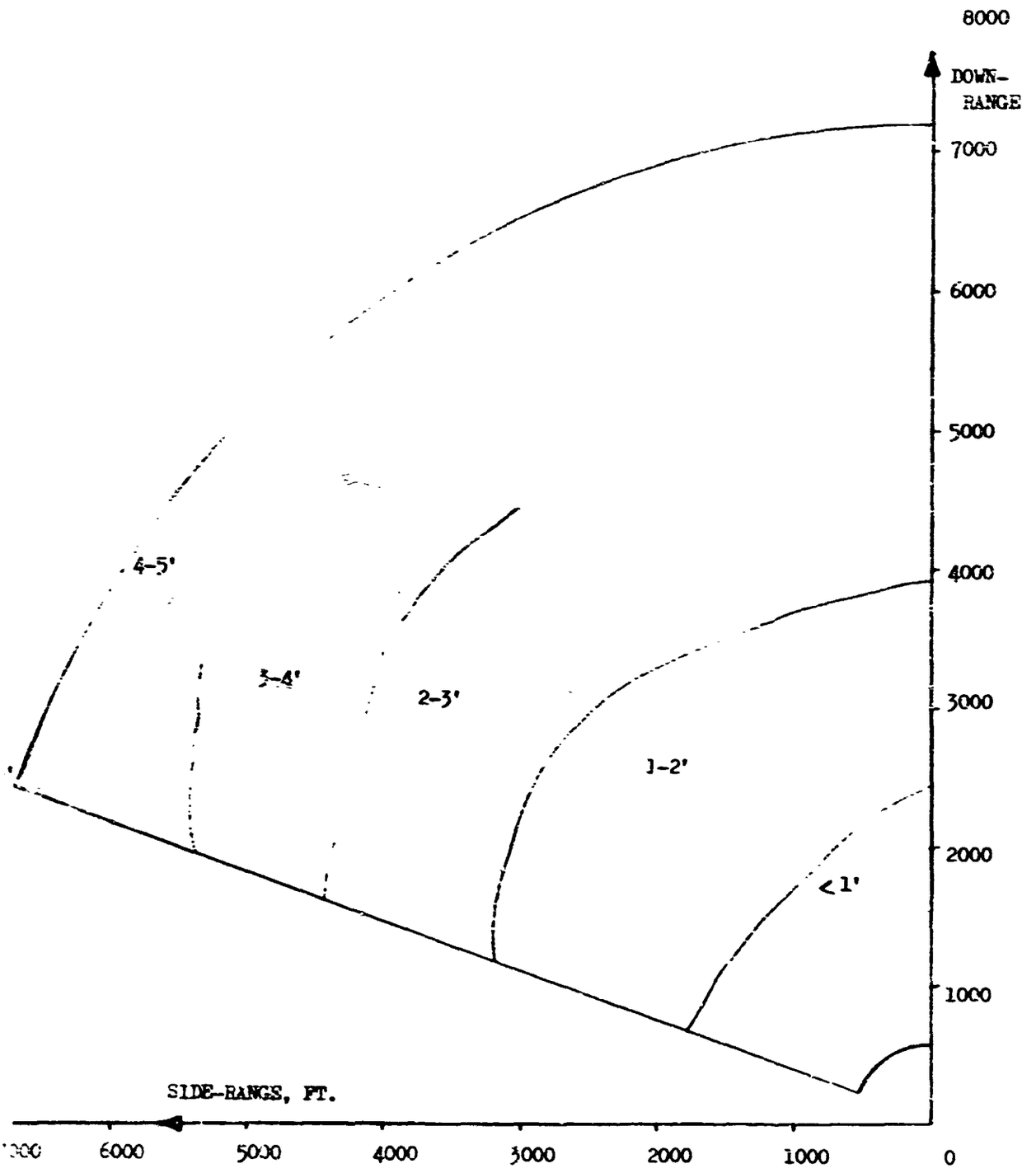

BRIGHT SIDE VIS.

SUN ϕ = 15°, h = 1000

SAND CRATERS

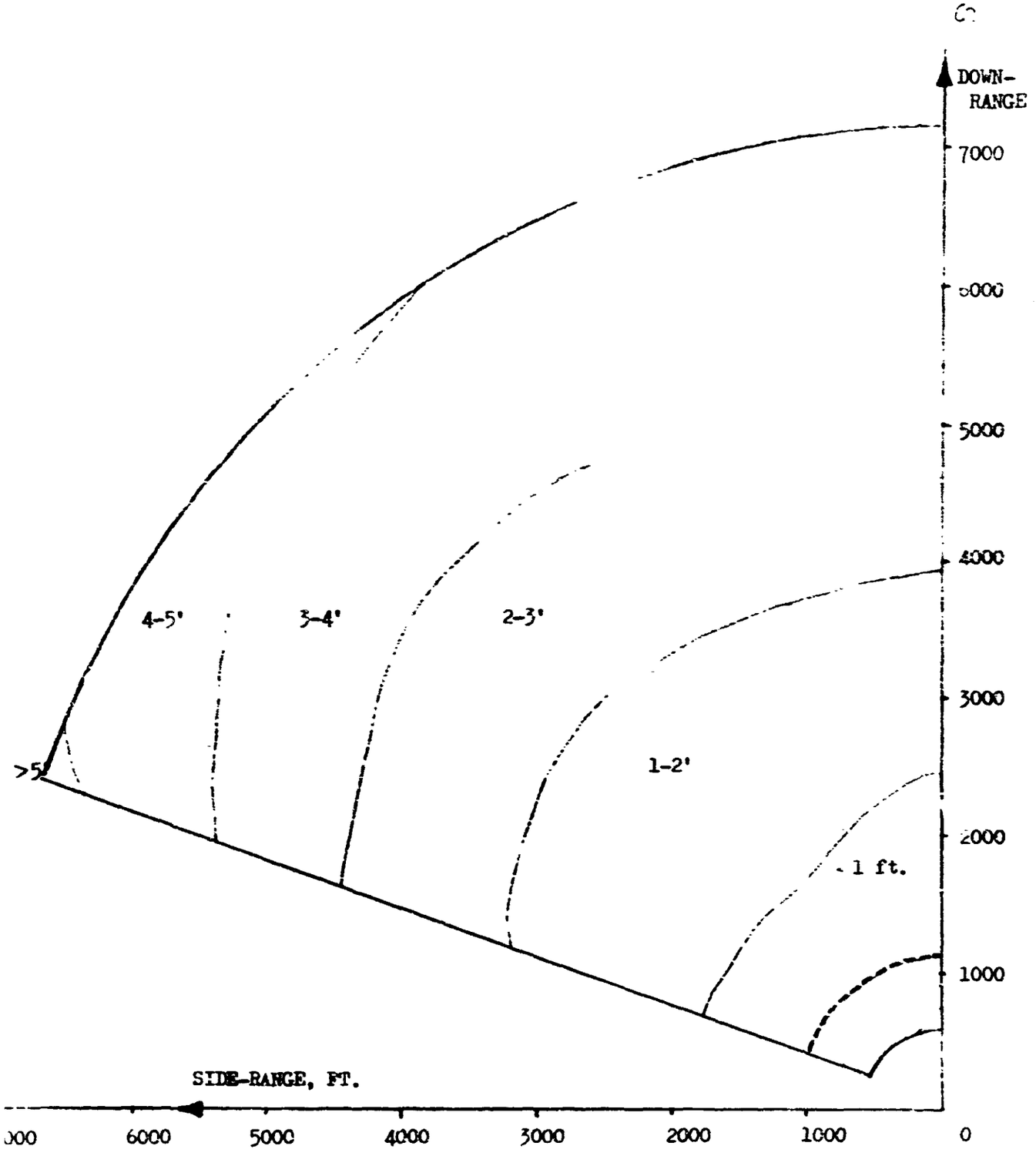

COMBINED VISIBILITY
SAND CRATERS
SUN = 15°, h = 1000 Ft.

FIGURE A4

BRIGHT SIDE GIVES BEST VISIBILITY

PHOTOMETRIC SHADOW GIVES BEST VISIBILITY

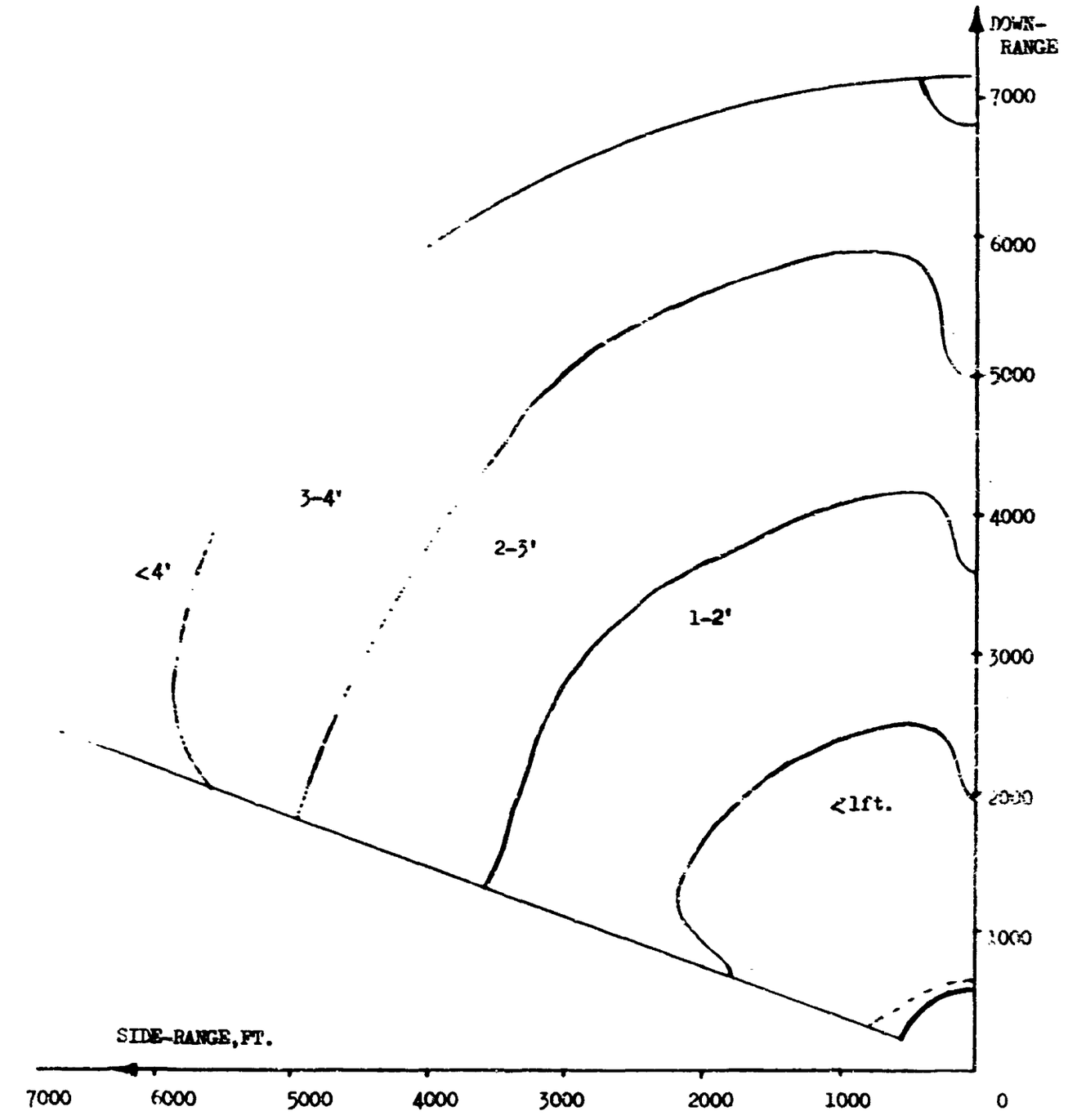

COMBINED VISIBILITY
SAND CRATERS
SUN ϕ = 30° h = 1000 ft.

BRIGHT SIDE GIVES BEST VISIBILITY

PHOTOMETRIC SHADOW GIVES BEST VISIBILITY

FIGURE A5

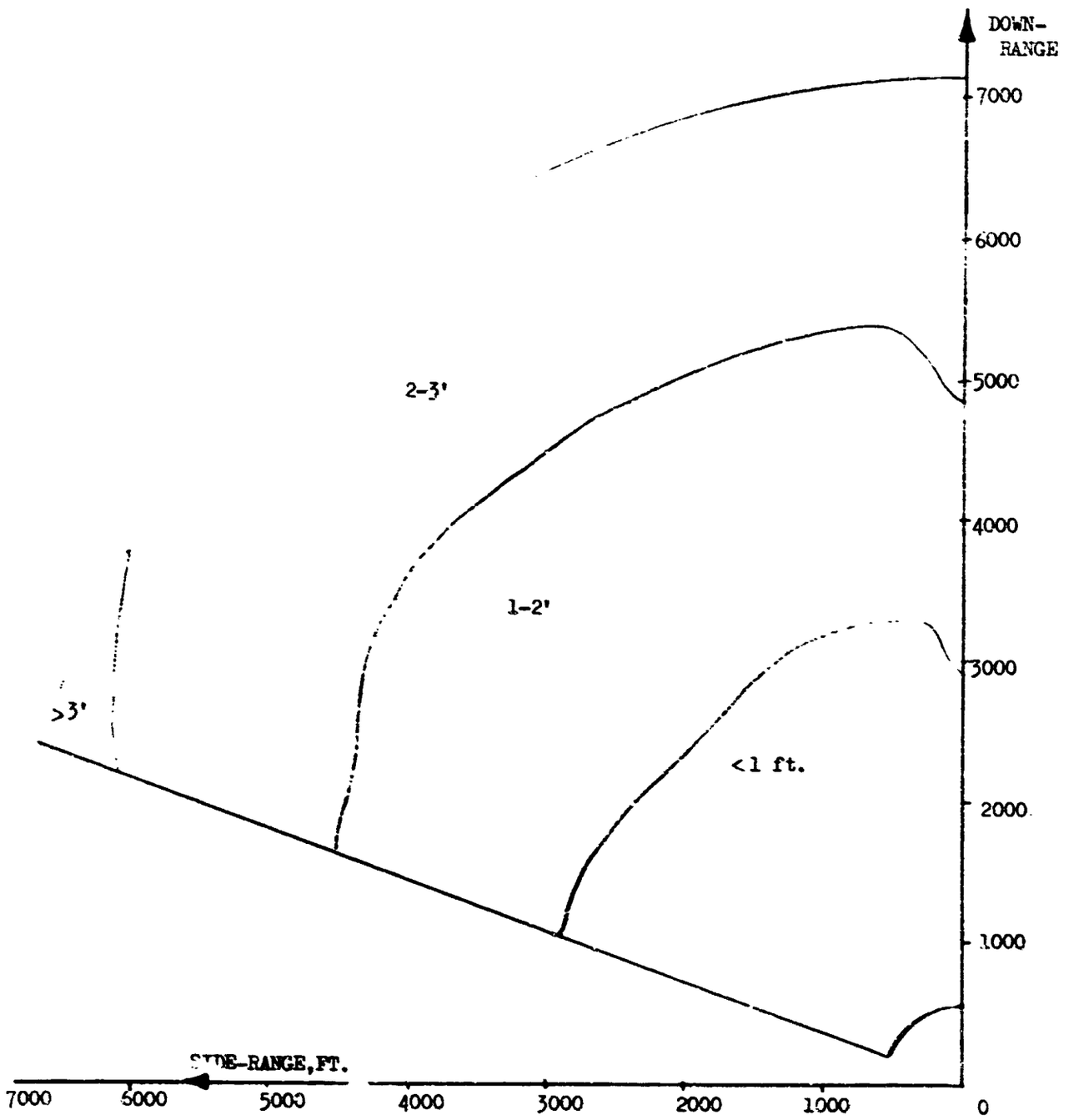

BEST VISIBILITY IS
DUE TO BRIGHT SIDE ONLY.

COMBINED VISIBILITY
SAND CRATERS
ψ_{SUN} 4 = 45° h = 1000 ft.

APPENDIX B

Simulated Crater Visibility Tests - A 1/250 scale model was constructed containing eight spherical depressions (10:1 diameter-to-depth ratio) of various sizes as illustrated in Figure B1. This model was dusted with copper oxide and the test was arranged as shown in Figure B2. The observer was asked to count the number of craters he could detect at any given range. The test was done for ten observers, sun angles of 10° and 30°, ranges of 4' to 28' in 4-foot steps and observer azimuths relative to the sun plane of 0°, 10°, and 20°. A weighted average was taken of the observations and the final number of craters detectable at each point inerpreted as a minimum detectable size. The results were plotted and compared to the computer generated results as shown in Figure B3.

The results of the comparison indicate that the revised method discussed earlier is the most accurate approach to evaluating crater visibility. The fact that the observed data differs by about 50% from the calculated data in some instances can be attributed to the use of untrained observers in the experiment and also to the inaccuracies inherent in this type of simulation. It should also be noted that the observers were limited to 30 seconds search time and the computer data was calculated with the assumption of no limit on search time.

CRATERS OF 10:1 DEPTH/DIAMETER RATIO MACHINED IN PLEXIGLASS

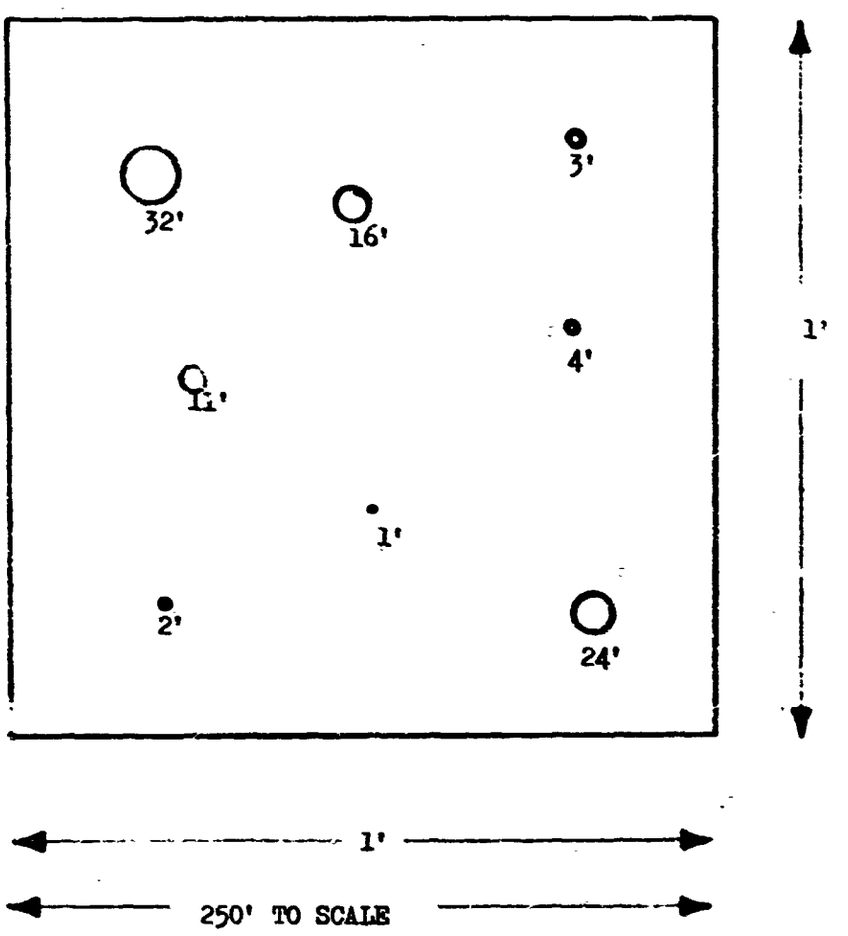

MODEL LAYOUT, GEOMETRIC CRATER VISIBILITY SIMULATION

FIGURE B1

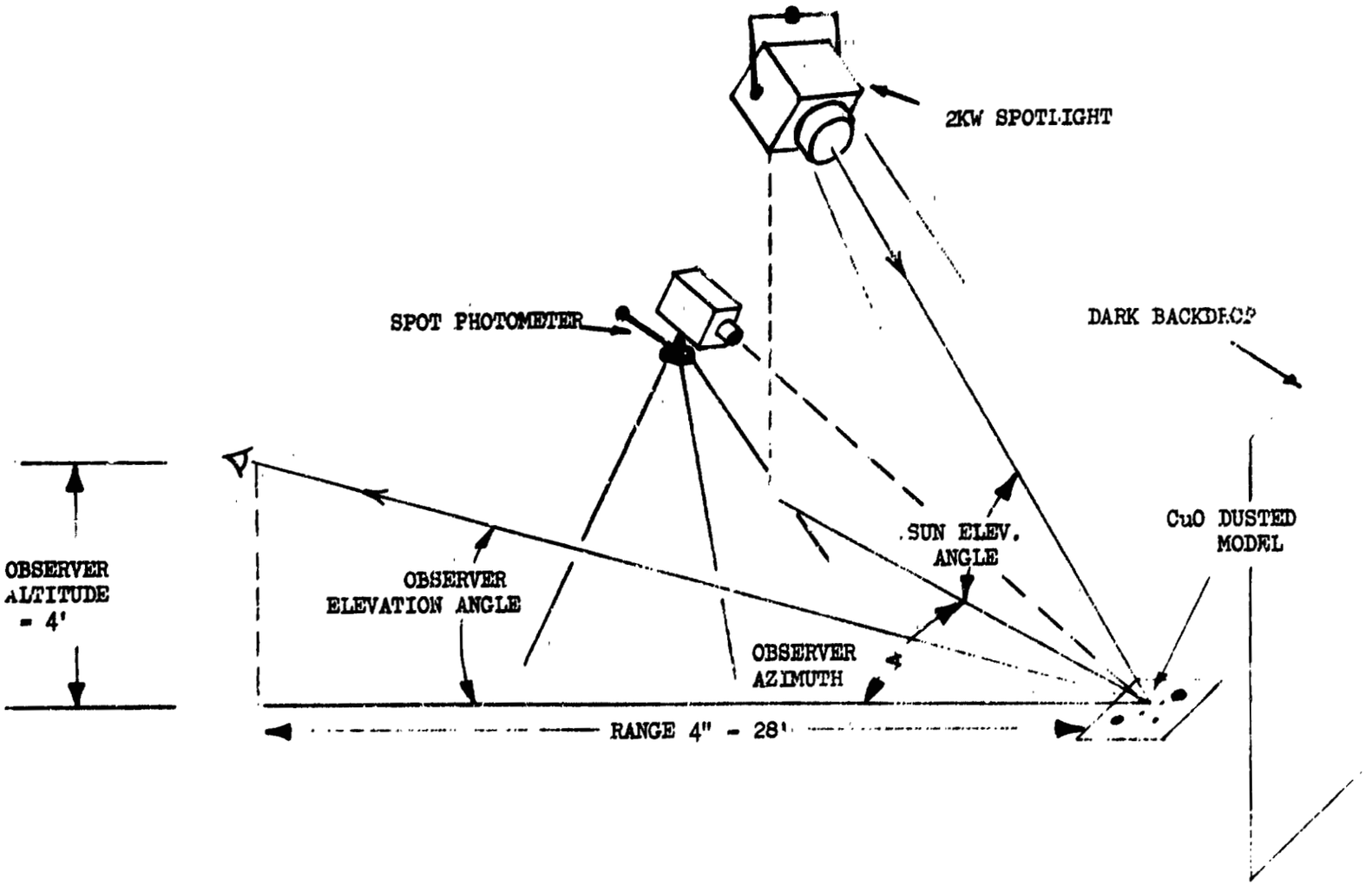

CRATER VISIBILITY SIMULATION

FIGURE B2

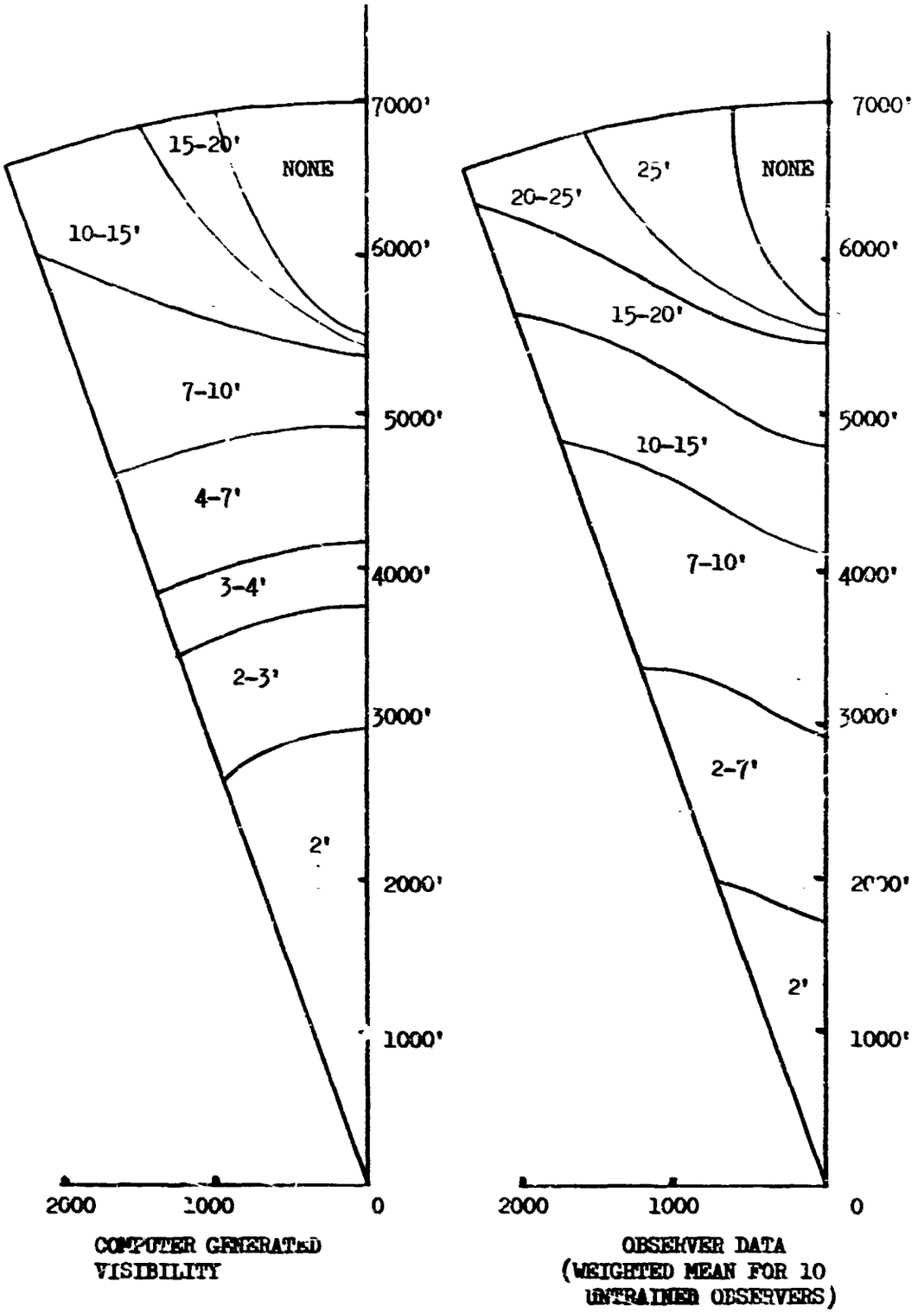

COMPARISON OF OBSERVED AND COMPUTER DATA

10° SUN ELEVATION ANGLE

FIGURE 33